Quantum fluids in low dimension and Kosterlitz–Thouless transition

Jean Dalibard
Collège de France, chaire *Atomes and rayonnement*

Lecture series 2016-17

COLLÈGE
DE FRANCE
1530

Contents

Introduction

This year's course has its origins in a simple question: what would become of the ordered objects of our physical world - crystals, magnets, superfluids - if we lived in a space with a lower dimension, on a plane for example? The analysis initiated by Peierls in 1935 had shown that thermal and quantum fluctuations would then be of greater importance, preventing the appearance of an order similar to that observed in our three-dimensional space. This result was reinforced in the 1960s by Mermin & Wagner (1966) and Hohenberg (1967).

However, if a conventional "order-disorder" transition cannot occur in reduced dimension, this does not mean that all phase transitions have disappeared: in the early 1970s, studies by Vadim Berezinskii on the one hand, and J. Michael Kosterlitz and David J. Thouless on the other, showed that a new mechanism could emerge, linked to the appearance of topological defects.

Let us start by saying a few words about this link between topology and physics, which the 2016 Nobel Jury saluted by rewarding David J. Thouless, F. Duncan M. Haldane and J. Michael Kosterlitz *for theoretical discoveries of topological phase transitions and topological phases of matter*. These two disciplines, topology and physics, seem far apart. Topology is a branch of mathematics concerned with establishing abstract equivalences between different objects, equivalences based on the shape – to be understood in a broad sense – of these objects. This kind of preoccupation might seem disconnected from research into the physical properties of matter, which is concerned with the phases that may appear as a function of density, temperature or interactions within a material.

To understand how "everyday" physics can benefit from notions of topology, it is useful to take a detour into geometry, more specifically the

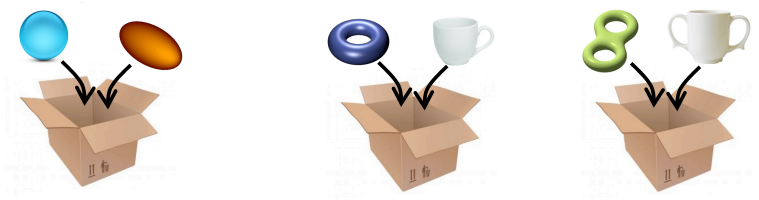

Figure 1. *Objects with genus $g = 0, 1, 2$.*

link between topology and geometry established by Gauss (who did not publish it) and Bonnet (who published it in 1848). In its simple version, the Gauss-Bonnet theorem concerns the study of regular surfaces in three-dimensional space, surfaces that we will assume here to be orientable and edgeless (i.e. closed). At each point $\boldsymbol{r}$ on the surface $\mathcal{S}$, we can define its curvature $\Omega(\boldsymbol{r})$. The Gauss-Bonnet theorem proves the quantization of the integral of $\Omega(\boldsymbol{r})$ on the surface $\mathcal{S}$ and gives an interpretation to this quantization:

$$\frac{1}{4\pi}\int_{\mathcal{S}} \Omega(\boldsymbol{r})\, \mathrm{d}^2 r = 1 - g \tag{.1}$$

where g is an integer, called the *genus* of the surface, which counts its number of holes. A sphere or the surface of a bowl has no hole (or no handle), so $g = 0$; a torus or a normal coffee cup has one handle, so $g = 1$; more complex objects have two, three handles (figure 1).

With this theorem emerges the notion of "topological protection": starting with a torus, for example, we can continuously deform it into a cup without closing the handle (figure 2). In this deformation, the curvature

Figure 2. *Continuous deformation of a cup into a torus. The curvature integral (.1) remains constant during this deformation (and equal to 0 for this one-handled object). Figure taken from the* Scientific American *web page and created by Keenan Crane (Columbia U.).*

at each point will of course change, but its integral over the surface will remain constant: this integral is therefore a robust quantity, protected from deformation. In fact, the only way to modify it is to plug the loop (or create a second one). At the precise moment when the hole is plugged, the surface is no longer regular and Gauss-Bonnet's theorem does not apply. As soon as the handle is plugged, the surface becomes regular again, but it now belongs to the $g = 0$ class of spheres and bowls...

When transposed to physical objects, this topological robustness is of great practical interest. Suppose a physical quantity can be written as the integral over a closed surface of a quantity Ω that can be assimilated to a curvature. We then know that this quantity will be robust, insensitive to changes in the detail of the object under consideration. This is precisely the situation encountered in the integer quantum Hall effect, where conductivity is obtained by integrating the Berry curvature over a closed surface, in this case the Brillouin zone associated with the populated energy band. We will not go into this aspect of the link between topology and physics in this lecture series, but it undoubtedly falls within the field rewarded by the Nobel jury, notably with the famous article TKNN (Thouless, Kohmoto, et al. 1982), which we had the opportunity to discuss in the 2013-14 course and that we will revisit in detail in next year course.

Another example of a topologically robust object that will feature prominently in this year's course is a vortex in a two-dimensional particle fluid obeying the Bose-Einstein statistic. Let us briefly introduce the notion of vortex in this context. We suppose[1] that the fluid is described by a matter wave field $\psi(\boldsymbol{r})$ with $\boldsymbol{r} = (x, y)$. This field is complex and is therefore characterized by its amplitude and phase. Traditionally, it is written

$$\psi(\boldsymbol{r}) = \sqrt{\rho(\boldsymbol{r})}\, \mathrm{e}^{\mathrm{i}\theta(\boldsymbol{r})}, \tag{.2}$$

where $\rho(\boldsymbol{r}) = |\psi(\boldsymbol{r})|^2$ represents the density at point $\boldsymbol{r}$. The phase $\theta(\boldsymbol{r})$ is defined modulo 2π, since the only constraint on the field ψ is that it be single-valued. Knowing the field ψ, we determine the fluid velocity as a function of the gradient of the phase $\theta(\boldsymbol{r})$, at any point $\boldsymbol{r}$ where the density is non-zero:

$$\boldsymbol{v}(\boldsymbol{r}) = \frac{\hbar}{m}\, \boldsymbol{\nabla}\theta(\boldsymbol{r}). \tag{.3}$$

It is important that the density is non-zero at $\boldsymbol{r}$ so that the phase $\theta(\boldsymbol{r})$ is itself well-defined in the vicinity of $\boldsymbol{r}$ and we can calculate its gradient. Since the velocity is proportional to the gradient of the phase, we deduce that for any closed contour $\mathcal{C}$ on which the phase is defined (figure 3):

$$\oint_{\mathcal{C}} \boldsymbol{\nabla}\theta(\boldsymbol{r}) \cdot \mathrm{d}\boldsymbol{r} = n\, 2\pi \qquad \longrightarrow \qquad \oint_{\mathcal{C}} \boldsymbol{v}(\boldsymbol{r}) \cdot \mathrm{d}\boldsymbol{r} = n\frac{2\pi\hbar}{m}, \qquad n \in \mathbb{Z}. \tag{.4}$$

This circulation is a quantized and topologically protected quantity: it can only change if the contour $\mathcal{C}$ is deformed to pass over a point where $\theta(\boldsymbol{r})$ is not defined, i.e. a zero of ψ.

The zeros of ψ correspond to vortices. The ones we will encounter in this course are simple zeros, corresponding to the cases $n = \pm 1$. A vortex in $\boldsymbol{r} = 0$ is obtained by taking, for example, a field $\psi(\boldsymbol{r})$ of the form

$$\psi(\boldsymbol{r}) = (x \pm \mathrm{i}y)\, F\left(x^2 + y^2\right) = r\, F(r^2)\, \mathrm{e}^{\pm i\varphi} \tag{.5}$$

where F is a regular function. The number $n = \pm 1$ determining the phase winding $\pm 2\pi$ on a contour surrounding a vortex is called the *topological charge* of the vortex.

Because of the protection of $\oint_{\mathcal{C}} \boldsymbol{v}(\boldsymbol{r}) \cdot \mathrm{d}\boldsymbol{r}$ for any contour surrounding a vortex, these vortices are referred to as "topological defects". A field $\psi(\boldsymbol{r})$ containing a vortex cannot be deformed continuously into a field $\psi(\boldsymbol{r})$

[1] We will come back to this assumption at length in the chapters that follow. Possible references on this subject include Pitaevskii & Stringari (2016), Leggett (2006) or Svistunov, Babaev, et al. (2015).

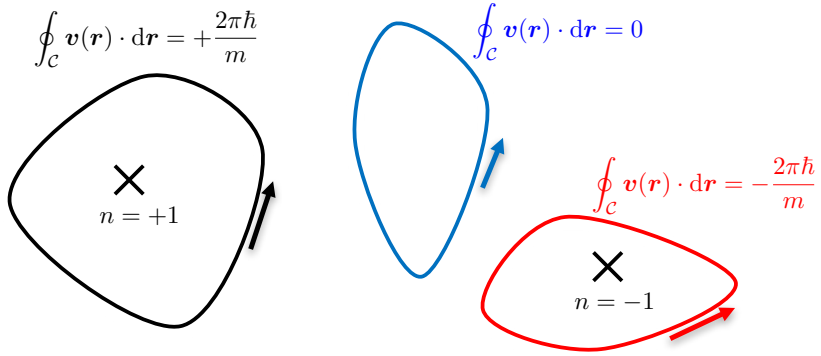

Figure 3. *Circulation of the velocity field on a closed contour $\mathcal{C}$ in a two-dimensional Bose gas. This circulation is non-zero if the contour encompasses a vortex. The value is then quantized [equation (.4)] with the integer n giving the charge of the vortex (or the sum of the charges if several vortices are located inside the contour).*

without a vortex. On the contrary, a field $\psi(\boldsymbol{r})$ exhibiting only smooth oscillations of $\rho(\boldsymbol{r})$ and $\theta(\boldsymbol{r})$, with $\rho(\boldsymbol{r})$ non-zero everywhere, can be continuously deformed into a completely uniform field ψ_0 (figure 4). We will later interpret these smooth oscillations as phonons.

This notion of topological defect plays a central role in the mechanism discovered by Kosterlitz & Thouless (1973). In fact, their work parallels that of Berezinskii (1971), and in this course we will refer to it as the BKT mechanism. The BKT mechanism consists of a "pairing-unpairing" transition of topological defects (figure 5):

- Let us consider the situation where the defects are paired; in the case of a Bose fluid, this means that in the immediate vicinity of any vortex of charge $+1$, we find a vortex of charge -1. If we restrict ourselves to large enough contours $\mathcal{C}$, the two vortices will almost always be inside the contour, leading to a zero integral. The state $\psi(\boldsymbol{r})$ can be seen, at least in the context of a coarse-grained average, as similar to the uniform state expected at zero temperature. This state is referred to as topologically ordered.

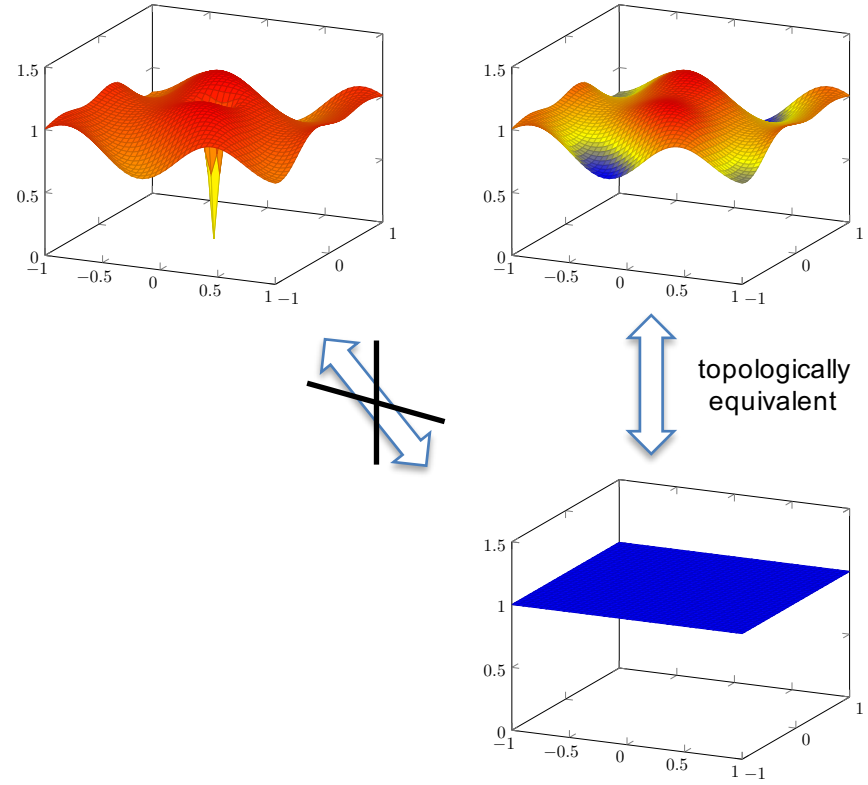

Figure 4. *Left: amplitude of a field $\psi(\boldsymbol{r})$ containing a vortex. This "defect" is topologically protected by the phase winding $\pm 2\pi$ around it. Right: amplitude of a field $\psi(\boldsymbol{r})$ exhibiting only smooth oscillations of $\rho(\boldsymbol{r})$ and $\theta(\boldsymbol{r})$, with $\rho(\boldsymbol{r})$ non-zero everywhere. This field can be continuously deformed into a uniform field, corresponding to the expected state at zero temperature.*

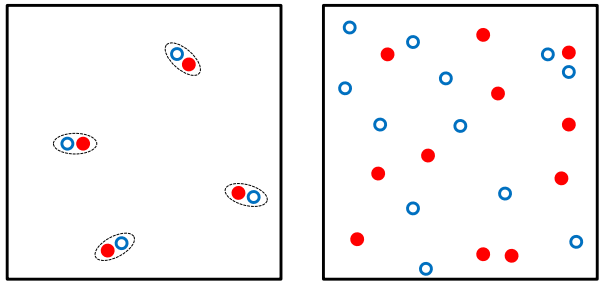

Figure 5. *Left: low temperature state with paired topological defects. If we do a coarse-grained average of the state of the system, we recover the situation with no defects. Right: high temperature, unpaired topological defects; the phase obtained is radically different from that expected at low temperature.*

- On the other hand, if the defects are unpaired, a contour $\mathcal{C}$ will generally encompass a different number of positive and negative vortices. The state $\psi(\boldsymbol{r})$ cannot be continuously deformed towards the uniform state and it is not topologically equivalent to the zero-temperature state.

In the thermodynamic limit, the corresponding transition is a phase transition. In the particular case of a Bose fluid of fixed density, it occurs for a critical temperature T_c that can be calculated. The BKT mechanism applies to a wide variety of systems, both classical and quantum. The corresponding phase transition is radically different from those described in the Landau classification. In fact, the BKT transition can be seen as an infinite-order transition, since all thermodynamic functions are continuous at T_c.

The plan for this lecture series is as follows:

- The first chapter is devoted to Peierls' argument, showing why conventional crystalline order cannot exist in one and two dimensions due to thermal fluctuations. We also give some illustrations of the topological order likely to appear in a fluid of interacting particles.
- We then turn to quantum fluids, starting with the ideal gas. We return to the impossibility of achieving long-range order and show how confinement effects can nevertheless lead to the emergence of a Bose-Einstein condensate. We illustrate this point with photon condensation experiments in an electromagnetic cavity. We conclude this chapter by describing how to take into account interactions between two particles in dimension two.
- Chapter 3 is devoted to the case of an interacting 2D Bose gas, in the low-temperature limit where a Bogoliubov-type approach is relevant. In agreement with the Mermin–Wagner–Hohenberg result, we show that the phase ordering well-known in 3D cannot appear in 2D, and we explain that it is replaced by a quasi-order with an algebraic decay of the one-body correlation function G_1 for a uniform gas:

$$G_1(\boldsymbol{r}) = \langle \hat{\psi}^\dagger(\boldsymbol{r})\, \hat{\psi}(0) \rangle \propto \frac{1}{r^\eta}, \tag{.6}$$

  where the exponent η can be related to the phase-space density of the gas.
- The role of topological defects (vortices) is discussed in detail in Chapter 4, where we see why the existence of isolated vortices destroys superfluidity, whereas pairs of bound vortices have no major consequences. We describe in semi-quantitative terms the now-standard methods for analyzing the critical point of the BKT transition. We also look at how the first experiments carried out on helium films in the late 1970s confirmed these predictions.
- Chapter 5 is devoted to comparing BKT predictions with experiments carried out on dilute quantum fluids, atomic gases or cavity polaritons. In particular, we show that it is not easy to design a single physical system capable of demonstrating all characteristics of the BKT transition at once.
- Finally, in Chapter 6, we look at the difference between the classical and quantum aspects of degenerate 2D gases. The BKT transition emerges when we describe these fluids by a *classical* field $\psi(\boldsymbol{r})$, the only quantization being that of the velocity circulation (.4). This "classical field" approach brings a bonus: the scale invariance. On the contrary, a completely quantum description of the fluid breaks this invariance. We present some recent experiments on this subject.

Clearly, in the limited space available for this course, it is not possible to provide a comprehensive overview of research dedicated to the BKT transition. The latter has been the subject of numerous books and journal articles, and we refer readers wishing to learn more to the recent book edited by José (2013), which contains numerous references on the subject.

Chapter I

Crystalline order in low dimension

Most of this year's course will be devoted to the study of quantum gases in reduced dimensions, essentially in dimension two. Because of this reduction of dimensionality, the condensation phenomenon associated with Bose-Einstein statistics is absent, at least in the thermodynamic limit, i.e. for an infinite system. In other words, the long-range order that characterizes a Bose-Einstein condensate, i.e. the phase coherence of the wave function that describes the gas, disappears in two or one dimensions. Thermal fluctuations play a more important role than in three dimensions, destroying the order that statistics and interactions tend to create.

Rudolf Peierls, originally from Germany but working in England from 1933, formalized this possible loss of long-range order in systems of reduced dimension (Peierls 1934; Peierls 1935). Peierls was not interested in Bose-Einstein condensates, but in the translational order of a solid, and he showed that a crystal could not exist in a one- or two-dimensional world.

In this chapter, we will start by examining Peierls' arguments in one and two dimensions. We will then describe some recent experiments on colloids that have tested Peierls' prediction. We will also see that the absence of crystalline order does not mean complete disorder: these colloidal assemblies can be "almost" crystalline at low temperatures, before becoming completely liquid at higher temperatures. This will be our first encounter with a phase transition induced by topological defects, a concept formalized by Kosterlitz & Thouless (1973).

1 Peierls argument in 1D

We start with a one-dimensional system, i.e. a chain of atoms. We restrict ourselves to the case of nearest-neighbor interactions to arrive at Peierls' simple result: such a system cannot exhibit crystalline order. Even if the position of a given atom in the chain is known precisely, the position of another atom is completely undefined on the scale of the spatial period of the crystal, provided this second atom is chosen far enough away from the first.

1-1 A simple argument: piling up defects

Consider a chain of atoms with nearest-neighbor interaction described by the potential $U(x)$. If we label the atoms with the index j and assume $\cdots < x_{j-1} < x_j < x_{j+1} < \cdots$, the interaction energy of the system is equal to

$$V_{\rm int}(\{x_j\}) = \sum_j U(x_{j+1} - x_j). \tag{I.1}$$

To favor the emergence of crystalline order, let us assume that the potential $U(x)$ has a local minimum at $x = a$, so that at zero temperature and in the absence of any quantum fluctuations, the chain of atoms is regular, with a spacing between adjacent atoms equal to a (figure I.1).

Suppose now that the system is at non-zero temperature T. Taking the

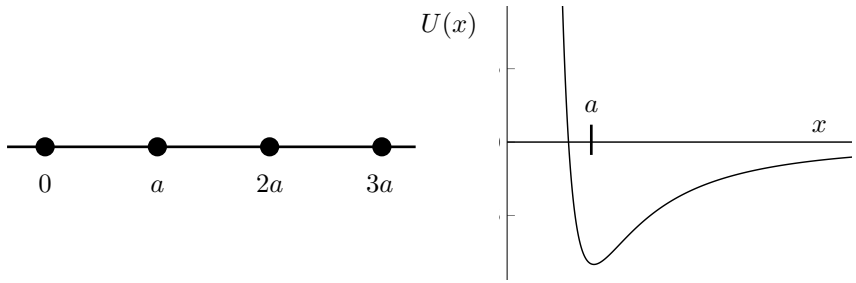

Figure I.1. *One-dimensional chain of atoms with nearest-neighbor interactions described by the potential $U(x)$. This potential has a minimum at $x = a$, which leads to the formation of a crystal, at least for a gas of particles at zero temperature described by classical physics (no thermal or quantum fluctuations).*

position x_0 of atom 0 as a reference, the position x_1 of its neighbor on the right will fluctuate around its equilibrium position with a root-mean-square deviation δ_1 which can be deduced from the equipartition theorem:

$$x_1 = x_0 + a + \delta_1 \qquad \text{with} \quad \langle \delta_1 \rangle = 0, \qquad \langle \delta_1^2 \rangle \sim \frac{k_{\rm B}T}{\kappa}, \quad \kappa = \left. \frac{{\rm d}^2 U}{{\rm d}x^2} \right|_{x=a}. \tag{I.2}$$

We have restricted ourselves here to the case where $|\delta| \ll a$, so we can use a quadratic approximation to estimate the variations of the potential $U(x)$ in the vicinity of its minimum $x = a$. Furthermore, we have added a $\sim$ sign and not a $=$ sign, as the treatment here can only give an order of magnitude of $\langle \delta_1^2 \rangle$. Indeed, the position of atom 1 must not only be located in relation to its left-hand neighbor, atom 0, but also in relation to its right-hand neighbor, atom 2. Correctly taking all these interactions into account leads to a set of coupled equations that we will look at later (§ 1-2).

The same argument can be used to evaluate fluctuations in the position of atom j relative to its neighbor $j-1$:

$$x_j = x_{j-1} + a + \delta_j \qquad \text{with} \quad \langle \delta_j^2 \rangle \sim \frac{k_{\rm B}T}{\kappa} \tag{I.3}$$

With respect to the initial atom 0, the position of atom j is given by

$$x_j = x_0 + ja + \Delta_j \tag{I.4}$$

where the quantity Δ_j is the sum of the j independent random variables:

$$\Delta_j = \delta_1 + \cdots + \delta_j. \tag{I.5}$$

This quantity also has zero mean value and its variance reads:

$$\langle \Delta_j^2 \rangle \sim \frac{k_{\rm B}T}{\kappa}\, j. \tag{I.6}$$

We can thus see that the uncertainty in the position of atom j increases as $\sqrt{j}$ as we move away from the reference atom. For j large enough, typically

$$\langle \Delta_j^2 \rangle \gtrsim a^2 \qquad \longrightarrow \qquad j \gtrsim \frac{\kappa a^2}{k_{\rm B}T}, \tag{I.7}$$

the uncertainty Δ_j becomes larger than the lattice period a and crystal order is lost: even if we know exactly where the reference atom 0 is, we have no information on the position of the atom j on the scale of the crystal period.

This very simple argument is conclusive in the one-dimensional case, but is difficult to generalize to higher dimensions. We are therefore going to use a slightly more elaborate treatment, in which we consider the vibrations (phonons) of the lattice, a treatment that can be transposed to dimensions 2 and 3. This treatment is similar to the one we will be using later to study superfluidity.

1-2 Classical harmonic crystal

We consider the same chain of atoms as in the previous paragraph, choosing periodic boundary conditions to simplify calculations. Noting the total atom number as N, we identify atom N and atom 0, which amounts to positioning the atoms on a circle (figure I.2). We limit ourselves to small variations of the distances $x_{j+1} - x_j$ around their equilibrium value a, so that the total energy (kinetic + interactions) of the system is written in the

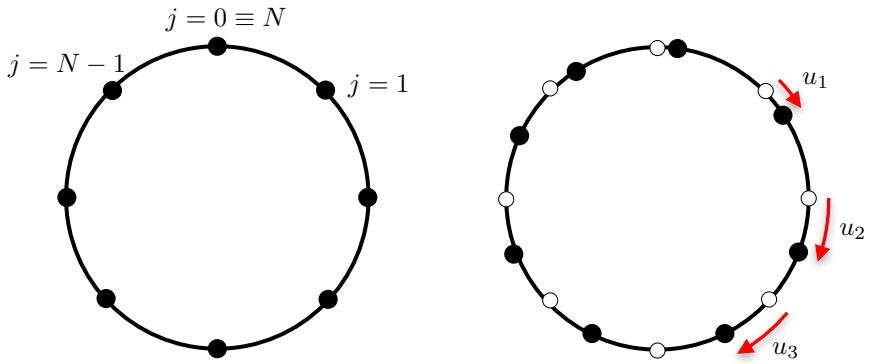

Figure I.2. *Left: ordered chain of N atoms with periodic boundary conditions, leading to identification of atom $j = 0$ and atom $j = N$. Right: definition of displacements u_j relative to equilibrium positions. We assume that $|u_{j+1} - u_j| \ll a$, but not necessarily that $|u_j| \ll a$.*

harmonic approximation

$$E = \sum_{j=1}^{N} \frac{1}{2} m \dot{u}_j^2 \; + \; \frac{\kappa}{2} (u_{j+1} - u_j)^2 \tag{I.8}$$

where u_j denotes the deviation of atom j from its equilibrium position X_j:

$$u_j = x_j - X_j \qquad \text{with} \quad X_j = ja \tag{I.9}$$

(with the convention $u_{N+1} \equiv u_1$). Note that the assumption of small variation in the distance between nearest neighbors:

$$|u_{j+1} - u_j| \ll a \tag{I.10}$$

does not imply that u_j and u_{j+1} are separately small in front of a. Atoms j and $j+1$ may each be strongly deviated from their equilibrium positions X_j and X_{j+1}, but we make the assumption that their deviations u_j and u_{j+1} are close; in other words, there can be local order without having long-range order.

The equations of motion lead to a system of N coupled linear equations:

$$m \ddot{u}_j = \kappa (u_{j+1} - 2u_j + u_{j-1}), \tag{I.11}$$

whose solutions are the eigenmodes of the system, i.e. the phonons. Solving this system of equations is a classic in solid-state physics textbooks [see, for example, Ziman (1960) and Ashcroft & Mermin (1976)]. We introduce the coefficients $\hat{u}_q$ (with N even)

$$\hat{u}_q = \frac{1}{\sqrt{N}} \sum_j \mathrm{e}^{-\mathrm{i}\, qX_j} \; u_j, \qquad q = -\frac{\pi}{a}, \ldots, -\frac{2\pi}{Na}, \; 0, \; \frac{2\pi}{Na}, \ldots, +\frac{\pi}{a} \tag{I.12}$$

where the two extreme values $q = \pm\pi/a$ lead to the same coefficient $\hat{u}_q$. The $u_j \to \hat{u}_q$ transformation is simply a discrete Fourier transform that associates the deviations u_j with the amplitudes $\hat{u}_q$ of the momenta q. This transformation is inverted to give

$$u_j = \frac{1}{\sqrt{N}} \sum_q \mathrm{e}^{\mathrm{i}\, qX_j} \; \hat{u}_q. \tag{I.13}$$

Since the N positions u_j are real, the complex amplitudes $\hat{u}_q$ satisfy

$$\hat{u}_q^* = \hat{u}_{-q}, \qquad \hat{u}_0, \; \hat{u}_{\pm\pi/a} \in \mathbb{R}. \tag{I.14}$$

We therefore have N independent real variables, both in position space and in Fourier space.

The total energy (I.8) can be written as a function of the phononic modes $\hat{u}_q$:

$$E = \sum_q \frac{1}{2} \, m \, \dot{\hat{u}}_q \dot{\hat{u}}_{-q} + \frac{1}{2} \, m \, \omega_q^2 \, \hat{u}_q \hat{u}_{-q} \tag{I.15}$$

where

$$\omega_q = 2\sqrt{\frac{\kappa}{m}} \, |\sin \frac{qa}{2}|. \tag{I.16}$$

We have therefore decomposed the problem into N independent phonon modes, governed by the equation of motion:

$$\ddot{\hat{u}}_q + \omega_q^2 \hat{u}_q = 0. \tag{I.17}$$

- The $\hat{u}_0$ mode, with equation of motion $\ddot{\hat{u}}_0 = 0$, corresponds to the motion of the center of mass of the entire chain. Nothing constrains the position of this center of mass, since the total energy is invariant in a global translation of the N atoms.

- The $N-1$ modes $\hat{u}_q$ with $q \neq 0$ form decoupled harmonic oscillators of frequency ω_q.

Modes (I.12-I.16) correspond to a discretized version of the traveling waves $\mathrm{e}^{\mathrm{i}qx}$, with the positions $x = X_j \equiv ja$. For small wave numbers ($q \ll \pi/a$), we find a linear dispersion relation

$$\omega_q = c\,|q| \qquad \text{with} \quad c = a\sqrt{\frac{\kappa}{m}}, \tag{I.18}$$

corresponding to sound waves traveling at velocity c.

1-3 Correlation of the deviations u_j

At thermal equilibrium, we deduce from the energy expression (I.15) that each mode $\hat{u}_q$ for $q \neq 0$ has a zero mean value and a variance given by the equipartition theorem:

$$\frac{1}{2}m\omega_q^2\langle|\hat{u}_q|^2\rangle = \frac{1}{2}k_{\mathrm{B}}T \qquad \langle\hat{u}_q\hat{u}_{q'}^*\rangle = 0 \text{ if } q \neq q'. \tag{I.19}$$

To establish this relationship (with the correct factors!), remember that we are working with complex oscillators [*cf.* (I.14)]. In case of doubt, one should think in terms of independent real oscillators, for example by considering the real and imaginary parts of $\hat{u}_q$, taking the sum (I.15) and restricting it to the independent variables corresponding to $q \geq 0$.

It is then easy to calculate the correlation between the displacement of atom j and that of atom 0 ($\equiv N$). Let us start with

$$u_j - u_0 = \frac{1}{\sqrt{N}}\sum_q \left(\mathrm{e}^{\mathrm{i}qX_j} - 1\right)\hat{u}_q, \tag{I.20}$$

which gives in average

$$\begin{aligned}\langle(u_j-u_0)^2\rangle &= \frac{4}{N}\sum_q \sin^2\left(qX_j/2\right)\,\langle|\hat{u}_q|^2\rangle &\text{(I.21)}\\ &= \frac{k_{\mathrm{B}}T}{m}\,\frac{4}{N}\sum_q \frac{\sin^2\left(qX_j/2\right)}{\omega_q^2}. &\text{(I.22)}\end{aligned}$$

At this point, it is useful to replace the sum over the discretized momenta q by an integral using the relationship deduced from (I.12):

$$\sum_q \longrightarrow \frac{Na}{2\pi}\int_{-\pi/a}^{\pi/a}\mathrm{d}q, \tag{I.23}$$

which leads to

$$\begin{aligned}\langle(u_j-u_0)^2\rangle &= \frac{2}{\pi}\,\frac{k_{\mathrm{B}}Ta}{m}\int_{-\pi/a}^{\pi/a}\frac{\sin^2(qX_j/2)}{\omega_q^2}\,\mathrm{d}q\\ &= \frac{4}{\pi}\,\frac{k_{\mathrm{B}}Ta}{m}\int_{0}^{\pi/a}\frac{\sin^2(qX_j/2)}{\omega_q^2}\,\mathrm{d}q\\ &\approx \frac{4}{\pi}\,\frac{k_{\mathrm{B}}T}{\kappa a}\int_{0}^{\pi/a}\frac{\sin^2(qX_j/2)}{q^2}\,\mathrm{d}q &\text{(I.24)}\end{aligned}$$

where we have replaced in the last line the frequency ω_q by its linearized expression $\omega_q = cq$, and used the expression (I.18) for the speed of sound c. This approximation will be justified once we know which modes q contribute most to this integral.

We take the case where atom j is far from atom 0, since we are interested in long-range order. To evaluate this integral, we will first use an approximate method. It consists in cutting up the integration interval, then evaluating each piece. This method will simply give us the scaling law for $\langle(u_j-u_0)^2\rangle$ and will be directly transposable to the two-dimensional case. We will then look at a second method, specific to the 1D case, which will allow us to calculate this integral (almost) exactly.

Cutting the integral. The structure of the integrand suggests splitting the integration interval into two parts (figure I.3):

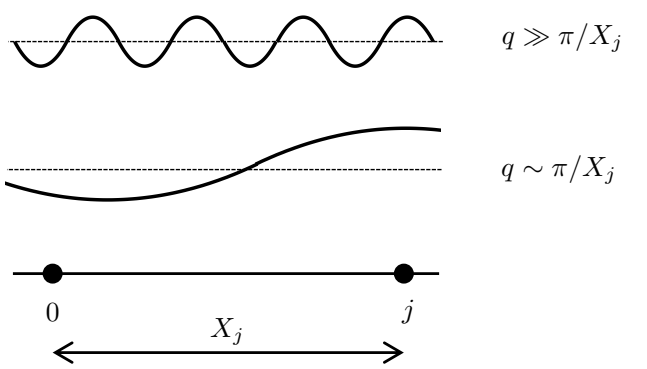

Figure I.3. *The two types of modes likely to contribute to the integral (I.24), for a given distance X_j between the two sites considered.*

- Values such as $q \gtrsim \pi/X_j$, for which we can replace the $\sin^2$ by its mean $1/2$, i.e.

$$\approx \frac{2}{\pi}\,\frac{k_\mathrm{B}T}{\kappa a}\int_{\pi/X_j}^{\pi/a}\frac{1}{q^2}\,\mathrm{d}q \approx \frac{2}{\pi^2}\,\frac{k_\mathrm{B}T}{\kappa a}\,X_j \tag{I.25}$$

  where we used the fact that $X_j \gg a$.

- Values such as $q \lesssim \pi/X_j$ for which we can replace the sine by its argument:

$$\approx \frac{1}{\pi}\,\frac{k_\mathrm{B}T}{\kappa a}\,{X_j}^2\int_0^{\pi/X_j}\mathrm{d}q = \frac{k_\mathrm{B}T}{\kappa a}\,X_j \tag{I.26}$$

In this form, we can see that the two contributions are of roughly the same order, their precise relative value depending on the position of the boundary between the two domains (here π/X_j). They each lead to a linear divergence of $\langle(u_j-u_0)^2\rangle$ with j. We can also see that the values of q that contribute most to these two integrals are those around $q \sim 1/X_j \ll 1/a$, i.e. modes whose wavelength is of the order of the distance between the two sites 0 and j considered here. This observation justifies the linearization of the frequency $\omega_q \propto \sin(qa/2)$ made in equation (I.24).

(Almost) exact calculation of the integral (I.24). A change of variable in this integral leads to:

$$\langle(u_j-u_0)^2\rangle = \frac{2}{\pi}\,\frac{k_\mathrm{B}T}{\kappa a}\,X_j\int_0^{\pi X_j/a}\frac{\sin^2 z}{z^2}\,\mathrm{d}z. \tag{I.27}$$

In the limit $j \gg 1$, the upper bound of the integral can be extended to $+\infty$ and the value of the integral is then $\pi/2$; we recover thus the result found in the first paragraph [*cf.* (I.6)]:

$$\langle(u_j-u_0)^2\rangle = \frac{k_\mathrm{B}T}{\kappa a}X_j = \frac{k_\mathrm{B}T}{\kappa}j. \tag{I.28}$$

This result also coincides (to within 20%) with the sum of the two contributions (I.25) and (I.26).

This calculation therefore confirms the conclusion of the simplified analysis in paragraph § 1-1: at non-zero temperature, there is no long-range order, and the memory of the atom's position $j = 0$ is lost after a distance that varies as $1/T$. On the other hand, at zero temperature, long-range order does exist in this classical model, with each atom occupying exactly its equilibrium position.

1-4 The quantum case

Before moving on to the multi-dimensional case, it is interesting to see how the previous results are modified when the influence of quantum fluctuations is taken into account. Let us place ourselves at zero temperature to simplify the analysis. To begin with, let us note that energy (I.8) is a quadratic function of positions and velocities, so the quantum treatment can be modelled on the classical one. In particular, the identification of phonon modes is unchanged, and we find for the potential energy of each oscillator $\hat{u}_q$:

$$\frac{1}{2}m\omega_q^2\langle|\hat{u}_q|^2\rangle = \frac{1}{4}\hbar\omega_q, \tag{I.29}$$

this expression replaces the classical equipartition of energy given in (I.19).

Let us inject this result into the expression (I.21) giving the variance of

the random variable $u_j - u_0$:

$$\langle (u_j - u_0)^2 \rangle = \frac{2\hbar}{mN} \sum_q \frac{\sin^2(qX_j/2)}{\omega_q} \quad \text{(I.30)}$$

$$\approx \frac{2}{\pi} \frac{\hbar}{\sqrt{\kappa m}} \int_0^{\pi/a} \frac{\sin^2(qX_j/2)}{q} \, \mathrm{d}q \quad \text{(I.31)}$$

where ω_q has been replaced by cq. As we did in (I.25-I.26), we can separate this integral into two parts, according to the relative value of q and $1/X_j$:

- For $q \gtrsim \pi/X_j$, we have for $X_j \gg a$

$$\approx \frac{1}{\pi} \frac{\hbar}{\sqrt{\kappa m}} \int_{\pi/X_j}^{\pi/a} \frac{1}{q} \, \mathrm{d}q = \frac{1}{\pi} \frac{\hbar}{\sqrt{\kappa m}} \ln(X_j/a) \quad \text{(I.32)}$$

- For $q \lesssim \pi/X_j$, we find:

$$\approx \frac{1}{2\pi} \frac{\hbar}{\sqrt{\kappa m}} X_j^2 \int_0^{\pi/X_j} q \, \mathrm{d}q = \frac{\pi}{4} \frac{\hbar}{\sqrt{\kappa m}}. \quad \text{(I.33)}$$

For $X_j \gg a$, the first contribution is dominant since it diverges as $\ln(X_j)$. We therefore find, up to an additive constant

$$\langle (u_j - u_0)^2 \rangle \sim \frac{a_{\mathrm{oh}}^2}{\pi} \ln(X_j/a), \quad \text{(I.34)}$$

where we set $a_{\mathrm{oh}} = (\hbar^2/m\kappa)^{1/4}$, which is the characteristic size of the ground state of a quantum harmonic oscillator of mass m and stiffness κ.

This divergence indicates that a one-dimensional quantum crystal cannot exist even at zero temperature, at least if we restrict ourselves to nearest-neighbor interactions. This divergence is weak since it is logarithmic, but it is enough to prevent crystalline long-range order.

In the following paragraph, we will find again a logarithmic divergence for a classical 2D crystal at non-zero temperature, with a mathematical treatment directly inspired by the one we have just used. Note that this relationship between a d-dimensional quantum system at zero temperature and its $d+1$-dimensional classical equivalent at finite temperature is not accidental. It can be fully formalized for certain problems, as discussed, for example, in the review article by Sondhi, Girvin, et al. (1997).

2 2D and 3D crystals

The above analysis can be transposed to the multi-dimensional case (Mermin 1968; Mermin 1979; Mermin 2006). The search for the system's eigenmodes is carried out in the same way, by linearizing the interaction potential between atoms in the vicinity of their equilibrium position in the crystal. The translational invariance of the system also allows us to search for the system's eigenmodes in the form of plane waves characterized by their wave vector $\boldsymbol{q}$.

A further complication arises in a lattice of dimension greater than 1. To fully specify the structure of an eigenmode, we need to know its polarization $\boldsymbol{\epsilon}$, i.e. the direction of oscillation of the atoms with respect to the wave vector. In one dimension, the problem does not arise, since oscillation necessarily takes place longitudinally, along the crystal's axis. In two (resp. three) dimensions, there are two (resp. three) independent polarizations for a given vector $\boldsymbol{q}$. The situation is simplified in the case of an isotropic crystal, for which one can always choose a solution polarized parallel to $\boldsymbol{q}$ and the other (or the other two in 3D) perpendicular to $\boldsymbol{q}$ (Ashcroft & Mermin 1976).

Once the eigenmodes have been identified, we can repeat the previous reasoning to evaluate the variance of the difference between the displacements $\boldsymbol{u}_0$ and $\boldsymbol{u}_{\boldsymbol{R}}$ of two atoms separated by $\boldsymbol{R}$. The exact treatment is complicated by the need to separate the contributions of the different polarizations of the modes, but fortunately the use of scaling laws is sufficient to conclude.

2-1 Deviations at thermal equilibrium in the 2D case

Let us consider a square lattice of period a, with N sites along each direction and periodic boundary conditions along each axis (figure I.4). Each site in the lattice is labelled by a pair of integers, $(j_x, j_y) \equiv \boldsymbol{j}$, corresponding to the position

$$\boldsymbol{R_j} = a\,(j_x \hat{\mathbf{x}} + j_y \hat{\mathbf{y}}) \quad \text{(I.35)}$$

where $\hat{\mathbf{x}}$ and $\hat{\mathbf{y}}$ are two unit vectors along the x and y axes. The position $\boldsymbol{r_j}$ of an atom is identified by its deviation $\boldsymbol{u_j}$ from the equilibrium position

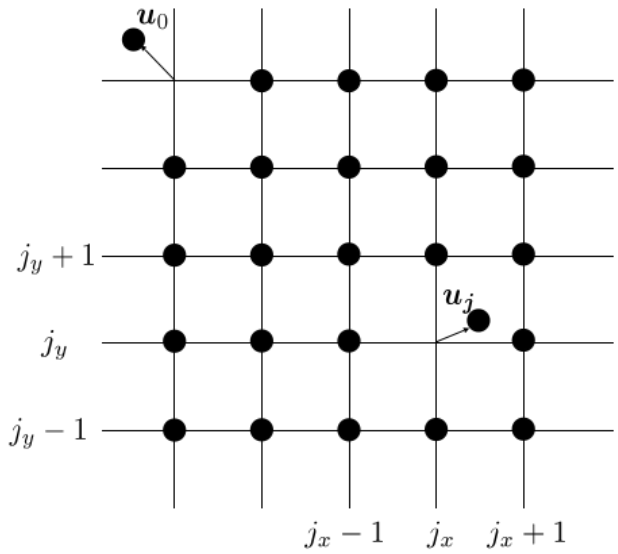

Figure I.4. *Two-dimensional lattice, with equilibrium positions $\boldsymbol{R_j}$, $\boldsymbol{j} = (j_x, j_y)$ and the deviation $\boldsymbol{u_j}$.*

$\boldsymbol{R_j}$:

$$\boldsymbol{r_j} = \boldsymbol{R_j} + \boldsymbol{u_j}. \tag{I.36}$$

Under the assumption $|\boldsymbol{u_j} - \boldsymbol{u_{j'}}| \ll a$ if $\boldsymbol{j}$ and $\boldsymbol{j'}$ are close neighbors, the interaction energy between atoms can be reduced to a quadratic Hamiltonian for the variables $\boldsymbol{u_j}$, and the eigenmodes (phonons) can then be determined exactly, in particular their dispersion relation $\omega_{\boldsymbol{q}}$.

Equipartition of energy applied to each mode leads to a result that has the same structure as in the one-dimensional case (I.22):

$$\langle (\boldsymbol{u_j} - \boldsymbol{u}_0)^2 \rangle \sim \frac{k_{\mathrm{B}}T}{m} \, \frac{8}{N^2} \sum_{\boldsymbol{q}} \frac{\sin^2(\boldsymbol{q}\cdot\boldsymbol{R_j}/2)}{\omega_{\boldsymbol{q}}^2}, \tag{I.37}$$

where a multiplicative factor of 2 has been introduced to account for the two directions of space.

The transition from a discrete sum to an integral on $\boldsymbol{q}$ is done by:

$$\text{(2D):} \qquad \sum_{\boldsymbol{q}} \longrightarrow \left(\frac{Na}{2\pi}\right)^2 \int_{\mathrm{BZ}} \mathrm{d}^2 q, \tag{I.38}$$

where the integral covers the entire Brillouin zone (BZ): $-\pi/a < q_x,\ q_y \leq \pi/a$. Replacing $\omega_{\boldsymbol{q}}$ by $c|\boldsymbol{q}|$, which is possible because – as in the 1D case – we will see that the dominant contribution comes from the small values of q ($q \ll 1/a$), we arrive at:[1]

$$\text{(2D):} \qquad \langle (\boldsymbol{u_j} - \boldsymbol{u}_0)^2 \rangle \sim \frac{k_{\mathrm{B}}T}{\kappa} \, \frac{2}{\pi^2} \int_{\mathrm{BZ}} \frac{\sin^2(\boldsymbol{q}\cdot\boldsymbol{R_j}/2)}{q^2} \, \mathrm{d}^2 q. \tag{I.39}$$

We define $mc^2 = \kappa a^2$ where κ is (as in 1D) an estimate of the spring constant associated with the restoring force acting on an atom towards its equilibrium position.

As in the one-dimensional case, we can approximate this integral by splitting it into two parts:

- For $q \gtrsim \pi/R_{\boldsymbol{j}}$, replacing the $\sin^2(\ldots)$ by its mean value $1/2$, we arrive at
$$\approx \frac{1}{\pi^2} \, \frac{k_{\mathrm{B}}T}{\kappa} \int_{\pi/R_{\boldsymbol{j}}}^{\pi/a} \frac{1}{q^2} \, 2\pi q \, \mathrm{d}q \approx \frac{2}{\pi} \frac{k_{\mathrm{B}}T}{\kappa} \log(R_{\boldsymbol{j}}/a). \tag{I.40}$$
- For $q \lesssim \pi/R_{\boldsymbol{j}}$, replacing the sine by its argument, we find
$$\sim \frac{1}{2\pi^2} \, \frac{k_{\mathrm{B}}T}{\kappa} \, R_{\boldsymbol{j}}^2 \int_0^{\pi/R_{\boldsymbol{j}}} \pi q \, \mathrm{d}q \sim \frac{\pi}{4} \, \frac{k_{\mathrm{B}}T}{\kappa}. \tag{I.41}$$

The main contribution therefore comes from the first term, which diverges logarithmically with distance $R_{\boldsymbol{j}}$:

$$\langle (\boldsymbol{u_j} - \boldsymbol{u}_0)^2 \rangle \sim \frac{2}{\pi} \, \frac{k_{\mathrm{B}}T}{\kappa} \log\left(\frac{R_{\boldsymbol{j}}}{a}\right). \tag{I.42}$$

As in the 1D case, this divergence comes from momenta q of the order of $1/R_{\boldsymbol{j}}$, i.e. long wavelengths of the order of the distance $R_{\boldsymbol{j}}$.

[1] Strictly speaking, we should take into account here the fact that the speed of sound is not the same for longitudinal and transverse vibrations. Since we are only interested in scaling laws here, we will omit this refinement.

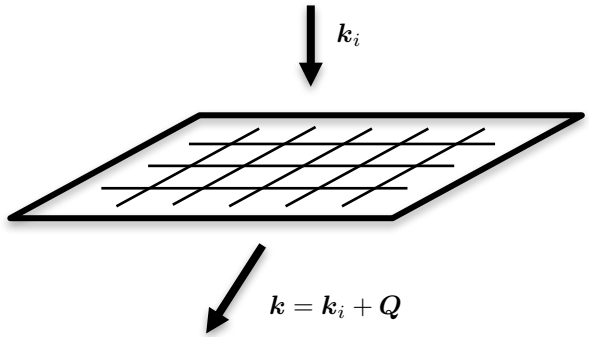

Figure I.5. *Bragg diffraction of an incident wave with wave vector k_i to a final wave vector k. We have chosen k_i orthogonal to the plane of the atoms. The intensity $I(k)$ reveals a possible crystalline order or quasi-order.*

2-2 A possible order parameter: the Bragg peaks

To test experimentally whether or not crystalline order is present in a sample, a standard method is to diffract a wave (photons, electrons, neutrons) with incident wave vector k_i onto the sample. For a crystal characterized by the basis vectors a_α, with $\alpha = 1, 2$ in 2D, we expect to observe Bragg peaks for wave vectors k such that

$$k = k_i + Q, \tag{I.43}$$

where Q is a vector of the reciprocal lattice defined by

$$Q \cdot a_\alpha = 0 \quad \text{modulo } 2\pi. \tag{I.44}$$

The variation of the diffracted intensity around Q then reveals the crystalline order (or absence of).

To simplify the analysis, let us assume that k_i is orthogonal to the plane of atoms (figure I.5). The intensity diffracted in direction k reads after averaging over the thermal fluctuations of the deviations u_j:

$$\begin{aligned} I(k) &\propto \langle \Big| \sum_j \mathrm{e}^{\mathrm{i}k\cdot(R_j+u_j)} \Big|^2 \rangle \\ &\propto \sum_{j,j'} \mathrm{e}^{\mathrm{i}k\cdot\left(R_j-R_{j'}\right)} \, \langle \mathrm{e}^{\mathrm{i}k\cdot\left(u_j-u_{j'}\right)} \rangle \end{aligned} \tag{I.45}$$

After decomposition on the phonon modes, the relative displacement $u_j - u_{j'}$ is written as a sum of independent variables. We can then use the classic result for a Gaussian variable $\langle \mathrm{e}^{\mathrm{i}\theta} \rangle = \mathrm{e}^{-\langle\theta^2\rangle/2}$, which gives:

$$\begin{aligned} \langle \exp\left[\mathrm{i}k\cdot(u_j - u_{j'})\right] \rangle &= \exp\left[-\frac{k^2}{4}\langle (u_j - u_{j'})^2 \rangle\right] \\ &\approx \exp\left[-\frac{k^2\, k_\mathrm{B}T}{2\pi\kappa} \ln\left(\frac{R_j}{a}\right)\right] \\ &\approx \left(\frac{a}{R_{jj'}}\right)^\eta \end{aligned} \tag{I.46}$$

where the exponent η is defined by :

$$\eta = \frac{k^2\, k_\mathrm{B}T}{2\pi\kappa}. \tag{I.47}$$

Recall that the stiffness κ entering here heuristically describes the bonding potential between atoms. A more rigorous treatment makes use of the *Lamé elastic constants* of the solid (Nelson & Halperin 1979).

In the absence of thermal fluctuations, $\eta = 0$, all the coefficients $\langle \mathrm{e}^{\mathrm{i}k\cdot\left(u_j-u_{j'}\right)} \rangle$ are equal to 1 and the diffracted intensity

$$I(k) \propto \sum_{j,j'} \mathrm{e}^{\mathrm{i}k\cdot\left(R_j-R_{j'}\right)} \tag{I.48}$$

consists of Dirac peaks (at the limit of an infinite lattice) located on the vectors Q of the reciprocal lattice.

In the presence of thermal fluctuations, the coefficients $\langle \mathrm{e}^{\mathrm{i}k\cdot\left(u_j-u_{j'}\right)} \rangle$ decrease algebraically with distance $R_{jj'}$ with exponent η. Bragg peaks are then broadened, as the intensity varies in the vicinity of a given vector Q

as

$$I(\boldsymbol{k}) \propto \sum_{j,j'} \mathrm{e}^{\mathrm{i}\boldsymbol{k}\cdot(\boldsymbol{R}_j-\boldsymbol{R}_{j'})} \left(\frac{a}{R_{jj'}}\right)^{\eta} \propto \int \mathrm{e}^{\mathrm{i}(\boldsymbol{k}-\boldsymbol{Q})\cdot\boldsymbol{R}} \left(\frac{a}{R}\right)^{\eta} \mathrm{d}^2R \tag{I.49}$$

leading to

$$I(\boldsymbol{k}) \propto |\boldsymbol{k}-\boldsymbol{Q}|^{\eta-2}. \tag{I.50}$$

Note that this result is significantly different from that for a completely disordered assembly of atoms. In the latter case, there would be no marked structure in a given direction $\boldsymbol{Q}$. Here, on the contrary, we continue to observe significant diffraction in specific directions in space, but the structure of the diffracted profile is less peaked than for perfect crystalline order. One thus speaks of a crystalline quasi-order (Nelson & Halperin 1979; Strandburg 1992).

2-3 The 3D crystal

To understand the specificity of the low-dimensional case, it is interesting to repeat the above treatment for a 3D crystal. The starting point is unchanged: after introducing the deviations $\boldsymbol{u_j}$ from the equilibrium positions $\boldsymbol{R_j}$ with here $\boldsymbol{j}=(j_x,j_y,j_z)$, we again reduce to a quadratic Hamiltonian for the $\boldsymbol{u_j}$'s. The eigenmode decomposition and the energy equipartition theorem lead to an estimate of the variance of the relative displacements of atom 0 and atom j:

$$\langle(\boldsymbol{u_j}-\boldsymbol{u}_0)^2\rangle \sim \frac{k_\mathrm{B}T}{m}\,\frac{12}{N^3}\sum_{\boldsymbol{q}}\frac{\sin^2(\boldsymbol{q}\cdot\boldsymbol{R_j}/2)}{\omega_{\boldsymbol{q}}^2}, \tag{I.51}$$

for a crystal of $N\times N\times N$ sites, with periodic boundary conditions.

Passing from a discrete sum to an integral then gives

$$\langle(\boldsymbol{u_j}-\boldsymbol{u}_0)^2\rangle \sim \frac{k_\mathrm{B}T}{m}\,\frac{12}{N^3}\left(\frac{Na}{2\pi}\right)^3\int_{\mathrm{BZ}}\frac{\sin^2(\boldsymbol{q}\cdot\boldsymbol{R_j}/2)}{\omega_{\boldsymbol{q}}^2}\,\mathrm{d}^3q \sim \frac{3}{2\pi^3}\,\frac{ak_\mathrm{B}T}{\kappa}\int_{\mathrm{BZ}}\frac{\sin^2(\boldsymbol{q}\cdot\boldsymbol{R_j}/2)}{q^2}\,\mathrm{d}^3q, \tag{I.52}$$

where, as before, we have replaced the frequency ω_q by its linearized expression[2] cq, and introduced a characteristic stiffness κ such that $mc^2=\kappa a^2$.

Let us apply the same treatment to this integral as in one and two dimensions, by splitting the integration domain into two parts:

- For $q \gtrsim \pi/R_{\boldsymbol{j}}$, substituting the $\sin^2$ function by its mean value $1/2$ gives
$$\sim \frac{3}{2\pi^3}\,\frac{ak_\mathrm{B}T}{\kappa}\int_{\pi/R_{\boldsymbol{j}}}^{\pi/a}\frac{1}{2q^2}\,4\pi q^2\mathrm{d}q \sim \frac{k_\mathrm{B}T}{\kappa}. \tag{I.53}$$
- For $q \lesssim \pi/R_{\boldsymbol{j}}$, substituting the $\sin$ function by its argument gives
$$\sim \frac{k_\mathrm{B}T}{\kappa}\,\frac{a}{R_{\boldsymbol{j}}}. \tag{I.54}$$

As in two dimensions, the contribution of the first term is dominant:

$$\langle(\boldsymbol{u_j}-\boldsymbol{u}_0)^2\rangle \sim \frac{k_\mathrm{B}T}{\kappa}, \tag{I.55}$$

but the form of this contribution is very different: it is now dominated by large values of q, typically $q\sim 1/a$, i.e. wavelengths of the order of the lattice period. An essential consequence is that this contribution is independent of the distance $R_{\boldsymbol{j}}$. This means that crystalline order can exist as long as this term is small compared to the square of the lattice period:

$$\frac{k_\mathrm{B}T}{\kappa} \ll a^2. \tag{I.56}$$

When this condition is verified, the position of atom $\boldsymbol{j}$ will be well defined relative to that of atom 0 on the scale of a single lattice period, whatever the distance $R_{\boldsymbol{j}}$ separating these two sites. More precisely, Lindeman's criterion indicates that crystalline order will be possible as long as (Nelson 2002)

$$\left[\langle(\boldsymbol{u_j}-\boldsymbol{u}_0)^2\rangle\right]^{1/2} \sim 0.15 \;-\; 0.30\;a. \tag{I.57}$$

[2] In fact, this linearization is not as well justified as in 1D or 2D, since large wave vector modes have a significant contribution at 3D, as we will see later. However, since we are only looking for scaling laws here, the approximation $\omega_q \approx cq$ is still sufficient.

2-4 The Mermin–Wagner–Hohenberg theorem

The conclusion that we have just reached on the existence or non-existence of crystalline order as a function of the number of spatial dimensions is only a special case of a very general result known as the Mermin–Wagner–Hohenberg theorem. We now state this theorem, which we will return to later in another case, that of the existence or non-existence of Bose-Einstein condensation.

This theorem was proved by Mermin & Wagner (1966) and independently by Hohenberg (1967)[3]. The Mermin-Wagner paper was concerned with ferromagnetism or antiferromagnetism in 1D or 2D systems, whereas Hohenberg used the Bose liquid or Cooper pairs in a superconducting system as examples. Their approaches were similar: starting from an inequality established by Bogoliubov (1962), they arrived at a result that can be formulated in the following general way:

For a system of dimension less than or equal to 2 and short-range interactions, there can be no spontaneous breaking of a continuous symmetry at non-zero temperature.

We will not be proving this theorem in the general case [see, for example, Herbut (2007) or Mudry (2014)], but we will emphasize a few important points:

- Interactions must be short-ranged. If the range is infinite, mean-field theory can be safely applied and the standard phase transitions predicted by this theory can occur, whatever the dimension of space.

- We are interested in the breaking of a continuous symmetry: this is the case, for example, of the translational symmetry considered in this chapter. It can also be the $U(1)$ symmetry associated with the choice of phase of a macroscopic wave function, the breaking of which corresponds to Bose-Einstein condensation. On the other hand, the theorem does not apply as such to discrete symmetries. For example, for the Ising model where spins $\sigma_z = \pm 1$ are placed on a lattice with nearest-neighbor interactions, a phase transition occurs for a critical temperature $T_c > 0$ in the 2D case (Onsager 1944).

- We discuss here transitions occurring at $T \neq 0$. At zero temperature, the interacting 2D quantum Bose gas is condensed [Schick (1971) and Popov (1972) and more recently Pilati, Boronat, et al. (2005) and Mora & Castin (2009)]. We will come back to this problem in Chapter 6.

[3] These two papers were submitted within a week of each other. The Mermin-Wagner article appeared in 1966, while Hohenberg's appeared in 1967; however, Mermin and Wagner were aware of Hohenberg's work, since they explicitly cite him as *unpublished*.

3 2D crystals in the laboratory

In their 1973 paper, Kosterlitz and Thouless suggested applying their theoretical model of a defect-induced phase transition to the case of two-dimensional crystals. However, the situation is more complex than that encountered later in this course for superfluids, as two successive transitions occur from the perfect triangular crystal expected at zero temperature to the liquid state at high temperatures. The quantitative theory of two-dimensional melting was made by Halperin & Nelson (1978a), Halperin & Nelson (1978b), Nelson & Halperin (1979), and Young (1979) [referred to as the KTHNY theory] and the main results are detailed in the review article by Strandburg (1988).

3-1 Scenario for the fusion of a 2D crystal

Let us summarize some salient points of the KTHNY model that are experimentally observed in colloidal systems [see for example Deutschländer, Dillmann, et al. (2015) and refs. in]. These points have also been validated by recent simulations carried out on a gas of 10^5 particles interacting via a Lennard–Jones potential (Wierschem & Manousakis 2011).

- At zero temperature, we have a perfect triangular crystal (at least if we neglect quantum fluctuations) corresponding to the densest arrangement. In this crystal, each particle has exactly 6 equally spaced neighbors.

- At very low temperatures, the crystal lattice is almost triangular, with phonons destroying long-range order as we saw above. We therefore

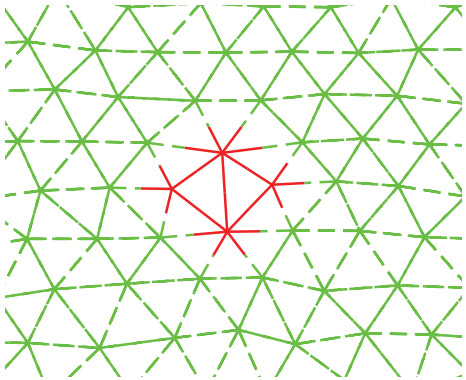

Figure I.6. *A local defect in a particle assembly exhibiting long-range translational quasi-order. This defect can be seen as a pair of dislocations, with two A_5 sites (with five neighbors) and two A_7 sites (with seven neighbors). Figure taken from Wierschem & Manousakis (2011).*

have a translational quasi-order, with a logarithmic growth of the root-mean-square deviation $\langle(\boldsymbol{u}_i - \boldsymbol{u}_j)^2\rangle$ with distance $R_{\boldsymbol{ij}}$, which induces an algebraic decrease in the order parameter (Bragg peaks), as we already discussed. We also have true orientational order, meaning that the correlation function of the local crystal orientation $\theta(\boldsymbol{r})$ does not tend towards 0 at infinity. There may be local defects, such as the one shown in figure I.6, but this does not change the general conclusion reached by our study of phonon modes.

- Above a certain temperature T_m, defects called *dislocations* have a significant probability of appearing. An example of a dislocation is shown in figure I.7. This type of defect is created by an $A_5 - A_7$ pair, i.e. a 5-neighbor site contiguous with a 7-neighbor site. The presence of a dislocation is equivalent to adding half a line of atoms (figure I.7, right).

  This intermediate phase is known as the hexatic phase. In this phase, the presence of dislocations destroys the translational quasi-order and transforms the decay of the order parameter into an exponential law.

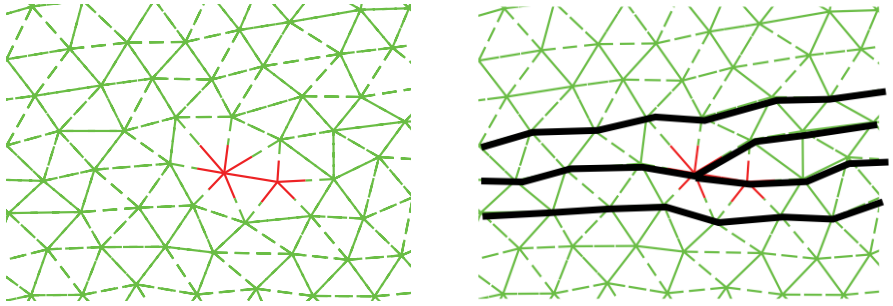

Figure I.7. *Isolated dislocation composed of an A_5 site and an A_7 site, equivalent to inserting an extra half-line of atoms. Figure taken from Wierschem & Manousakis (2011).*

Indeed, the addition of a half-line between the two sites $\boldsymbol{R}_i$ and $\boldsymbol{R}_j$ changes the distance $R_{\boldsymbol{ij}}$ by an amount that is of the order of the lattice period. We therefore expect complete decorrelation of the deviations $\boldsymbol{u_j}$ and $\boldsymbol{u_j}$ as soon as $R_{\boldsymbol{ij}}$ is of the order of the average distance between dislocations.

However, the right-hand image in figure I.6 shows that a dislocation does not completely destroy orientational order. Despite the addition of the half-line of atoms, the lattice axes remain approximately the same (in fact, the local orientation correlation function $\theta(\boldsymbol{r})$ decreases algebraically in this regime).

- Above a second critical temperature T_i, the two members A_5 and A_7 of the dislocations can move arbitrarily far apart. An isolated A_5 or A_7, a defect called *disclination*, changes the orientation of the crystal, as shown in figure I.8. In this case, orientational order is also lost, with the correlation function for the orientation $\theta(\boldsymbol{r})$ decreasing exponentially with distance.

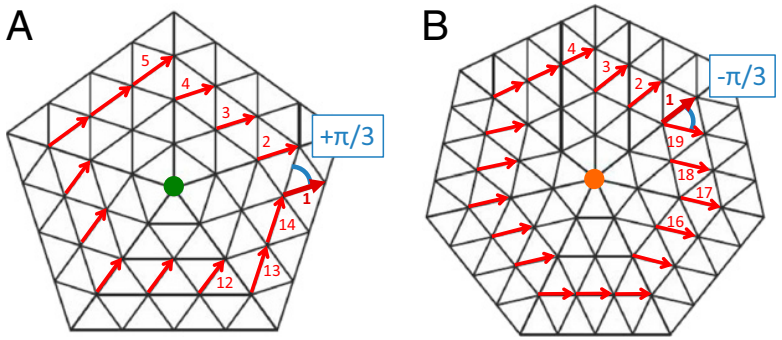

Figure I.8. *Disclinations corresponding to an A_5 or A_7 defect. The proliferation of this type of defects leads to a loss of orientational order. Figure taken from Deutschländer, Dillmann, et al. (2015).*

3-2 Studies on colloidal systems

The experimental demonstration of the KTHNY scenario has been the subject of a great deal of work since it was first proposed. Here we focus on recent results obtained by the Konstanz group, led by Peter Keim and Georg Maret, on colloidal monolayers. These experiments are carried out on polystyrene beads with a diameter of 4.5 microns immersed in water retained by capillarity in a glass cell (figure I.9), with a water-air interface for the lower surface (Deutschländer, Puertas, et al. 2014; Deutschländer, Dillmann, et al. 2015).

The density of the beads is 1.7, so they accumulate at the bottom of the water, at the water-air interface. They form a monolayer of about 10^5 particles, from which one selects those located within a window of 1 mm$\times$ 1 mm (figure I.10). There are around 4,000 beads in this window, and the position of each one is tracked using a sub-micrometer resolution imaging system.

These beads are doped with iron oxide nanoparticles, making them paramagnetic. By applying a magnetic field perpendicular to the plane of the cell, a magnetic dipole is induced in each bead. As these vertical dipoles are orthogonal to the segments joining two beads, the dipole-

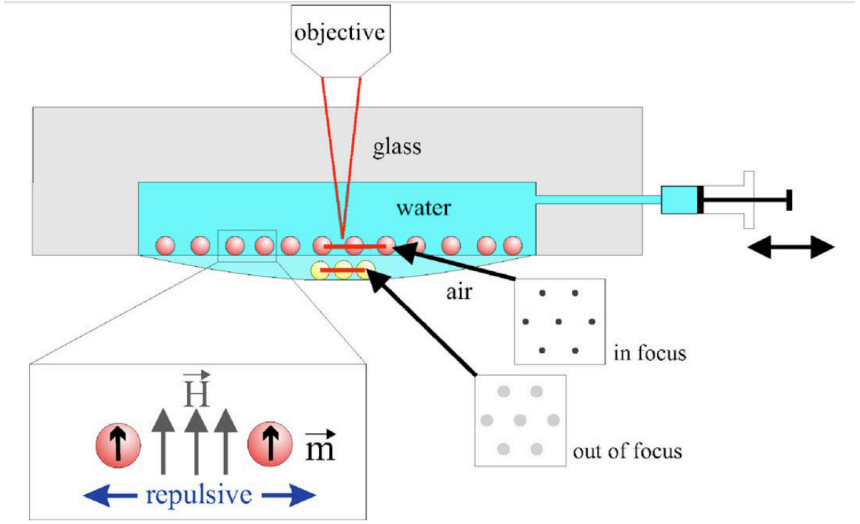

Figure I.9. *Experimental setup used in the Constance experiments. A droplet of water (diameter 8 mm) is suspended by capillary action. Polystyrene beads doped with iron oxide nanoparticles accumulate on the bottom plane, at the water-air interface. A vertical magnetic field induces a magnetic moment in the beads, creating a repulsive interaction between them. Figure taken from Keim, Maret, et al. (2007).*

dipole interaction is repulsive and isotropic in plane. It therefore tends to form a triangular crystalline order. For the experimental parameters of the Constance experiment, the average distance between beads is 13 μm. The experiment is carried out at room temperature, with sample horizontality controlled at the microradian level. Thermalization times can be up to a month, during which bead trajectories are tracked every second.

A typical image is shown in figure I.10 where the defects appearing in the spatial distribution of the beads are colored. The control parameter of the experiment is the ratio

$$\Gamma = \frac{E_{\mathrm{mag}}}{k_{\mathrm{B}}T}, \tag{I.58}$$

between the magnetic energy of two neighboring dipoles and the charac-

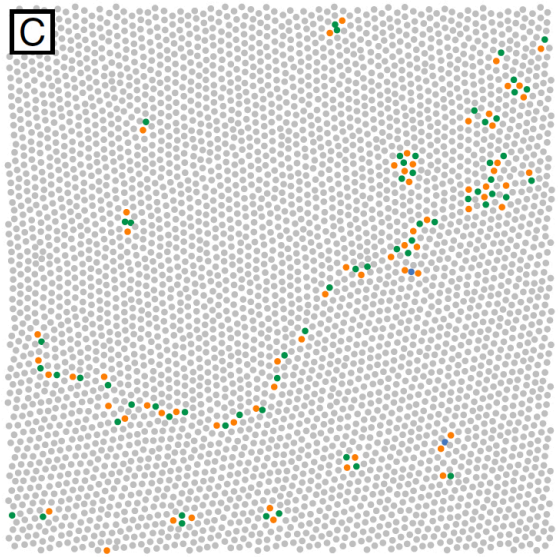

Figure I.10. *Identification of defects in an assembly of around 4000 paramagnetic beads. This figure was obtained for the ratio $\Gamma = 98$, after a quench of slope $\dot{\Gamma} = 1/(19\,\text{days})$. Figure taken from Deutschländer, Dillmann, et al. (2015).*

teristic thermal energy $k_\mathrm{B}T$. The two transitions shown above are obtained for (Deutschländer, Puertas, et al. 2014):

- $\Gamma_m = 70.3$ for the crystal/hexatic transition,
- $\Gamma_i = 67.3$ for the hexatic/isotope transition,

in good agreement with the values obtained by numerical simulation.

In fact, these remarkably rich experiments make it possible not only to validate predictions concerning the equilibrium state of two-dimensional materials, but also to study the temporal evolution of the system when the two phase transitions are crossed at finite speed $\dot{\Gamma}$. This is the Kibble–Zurek problem, which aims to characterize the number of defects generated as a function of the quench rate (Deutschländer, Dillmann, et al. 2015). Another recent study on these systems involved measuring density fluctuations on a large spatial scale (Illing, Fritschi, et al. 2017).

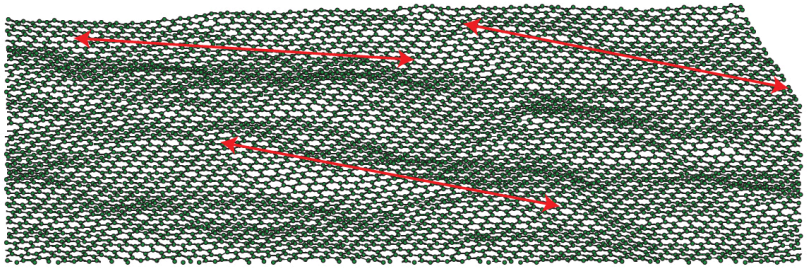

Figure I.11. *Numerical simulation of a graphene surface at 300 K, with $N = 8640$ atoms, showing that the surface is rippled under the effect of thermal fluctuations. Arrows have a length of 8 nm. Figure taken from Fasolino, Los, et al. (2007).*

3-3 What about graphene?

The most famous example of a two-dimensional crystalline order is graphene (Castro Neto, Guinea, et al. 2009). This raises the question of whether the existence of these sheets of carbon atoms is compatible with the Mermin-Wagner-Hohenberg theorem. In the literature, we find two classes of answers, both of which are compatible:

- Given the stiffness of the bonds in graphene, one finds a gigantic value for the characteristic distance over which the loss of crystalline order should manifest itself (Thompson-Flagg, Moura, et al. 2009). Finite-size effects alone are therefore sufficient to explain the apparent order in laboratory samples.
- The surface of graphene is not flat: it is rippled (figure I.11) and deviations from the plane can play, at least in principle, an important role (Fasolino, Los, et al. 2007; Schoelz, Xu, et al. 2015). The non-linear coupling between fluctuations of the height and displacements parallel to the surface changes the nature of the interactions by giving them a long-range effective component, which may invalidate the Mermin–Wagner–Hohenberg theorem.

Chapter II

The 2D quantum gas: From the ideal case to binary interactions

We now turn to the study of two-dimensional quantum fluids. Most of the chapter will be devoted to the ideal gas governed by Bose-Einstein statistics. We will look successively at the uniform case, for which there is no condensation at the thermodynamic limit, and the case of a trapped gas, for which condensation can occur. We will describe experiments carried out on a photon gas stored in a cavity and illustrating this prediction. In the final section, we will explain how to take particle interactions into account by looking at a binary collision between two identical atoms.

Let us start by recalling a few elements for dealing with the thermodynamic equilibrium of an ideal gas of Bose particles. Let us assume that we know the eigenstates $\psi_\alpha(\boldsymbol{r})$ of the one-particle Hamiltonian and the associated energies E_α, the index α being a discrete or continuous variable allowing us to identify each state unambiguously. The average population of a state ψ_α is then given by

$$N_\alpha = \frac{1}{\mathrm{e}^{(E_\alpha-\mu)/k_\mathrm{B}T}-1}, \tag{II.1}$$

where we have introduced two intensive thermodynamic variables, the temperature T and the chemical potential μ. For cold atom experiments, we can usually measure the temperature T and the total number of atoms N with good accuracy, from which we deduce the chemical potential by inverting the relation $N = \sum_\alpha N_\alpha$.

1 The 2D uniform Bose gas

In this paragraph, we consider a gas of particles confined in a square (two-dimensional) box of size $L \times L$. To simplify calculations, we will use the expression for eigenstates obtained by assuming periodic boundary conditions. These states are then plane waves identified by their momentum $\boldsymbol{p}$:

$$\psi_{\boldsymbol{p}}(\boldsymbol{r}) = \frac{1}{L}\mathrm{e}^{\mathrm{i}\boldsymbol{p}\cdot\boldsymbol{r}/\hbar}, \qquad \boldsymbol{p} = \frac{2\pi\hbar}{L}\boldsymbol{n}, \quad \boldsymbol{n} = (n_x, n_y) \in \mathbb{Z}^2. \tag{II.2}$$

We are going to look at the thermodynamic limit of this gas, by letting the size L of the box and the number N of particles tend to infinity, while keeping the spatial density constant:

$$L \to \infty,\ N \to \infty,\ \rho^{(2)} = \frac{N}{L^2}\text{: constant} \tag{II.3}$$

An important concept in the calculation of physical quantities is the density of states $D(E)$. Consider a physical quantity $F(\boldsymbol{p})$ varying relatively smoothly with $\boldsymbol{p}$, the population $N(\boldsymbol{p})$ of level $\boldsymbol{p}$ for example, and let us look at the sum $\sum_{\boldsymbol{p}} F(\boldsymbol{p})$. When passing to the thermodynamic limit, we can replace discrete sums on quantized momenta by an integral:

$$F(\boldsymbol{p}) \text{ regular}: \quad \sum_{\boldsymbol{p}} F(\boldsymbol{p}) \ \longrightarrow\ \left(\frac{L}{2\pi\hbar}\right)^2 \int F(\boldsymbol{p})\ \mathrm{d}^2p. \tag{II.4}$$

If the quantity $F(\boldsymbol{p})$ to be summed is a function of the energy $E(\boldsymbol{p}) = p^2/2m$ only, the integral over the angular distribution of the momentum $\boldsymbol{p}$ can be carried out analytically and we find

$$\sum_{\boldsymbol{p}} F(\boldsymbol{p}) \longrightarrow \int_0^{+\infty} F(E)\, D^{(2)}(E)\, \mathrm{d}E \qquad \text{with} \quad D^{(2)}(E) = \frac{mL^2}{2\pi\hbar^2}. \quad \text{(II.5)}$$

The variation of the density of states at low energies will play a crucial role in what follows: while this density in the 3D case tends to 0 as[1] $\sqrt{E}$ when $E \to 0$, it remains constant in 2D. This confirms what we had already seen in the first lecture, when we found that long-wavelength phonons were responsible for the destruction of crystal order in 2D.

1-1 The (non-)saturation of excited states

Reminder on the three-dimensional case. The Bose-Einstein condensation of the ideal 3D gas is covered in many statistical physics books, and we described it in detail in the 2015-16 lecture series. Recall that it is based on three properties of the distribution (II.1):

- At a fixed temperature T, each population N_α is an increasing function of the chemical potential μ.
- In order for N_α to be defined for any state α, including the ground state which we will note here $\alpha = 0$, we must restrict to $\mu < E_0$.
- This inequality on μ implies that for a given temperature T, there is an upper bound on the number of atoms $N_{\rm exc}(T,\mu)$ that can occupy the set of excited states:

$$N_{\rm exc}(T,\mu) < N_{\rm exc}^{\rm max}(T) \quad \text{(II.6)}$$

with

$$N_{\rm exc}(T,\mu) = \sum_{\alpha\neq 0} \frac{1}{\mathrm{e}^{(E_\alpha-\mu)/k_{\rm B}T}-1}, \qquad N_{\rm exc}^{\rm max}(T) = \sum_{\alpha\neq 0} \frac{1}{\mathrm{e}^{(E_\alpha-E_0)/k_{\rm B}T}-1}. \quad \text{(II.7)}$$

[1]The exact value is $D^{(3)}(E) = \frac{1}{4\pi^2}\left(\frac{2mL^2}{\hbar^2}\right)^{3/2}\sqrt{E}$.

For a 3D gas in the thermodynamic limit, consider the spatial density associated with these excited states

$$\rho_{\rm exc}^{(3)}(T,\mu) = \frac{N_{\rm exc}(T,\mu)}{L^3} \quad \text{(II.8)}$$

which can be calculated analytically by replacing the discrete sum by an integral:

$$\rho_{\rm exc}^{(3)}(T,\mu) = \frac{1}{L^3}\int_0^{+\infty} \frac{D^{(3)}(E)}{\frac{1}{Z}\mathrm{e}^{E/k_{\rm B}T}-1}\,\mathrm{d}E = \frac{1}{\lambda_T^3}\mathrm{Li}_{3/2}(Z) \quad \text{(II.9)}$$

where the thermal wavelength and the gas fugacity are defined by

$$\lambda_T = \frac{\hbar\sqrt{2\pi}}{\sqrt{mk_{\rm B}T}} \qquad Z = \mathrm{e}^{\mu/k_{\rm B}T} \quad \text{(II.10)}$$

and where the polylogarithm function is

$$\mathrm{Li}_\alpha(x) = \sum_{n=1}^{+\infty} \frac{x^n}{n^\alpha}. \quad \text{(II.11)}$$

For $\alpha > 1$, this function is defined at any point of the interval $x \in [0,1]$ and we find in particular[2] $\mathrm{Li}_{3/2}(1) = 2.612\ldots$

The limit $Z \to 1$ corresponds to $\mu \to E_0 = 0$ for this gas of non-interacting particles. The fact that $\mathrm{Li}_{3/2}(Z)$ remains finite when $Z \to 1$ means that the spatial density that can be placed in excited states is bounded by $2.612/\lambda_T^3$. The phase-space density associated with excited states, defined as

$$\mathcal{D}_{\rm exc} = \rho_{\rm exc}^{(3)}\lambda_T^3, \quad \text{(II.12)}$$

is therefore also upper bounded:

$$\mathcal{D}_{\rm exc} < \mathcal{D}_{\rm exc}^{\rm max} = 2.612. \quad \text{(II.13)}$$

Bose-Einstein condensation arises from this inequality: it occurs when the phase-space density $\mathcal{D}$ exceeds the critical value $\mathcal{D}_{\rm exc}^{\rm max}$. The surplus

[2]The constant $\mathrm{Li}_{3/2}(1)$ is also equal to the value of the Riemann function $\zeta(x)$ in $x = 3/2$: $\zeta(x) = \sum_{n=1}^{+\infty} n^{-x}$.

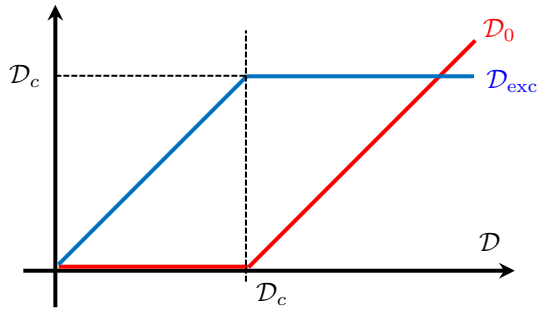

Figure II.1. *3D case: phase-space densities associated respectively with the ground state ($\mathcal{D}_0$) and the set of excited states $\mathcal{D}_{\rm exc}$, as a function of the total phase-space density $\mathcal{D}$. We have defined $\mathcal{D}_c \equiv \mathcal{D}_{\rm exc}^{\rm max} = 2.612$.*

of particles must accumulate in the single-particle ground state $\boldsymbol{p} = 0$. In other words, two cases are possible (figure II.1):

$$\mathcal{D} \leq 2.612 : \quad \mathcal{D} \approx \mathcal{D}_{\rm exc} = {\rm Li}_{3/2}(Z), \quad \mathcal{D}_0 \ll \mathcal{D}, \tag{II.14}$$

$$\mathcal{D} > 2.612 : \quad \mathcal{D} = \mathcal{D}_0 + \mathcal{D}_{\rm exc}^{\rm max} \quad \text{with } \mathcal{D}_{\rm exc}^{\rm max} = 2.612. \tag{II.15}$$

The pair of equations (II.14-II.15) constitutes the equation of state of the ideal 3D Bose gas.

The two-dimensional case. For a 2D gas, the calculation of the spatial density associated with excited states can be repeated in virtually the same way as in the 3D case, the only difference being in the expression of the density of states, which loses a factor $\sqrt{E}$. The proportion of states in the vicinity of $E = 0$ increases as we move from 3D to 2D; as we shall see, this causes the $E = 0$ state to lose its singular character and prevents condensation.

Again, replacing the discrete sum (II.7) by an integral, we find:

$$\rho_{\rm exc}^{(2)} = \frac{1}{L^2} \int_0^{+\infty} \frac{D^{(2)}(E)}{\frac{1}{Z}{\rm e}^{E/k_{\rm B}T} - 1} \, {\rm d}E = \frac{1}{\lambda_T^2} {\rm Li}_1(Z). \tag{II.16}$$

Note that the function ${\rm Li}_1(Z)$, which is calculated from the general expression (II.11), can be expressed in analytical form ${\rm Li}_1(Z) = -\ln(1-Z)$, which gives the phase-space density

$$\mathcal{D}_{\rm exc} = -\ln(1-Z). \tag{II.17}$$

This brings us to the crucial point that, unlike ${\rm Li}_{3/2}(Z)$, the function ${\rm Li}_1(Z)$ has no finite limit when $Z \to 1$. This means that even for an arbitrarily large phase-space density $\mathcal{D}$, we can always find (at a given temperature) a chemical potential μ such that $\mathcal{D} = \mathcal{D}_{\rm exc}(T, \mu)$. This does not mean that the population of the ground level is zero, but simply that it does not take on a "macroscopic" value at the thermodynamic limit. No singularity appears when the density is increased at constant temperature, and Bose-Einstein condensation does not occur.

It is important to identify the essential ingredient that causes this difference between the 3D and 2D cases. The question is whether the d-dimensional integral:

$$\rho_{\rm exc}^{(d)}(T) = \frac{1}{L^d} \int_0^{+\infty} \frac{D^{(d)}(E)}{\frac{1}{Z}{\rm e}^{E/k_{\rm B}T} - 1} \, {\rm d}E \tag{II.18}$$

has a finite limit in the highly degenerate case $Z \to 1$. As there is no problem of convergence of the integral when $E \to +\infty$, the difficulty is concentrated in $E \to 0$. We can then do an expansion of the integrand in the neighborhood of $E = 0$ in the limiting case $Z = 1$:

$$Z = 1, \ E \to 0 : \qquad \frac{D^{(d)}(E)}{\frac{1}{Z}{\rm e}^{E/k_{\rm B}T} - 1} \sim k_{\rm B}T \, \frac{D^{(d)}(E)}{E}. \tag{II.19}$$

For a power-law density of state in the vicinity of $E = 0$:

$$D^{(d)}(E) \propto E^{\nu} \tag{II.20}$$

then the integral will be convergent at $E = 0$ if

$$\nu > 0 \tag{II.21}$$

and this even if $Z = 1$, which is the maximum value allowed. This is the situation reached in 3D: the density in the excited states saturates and condensation occurs. In contrast, the 2D case corresponds to $\nu = 0$ and the integral is divergent for $Z = 1$. Whatever the chosen spatial density, we can always find a value of Z close enough to 1 to match this density.

The equation of state of the 2D gas. The result

$$\mathcal{D}(T,\mu) = -\ln(1-Z) \qquad Z \equiv \mathrm{e}^{\mu/k_\mathrm{B}T} \tag{II.22}$$

is the equation of state for the ideal 2D Bose gas. Two interesting limiting cases are:

- The non-degenerate case is obtained by taking the $Z \ll 1$ limit:

$$Z \ll 1 : \qquad \mathcal{D}(T,\mu) \approx Z = \mathrm{e}^{\mu/k_\mathrm{B}T} \ll 1, \tag{II.23}$$

  which corresponds to the well-known result for a Boltzmann gas.

- The case $Z \to 1$, obtained for $|\mu| \ll k_\mathrm{B}T$, corresponds on the contrary to a strongly degenerate gas:

$$Z \approx 1 : \quad 1 - Z \approx \frac{|\mu|}{k_\mathrm{B}T} \quad \to \quad \mathcal{D}(T,\mu) \approx \ln\left(\frac{k_\mathrm{B}T}{|\mu|}\right) \gg 1 \tag{II.24}$$

1-2 Momentum distribution

For an ideal gas, this distribution is written:

$$N(\boldsymbol{p}) = \frac{1}{\frac{1}{Z}\mathrm{e}^{p^2/(2mk_\mathrm{B}T)} - 1}. \tag{II.25}$$

To gain some intuition about the shape of this distribution (*cf.* figure II.2), we consider the two limiting cases of a non-degenerate gas ($Z \ll 1$) and of a strongly degenerate gas ($Z \approx 1$).

Non-degenerate case. In the $Z \ll 1$ case, we can make the approximation

$$Z \ll 1 : \qquad N(\boldsymbol{p}) \approx Z\ \mathrm{e}^{-p^2/(2mk_\mathrm{B}T)} \tag{II.26}$$

which yields the Maxwell-Boltzmann Gaussian distribution.

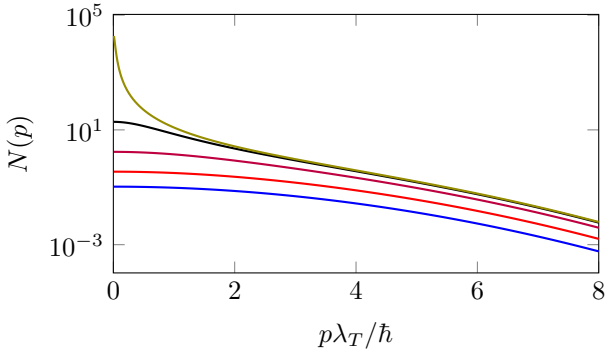

Figure II.2. *Momentum distributions for* $\mathcal{D} = 0.1,\ 0.3,\ 1,\ 3,\ 10$.

Highly degenerate case. To describe the $Z \approx 1$ case, corresponding to $|\mu| \ll k_\mathrm{B}T$, we separate the momenta into two classes:

- The momenta p such that $\frac{p^2}{2m} < k_\mathrm{B}T$, i.e. $p\lambda_T/\hbar < \sqrt{4\pi}$, for which we can linearize the exponential in the denominator of (II.25):

$$Z \approx 1, \quad \frac{p^2}{2m} < k_\mathrm{B}T : \qquad N(\boldsymbol{p}) \approx \frac{k_\mathrm{B}T}{\frac{p^2}{2m} + |\mu|} = \frac{4\pi\hbar^2}{\lambda_T^2}\frac{1}{p^2 + p_c^2} \tag{II.27}$$

  with

$$p_c = \sqrt{2m|\mu|} \ll \sqrt{2mk_\mathrm{B}T} \tag{II.28}$$

  (remember that μ is always negative).

- The momenta p such that $\frac{p^2}{2m} > k_\mathrm{B}T$ for which we can neglect the -1 "Bose" term in the denominator of (II.25) to recover a Gaussian distribution *à la Boltzmann*:

$$Z \approx 1, \quad \frac{p^2}{2m} > k_\mathrm{B}T : \qquad N(\boldsymbol{p}) \approx \mathrm{e}^{-p^2/(2mk_\mathrm{B}T)}. \tag{II.29}$$

The momentum distribution is therefore made up of two distinct parts: a central Lorentzian part of width p_c and Gaussian wings of width $\sqrt{mk_\mathrm{B}T}$. To go a step further, it is interesting to evaluate the respective weights of

these two distributions. For the central Lorentzian part, we find

$$\mathcal{D}_{\text{Lor.}} \approx \int_0^{\sqrt{2mk_{\text{B}}T}} \frac{2p}{p^2+p_c^2}\,\mathrm{d}p \approx \ln\left(\frac{k_{\text{B}}T}{|\mu|}\right) \tag{II.30}$$

i.e., using (II.24)

$$\mathcal{D}_{\text{Lor.}} \approx \mathcal{D}. \tag{II.31}$$

For the Gaussian wings, we have

$$\mathcal{D}_{\text{Gau.}} \approx \frac{\lambda_T^2}{2\pi\hbar^2}\int_{\sqrt{2mk_{\text{B}}T}}^{+\infty} \mathrm{e}^{-p^2/(2mk_{\text{B}}T)}\; p\,\mathrm{d}p \approx 1/e \;\ll\; \mathcal{D}. \tag{II.32}$$

The contribution $\mathcal{D}_{\text{Gau.}}$ is small compared to $\mathcal{D}$ since we have assumed a strongly degenerate gas. We can therefore consider that most atoms are located in the Lorentzian distribution of width $p_c \ll \sqrt{mk_{\text{B}}T}$. However, as a Lorentzian distribution is non-normalizable in 2D (unlike the 1D case), we need to put a cutoff on the integrals at the thermal momentum $\sqrt{2mk_{\text{B}}T}$.

1-3 One-body correlation function

Beyond the possible appearance of a macroscopic fraction of atoms in the ground state, another manifestation of Bose-Einstein condensation appears on the correlation function:

$$G_1(\boldsymbol{r},\boldsymbol{r}') = \langle \boldsymbol{r}|\hat{\rho}_1|\boldsymbol{r}'\rangle \tag{II.33}$$

where $\hat{\rho}_1$ is the one-body density operator. Recall that the translational invariance of the system ensures that the value of G_1 actually depends only on $\boldsymbol{r}-\boldsymbol{r}'$.

To evaluate G_1, let us start with the matrix element of $\hat{\rho}_1$ between two momentum states $\boldsymbol{p}$ and $\boldsymbol{p}'$. We introduce a double closure relation

$$\langle \boldsymbol{p}|\hat{\rho}_1|\boldsymbol{p}'\rangle = \iint \langle \boldsymbol{p}|\boldsymbol{r}\rangle\; G_1(\boldsymbol{r},\boldsymbol{r}')\; \langle \boldsymbol{r}'|\boldsymbol{p}'\rangle\; \mathrm{d}^2r\; \mathrm{d}^2r'. \tag{II.34}$$

with $\langle \boldsymbol{r}|\boldsymbol{p}\rangle = \mathrm{e}^{\mathrm{i}\boldsymbol{r}\cdot\boldsymbol{p}/\hbar}/L$. Using translation invariance, this result can be written

$$\langle \boldsymbol{p}|\hat{\rho}_1|\boldsymbol{p}'\rangle = \delta_{\boldsymbol{p},\boldsymbol{p}'}\int \mathrm{e}^{-\mathrm{i}\boldsymbol{r}\cdot\boldsymbol{p}/\hbar}\; G_1(\boldsymbol{r})\;\mathrm{d}^2r \tag{II.35}$$

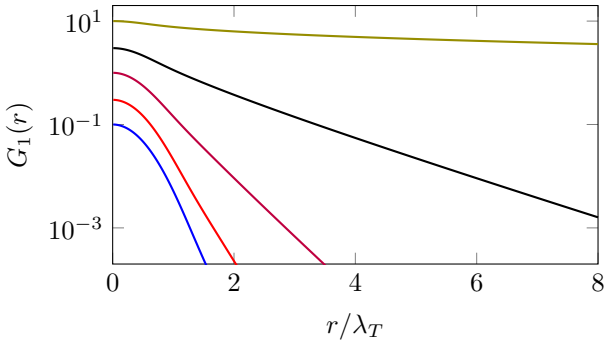

Figure II.3. *Correlation function $G_1(r)$ for an ideal two-dimensional Bose gas. Curves made for $\mathcal{D} = 0.1,\ 0.3,\ 1,\ 3,\ 10$.*

where, for simplicity, we have noted $G_1(\boldsymbol{r}) = G_1(\boldsymbol{r},0)$. The momentum distribution $N(\boldsymbol{p}) = \langle \boldsymbol{p}|\hat{\rho}_1|\boldsymbol{p}\rangle$ and the correlation function $G_1(\boldsymbol{r})$ are thus Fourier transforms of each other. Note that the proof of this result does not depend on whether the gas is ideal, nor on the dimension of the space.

The correlation function G_1 is obtained by taking the inverse Fourier transform

$$\begin{aligned} G_1(\boldsymbol{r}) &= \frac{1}{(2\pi\hbar)^2}\int \mathrm{e}^{\mathrm{i}\boldsymbol{r}\cdot\boldsymbol{p}/\hbar}\; N(\boldsymbol{p})\;\mathrm{d}^2p \\ &= \frac{1}{\lambda_T^2}\sum_{n=1}^{+\infty}\frac{Z^n}{n}\,\mathrm{e}^{-\pi r^2/(n\lambda_T^2)}. \end{aligned} \tag{II.36}$$

To analyze this result, let us concentrate on the two limiting cases already identified, that of the non-degenerate gas and that of the strongly degenerate gas.

In the non-degenerate case, the Gaussian character of the distribution $N(\boldsymbol{p})$ given in (II.26) leads to a correlation function G_1 that is also Gaussian:

$$Z \ll 1: \qquad G_1(\boldsymbol{r}) \approx \rho^{(2)}\;\mathrm{e}^{-\pi r^2/\lambda_T^2}. \tag{II.37}$$

The thermal wavelength λ_T therefore gives the extension of spatial coherence in this case.

In the highly degenerate case, we have seen that most of the distribution is concentrated in the central Lorentzian of width p_c. The 2D Fourier transform of this Lorentzian is defined at any point $\boldsymbol{r} \neq 0$ and is proportional to the Bessel function of imaginary argument $K_0(p_c r/\hbar)$. The asymptotic behavior of this function is

$$x \to \infty : \qquad K_0(x) \approx \sqrt{\frac{\pi}{2x}}\, \mathrm{e}^{-x} \tag{II.38}$$

and is dominated by exponential decay. We then have

$$G_1(r) \propto \frac{1}{\sqrt{r}} \mathrm{e}^{-r/\ell} \qquad \text{with} \quad \ell = \frac{\hbar}{p_c}. \tag{II.39}$$

Using the definition (II.28) of p_c and the link (II.24) between the phase-space density and the ratio $k_\mathrm{B}T/|\mu|$, we get the characteristic decay length of the G_1 function in the strongly degenerate case:

$$\ell \approx \frac{\lambda_T}{\sqrt{4\pi}}\, \mathrm{e}^{\mathcal{D}/2}. \tag{II.40}$$

Here we see the marginal character of the uniform 2D Bose gas. Although there is no long-range order strictly speaking, since the G_1 function tends exponentially to 0, the characteristic length of this exponential diverges exponentially fast with the phase-space density of the system. This underlines the important role for finite-size effects, which we examine in the next paragraph.

1-4 Finite size effects

In cold-atom experiments, phase-space densities in excess of 30 are commonly achieved. For these values of $\mathcal{D}$, we find $\ell \sim \lambda_T \times 10^6$. For a typical value of thermal wavelength $\lambda_T = 1\,\mu$m, the decay length ℓ of G_1 is of the order of a meter, and therefore undetectable on a realistic sample size. Under these conditions, the phase is essentially constant across the sample, as if we had a genuine Bose-Einstein condensate.

We can give ourselves two equivalent criteria for setting the threshold for the appearance of finite-size effects:

- The first is to compare the difference $E_0 - \mu$ with the gap $E_1 - E_0$ between the first excited state and the ground state. When $E_0 - \mu$ becomes smaller than $E_1 - E_0$, then the discretization of energy levels due to finite-size effects begins to play a significant role. Apart from a numerical factor of no importance here, $E_1 - E_0 \sim \hbar^2/mL^2$ so this first criterion is written:

$$|\mu| \lesssim \frac{\hbar^2}{mL^2} \quad \to \qquad \frac{k_\mathrm{B}T}{|\mu|} \gtrsim \frac{L^2}{\lambda_T^2} \tag{II.41}$$

  which for the degenerate case leads to [*cf.* (II.24)]:

$$\mathcal{D} \gtrsim \ln(L^2/\lambda_T^2). \tag{II.42}$$

- The second criterion is to compare the decay length ℓ of the function G_1 with the sample size L. Finite-size effects become significant when ℓ exceeds L, i.e. :

$$\ell \gtrsim L \quad \to \quad \mathrm{e}^{\mathcal{D}/2} \gtrsim \frac{L}{\lambda_T}, \tag{II.43}$$

  which is effectively equivalent to the criterion (II.42).

2 Bose gas in a 2D harmonic trap

Many experiments on atoms, light or hybrid systems use a harmonic confinement. The major effect of this confinement is to modify the density of states of the system and thus to change, for a given dimensionality, the existence or non-existence of the condensation phenomenon. In what follows, we consider an isotropic harmonic trap of frequency ω for which the energy levels are given by $E_j = j\,\hbar\omega$, with $j \in \mathbb{N}$ (up to an additive constant). In the case of a non-isotropic trap, most of the following results remain valid, provided we replace ω by the geometric mean of the trap frequencies.

2-1 The influence of the spatial dimension

To find out whether or not condensation is possible, let us return to the expression giving the number of atoms in the excited states of the one-

particle Hamiltonian

$$N_{\rm exc} = \sum_{\alpha\neq 0} \frac{1}{\frac{1}{Z}{\rm e}^{E_\alpha/k_{\rm B}T}-1} \tag{II.44}$$

where the subscript α denotes the energy levels in the trap. As in the uniform case, it is useful to replace this discrete sum by an integral, which is a good approximation if the thermal energy $k_{\rm B}T$ is large compared with the distance between consecutive energy levels. We then obtain

$$N_{\rm exc} = \int_0^{+\infty} \frac{D(E)}{\frac{1}{Z}{\rm e}^{E/k_{\rm B}T}-1}\,{\rm d}E \tag{II.45}$$

where $D(E)$ is the density of states for the trap.

As in the case of a box, the density of state in a harmonic trap depends on dimensionality. For a 1D trap, the levels $(j+1/2)\hbar\omega$ are non-degenerate ($\xi_j = 1$), equidistant and separated by $\hbar\omega$, i.e.

$$D^{(1)}(E) = \frac{1}{\hbar\omega}. \tag{II.46}$$

In dimension 2, the degeneracy of the energy level $E_j = (j+1)\hbar\omega$ is $\xi_j = j+1$. In dimension 3, the degeneracy of the level $E_j = (j+3/2)\hbar\omega$ is $\xi_j = (j+1)(j+2)/2$, so that

$$D^{(2)}(E) = \frac{E}{(\hbar\omega)^2}, \qquad D^{(3)}(E) = \frac{E^2}{2(\hbar\omega)^3}. \tag{II.47}$$

Let us return to the criterion found in (II.19-II.21). The density of states does indeed vary as E^ν and the exponent ν is strictly positive in dimension 3 and dimension 2 ($\nu = 2$ and $\nu = 1$ respectively). Condensation is therefore possible in both cases. On the other hand, dimension 1 remains (marginally) excluded, since it corresponds to $\nu = 0$.

2-2 The condensation point

The maximum number of atoms that can be placed in a harmonic trap is obtained by injecting the density of states (II.47) into the expression (II.45)

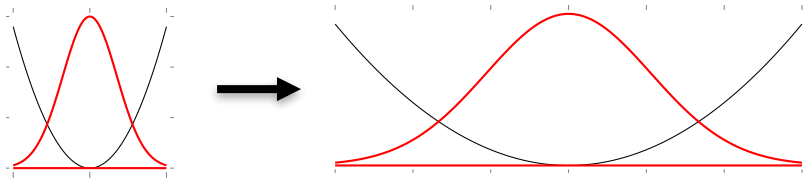

Figure II.4. *Thermodynamic limit in a trap. It is obtained by decreasing the frequency ω while increasing the number of atoms so as to keep the central density constant.*

for the maximum fugacity $Z = 1$. We obtain

$$\text{2D}: \quad N_{\rm exc}^{(\max)}(T) = {\rm Li}_2(1)\left(\frac{k_{\rm B}T}{\hbar\omega}\right)^2 \qquad \text{with} \quad {\rm Li}_2(1) = \sum_{n=1}^{+\infty}\frac{1}{n^2} = \frac{\pi^2}{6}, \tag{II.48}$$

and

$$\text{3D}: \quad N_{\rm exc}^{(\max)}(T) = {\rm Li}_3(1)\left(\frac{k_{\rm B}T}{\hbar\omega}\right)^3 \qquad \text{with} \quad {\rm Li}_3(1) = \sum_{n=1}^{+\infty}\frac{1}{n^3} = 1.202\ldots \tag{II.49}$$

Remember that these results are valid under the assumption $k_{\rm B}T \gg \hbar\omega$, necessary to replace the discrete sum (II.44) by an integral. The opposite case $k_{\rm B}T \ll \hbar\omega$ is conceptually trivial: particles accumulate in the ground state simply because the excited levels are not thermally activated.

Thermodynamic limit in a trap. For a gas in a square box, the notion of thermodynamic limit is simple: for a given temperature T, we take the limit where the number of particles N and the size of the box L tend to infinity, keeping the spatial density constant. In a harmonic trap, the thermodynamic limit is obtained in a similar way, but we now keep the central density $n(0)$ constant, while letting the number of particles N tend to infinity (De Groot, Hooyman, et al. 1950; Bagnato, Pritchard, et al. 1987). To understand how this is achieved, we can use the prediction for Maxwell-

Boltzmann statistics as an example:

$$\rho^{(\mathrm{d})}(\boldsymbol{r}) = \frac{1}{(2\pi)^{d/2}} \frac{N}{\sigma^d} \mathrm{e}^{-r^2/2\sigma^2} \qquad \text{with} \quad \frac{1}{2}m\omega^2\sigma^2 \equiv \frac{1}{2}k_{\mathrm{B}}T, \tag{II.50}$$

leading to

$$\rho^{(\mathrm{d})}(0) = \left(\frac{m}{2\pi k_{\mathrm{B}}T}\right)^{d/2} N\omega^d. \tag{II.51}$$

The thermodynamic limit is thus obtained by taking (figure II.4):

$$N \to +\infty, \quad \omega \to 0, \qquad \rho^{(\mathrm{d})}(0) \propto N\omega^d = \text{constant}. \tag{II.52}$$

Both results (II.48) and (II.49) on the saturation of excited states in 2D and 3D traps are relevant in this limit, since they are expressed in terms of the single variable $N_{\mathrm{exc}}^{(\max)}(T)\ \omega^d$:

$$N_{\mathrm{exc}}^{(\max)}(T)\ \omega^d = \mathrm{Li}_d(1) \left(\frac{k_{\mathrm{B}}T}{\hbar}\right)^d. \tag{II.53}$$

The one-dimensional case. In one dimension, the situation is more delicate than in 2D and 3D, since the integral (II.45) diverges when $Z \to 1$ (Bagnato & Kleppner 1991). We must therefore return to the discrete sum (II.44) to evaluate the maximum number of atoms that can be placed in a trap with frequency ω and temperature T. The calculation is described by Ketterle & vanDruten (1996) and leads to the result:

$$1\mathrm{D},\ k_{\mathrm{B}}T \gg \hbar\omega : \qquad N_{\mathrm{exc}}^{(\max)}(T) \approx \frac{k_{\mathrm{B}}T}{\hbar\omega}\ \ln\left(\frac{2k_{\mathrm{B}}T}{\hbar\omega}\right). \tag{II.54}$$

As expected, this result does not survive when we take the thermodynamic limit, since the product $N\omega$ required to reach the condensation threshold diverges. On the other hand, in a 1D trap with a fixed ω, a condensate forms when the number of atoms exceeds (II.54).

2-3 Semi-classical approximation

The equilibrium state of an ideal gas in a harmonic trap can be written in terms of the single-particle density operator

$$\hat{\rho}_1 = \frac{1}{\frac{1}{Z}\mathrm{e}^{\hat{H}/k_{\mathrm{B}}T} - 1}, \tag{II.55}$$

where $\hat{H} = \frac{\hat{\boldsymbol{p}}^2}{2m} + V_{\mathrm{trap}}(\hat{\boldsymbol{r}})$ is the single-particle Hamiltonian. The density operator $\hat{\rho}_1$ is diagonal in the eigenstate basis of $\hat{H}$ and the population of each state is given by the Bose–Einstein statistic (II.1).

The semi-classical approximation consists in "forgetting" the fact that $\hat{p}$ and $\hat{r}$ are non-commuting operators and in replacing them with classical variables (Bagnato, Pritchard, et al. 1987). The operator $\hat{\rho}_1$ then becomes a distribution in phase space:

$$W(\boldsymbol{r}, \boldsymbol{p}) = \frac{1}{(2\pi\hbar)^d} \frac{1}{\frac{1}{Z}\mathrm{e}^{[\frac{p^2}{2m} + V(\boldsymbol{r})]/k_{\mathrm{B}}T} - 1} \tag{II.56}$$

which can be integrated on either variable to determine the position and velocity distributions. The normalization constant of W will be justified later.

In reality, the concept of phase-space distribution does not exist in quantum physics. It is impossible to prepare a particle in such a state that both its position and momentum are perfectly defined. The object that comes closest is the Wigner distribution (Wigner 1932), a real but not always positive quantity. The link between the function $W(\boldsymbol{r}, \boldsymbol{p})$ defined above and the Wigner distribution is discussed in detail by Castin (2001). The upshot of this discussion is that (II.56) can validly be used if one is interested in phase-space structures with an extent much larger than $\hbar$. In other words, one should not try to resolve the contribution of each quantum state individually, but one should restrict to evaluating physical quantities that vary smoothly from a given state to a neighboring one. In particular, this must be the case for the population of these states, which means that $k_{\mathrm{B}}T \gg \hbar\omega$.

Within the framework of this approximation, it is straightforward to determine the d-dimensional spatial density profile, $\rho_{\mathrm{exc.}}^{(d)}(\boldsymbol{r})$, in a trap at a given temperature (remember that the ground state, if macroscopically

populated, is not included in this semi-classical distribution). Integration over momentum gives:

$$\begin{aligned}\rho^{(d)}_{\rm exc}(\boldsymbol{r}) &= \frac{1}{(2\pi\hbar)^d}\int \frac{Z\mathrm{e}^{-[\frac{p^2}{2m}+V(\boldsymbol{r})]/k_{\rm B}T}}{1-Z\mathrm{e}^{-[\frac{p^2}{2m}+V(\boldsymbol{r})]/k_{\rm B}T}}\,\mathrm{d}^d p \\ &= \frac{1}{(2\pi\hbar)^d}\sum_{j=1}^{+\infty} Z^j\int \mathrm{e}^{-j[\frac{p^2}{2m}+V(\boldsymbol{r})]/k_{\rm B}T}\,\mathrm{d}^d p \qquad \text{(II.57)} \\ &= \frac{1}{\lambda_T^d}\sum_{j=1}^{+\infty}\frac{1}{j^{d/2}}\left[Z\,\mathrm{e}^{-V(\boldsymbol{r})/k_{\rm B}T}\right]^j = \frac{1}{\lambda_T^d}\,\mathrm{Li}_{d/2}\left[Z\,\mathrm{e}^{-V(\boldsymbol{r})/k_{\rm B}T}\right].\end{aligned}$$

Note that for $Z \ll 1$, the first term ($j = 1$) of the sum is larger than all the others, and we recover the Boltzmann distribution

$$\rho^{(d)}_{\rm exc}(\boldsymbol{r}) \approx \rho^{(d)}_{\rm tot}(\boldsymbol{r}) = \frac{Z}{\lambda_T^d}\,\mathrm{e}^{-V(\boldsymbol{r})/k_{\rm B}T}. \qquad \text{(II.58)}$$

Number of atoms in the semi-classical approximation. The result (II.57) gives the density at any point in the trap. For the harmonic potential $V(\boldsymbol{r}) = m\omega^2 r^2/2$, we can now integrate this density over space and recover the results obtained previously:

$$\begin{aligned}N^{(d)}_{\rm exc} &= \frac{1}{\lambda_T^d}\sum_{j=1}^{+\infty}\frac{1}{j^{d/2}}Z^j\int \mathrm{e}^{-jm\omega^2 r^2/(2k_{\rm B}T)}\,\mathrm{d}^d r \\ &= \sum_{j=1}^{+\infty}\frac{Z^j}{j^{d/2}}\left(\frac{k_{\rm B}T}{\hbar\omega}\right)^d = \mathrm{Li}_d(Z)\left(\frac{k_{\rm B}T}{\hbar\omega}\right)^d. \qquad \text{(II.59)}\end{aligned}$$

2-4 The local density approximation (LDA)

In the absence of a trapping potential ($\omega = 0$), we recover the result given above for a uniform 2D gas [*cf.* (II.16)]:

$$\rho^{(\rm d)}_{\rm exc}(\boldsymbol{r}) = \frac{1}{\lambda_T^d}\,\mathrm{Li}_{d/2}\left(\mathrm{e}^{\mu/k_{\rm B}T}\right), \qquad \text{(II.60)}$$

which justifies the normalization constant introduced in (II.56). In the general case, the result (II.57), written as

$$\rho^{(\rm d)}_{\rm exc}(\boldsymbol{r}) = \frac{1}{\lambda_T^d}\,\mathrm{Li}_{d/2}\left(\mathrm{e}^{[\mu-V(\boldsymbol{r})]/k_{\rm B}T}\right) \qquad \text{(II.61)}$$

provides an illustration of the local density approximation: the density at any point in the trap is the density of a uniform gas of the same temperature and chemical potential $\mu - V(\boldsymbol{r})$. We will later generalize this approximation to a gas of interacting particles.

Condensation threshold for the semi-classical approach. Let us start with the 3D case. Condensation in the harmonic trap $V(\boldsymbol{r}) = m\omega^2 r^2/2$ is obtained when the fugacity Z tends towards 1, in which case the result (II.57) indicates that the central density of the trap is:

$$\rho^{(3)}_{\rm exc}(0) = \frac{1}{\lambda_T^3}\,\mathrm{Li}_{3/2}(1). \qquad \text{(II.62)}$$

So we arrive at a remarkable (and satisfying!) conclusion that links the uniform and trapped cases: condensation in the trap occurs when the central density is equal to the critical density of a uniform gas of the same temperature.

How does this result transfer to two dimensions? The answer does not seem obvious, since condensation occurs in the harmonic trap, but not in the uniform case. The answer lies in the fact that the central density $n(0)$ in the trap diverges when $Z \to 1$, although the integral of $n(\boldsymbol{r})$ over space remains convergent. The divergence of $n(\boldsymbol{r})$ around the point $\boldsymbol{r} = 0$ is indeed quite smooth:

$$\begin{aligned}Z = 1: \quad \rho^{(2)}_{\rm exc}(\boldsymbol{r}) &= \frac{1}{\lambda_T^2}\,\mathrm{Li}_1\left(\mathrm{e}^{-V(\boldsymbol{r})/k_{\rm B}T}\right) = -\frac{1}{\lambda_T^2}\,\ln\left(1-\mathrm{e}^{-m\omega^2 r^2/(2k_{\rm B}T)}\right) \\ &\overset{r\to 0}{\approx} -\frac{1}{\lambda_T^2}\,\ln(r^2) + \text{constant}. \qquad \text{(II.63)}\end{aligned}$$

This brings us back to the marginal aspect of two-dimensional condensation, at least in the thermodynamic limit: it can take place in a harmonic trap, but this means adding atoms until the central density becomes infinite. While this is possible in principle for an ideal gas, we can guess that it will be problematic in the presence of repulsive particle interaction.

3 An almost ideal 2D gas: photons in cavities

An example of Bose–Einstein condensation of an ideal gas in a 2D harmonic trap is provided by experiments carried out in Martin Weitz's group in Bonn since 2010 (Klaers, Schmitt, et al. 2010), and repeated more recently in Robert Nyman's group at Imperial College (Marelic & Nyman 2015; Marelic, Zajiczek, et al. 2016). It involves the two-dimensional condensation of photons in a Fabry-Perot cavity. *A priori*, the extension to photons of the notion of Bose–Einstein condensation, a phenomenon specific to massive particles, raises a number of questions:

- Photons are not massive particles in 3D space. How can they acquire a mass in 2D?
- To get a two-dimensional condensate, one needs to confine the particles, for example in a harmonic trap. How do we achieve this harmonic trapping for photons?
- Photons are generally assigned a zero chemical potential, on the grounds that their number is not conserved. In particular, this argument is used to establish the Planck law for blackbody radiation. How is it that photons can acquire a non-zero chemical potential in this type of experiment?
- Bose-Einstein condensation corresponds to the accumulation of a macroscopic number of particles in a single quantum state of the system, and the same is true for the laser. How do the experiments from the Bonn group differ from an ordinary laser?

3-1 Mass and harmonic potential for photons

Klaers' experimental scheme is shown in figure II.5. The experiment is carried out with photons of wavelength $\lambda \approx 570\,\text{nm}$. A Fabry-Perot cavity of high finesse (10^5) and low thickness $L \approx 1.5\,\mu\text{m}$ is used. The cavity is filled with a medium (methanol+dye) of index $n_0 = 1.33$, so that $L \approx N\frac{\lambda}{2n_0}$ with $N = 7$. Photons are stored in the cavity in the longitudinal mode $N = 7$.

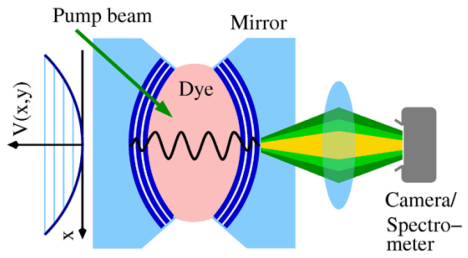

Figure II.5. *Fabry-Perot cavity filled with dye and laterally pumped by a laser. For a sufficiently high pumping rate, Bose-Einstein condensation of photons occurs in the $N = 7$ longitudinal mode and in the lowest transverse mode. Figure taken from Klaers, Schmitt, et al. (2011).*

The choice of the value of L is motivated by the fact that the free spectral range, i.e. the energy gap between the $N = 7$ mode and its neighbors $N = 6$ or 8, must be greater than (i) $k_\text{B}T$, where T is the ambient temperature, and (ii) the spectral width of the dye fluorescent light. When this condition is met, these other longitudinal modes play no role: the degree of freedom along z can be considered as frozen. The choice of $L = 1.5\,\mu$m leads to an energy gap of around $10\,k_\text{B}T$, which is more than sufficient.

How can photons be given a mass? In what follows, we focus on the dynamics and thermodynamics of photons in the xy plane, where z is the cavity axis. A photon resonant with the cavity has a wave vector $(\boldsymbol{k}_\perp, k_z)$ with $k_z = N\pi/L$. If we restrict ourselves to the paraxial approximation, i.e. to photons making a small angle with the z axis, we have $|\boldsymbol{k}_\perp| \ll k_z$. The energy of a photon in the medium of index n_0 filling the cavity can be written as

$$\hbar\omega(\boldsymbol{k}_\perp) = \frac{\hbar c}{n_0}\left(k_z^2 + \boldsymbol{k}_\perp^2\right)^{1/2} \approx \hbar\omega_0 + \frac{\hbar^2\boldsymbol{k}_\perp^2}{2m_\text{ph}}, \tag{II.64}$$

where

$$\hbar\omega_0 = \frac{N\pi\hbar c}{n_0 L}. \tag{II.65}$$

We obtain a massive particle dispersion relation and the effective mass of the photon for the motion in the xy plane is:

$$m_{\mathrm{ph}} = \frac{\hbar n_0 k_z}{c} = n_0^2 \frac{\hbar\omega_0}{c^2}. \tag{II.66}$$

This effective mass is 0.7×10^{-35} kg in the Bonn experiment, 100 000 times less than an electron!

How can one induce a harmonic potential in the xy plane? We are going to use a classical corpuscular reasoning here, which can be transposed into wave formalism if needed. The cavity is made up of two spherical mirrors of radius R, so that the distance L between the two mirrors varies with the distance from the axis $r = \left(x^2 + y^2\right)^{1/2}$:

$$L(r) = L_0 - 2\left(R - \sqrt{R^2 - r^2}\right). \tag{II.67}$$

The radius of curvature of the mirrors $R \approx 1\,\mathrm{m}$ is large compared to the typical distance to the optical axis, $r \approx 100\,\mu\mathrm{m}$ so that

$$L(r) \approx L_0 - \frac{r^2}{R}. \tag{II.68}$$

The variation in cavity length with the distance to axis induces a spatial variation in the energy of a photon stored in the longitudinal mode N. More precisely, if we inject the result for $L(r)$ into the definition (II.65) of $\hbar\omega_0$, we arrive at

$$\hbar\omega_0(r) = \hbar\omega_0(0) + \frac{1}{2} m_{\mathrm{ph}} \Omega^2 r^2 \tag{II.69}$$

where the frequency Ω is defined by:

$$\Omega = \frac{c}{n_0\sqrt{L_0 R/2}}. \tag{II.70}$$

The desired harmonic confinement is obtained, with an oscillation frequency $\Omega/(2\pi) \approx 40\,\mathrm{GHz}$ for the Bonn experiment.

At this point, the energy of a photon with transverse position $\boldsymbol{r}$ and transverse momentum $\hbar\boldsymbol{k}_\perp$ can be written as follows

$$E(\boldsymbol{r}, \boldsymbol{k}_\perp) = \frac{\hbar^2 \boldsymbol{k}_\perp^2}{2m_{\mathrm{ph}}} + \frac{1}{2} m_{\mathrm{ph}} \Omega^2 \boldsymbol{r}^2, \tag{II.71}$$

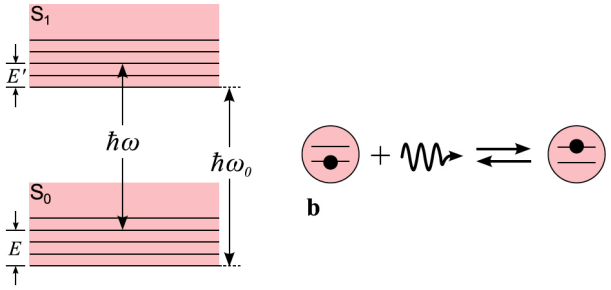

Figure II.6. *Absorption and emission of a photon by a dye molecule. Figure taken from Klaers, Schmitt, et al. (2011).*

which, from a kinematic point of view, is sufficient to apply the previous formalism.

3-2 Temperature and chemical potential

The cavity is filled with a dye (rhodamine 6G) which is illuminated from the side with a pump laser at 532 nm. A dye molecule can be considered as a system with two electronic levels g (ground) and e (excited), with a quasi-continuum of vibrational and rotational sublevels for each of these levels (figure II.6). In an $e \to g$ transition, a molecule emits a photon in the cavity mode $N = 7$. This photon can be reabsorbed by a molecule ($g \to e$ transition), then re-emitted multiple times before finally escaping the cavity.

This succession of absorption and emission processes leads to a thermal distribution for the photon energy. More precisely, using Kennard–Stepanov's law which relates the absorption and emission spectra of molecules, we can show that the photon energy distribution is characterized (roughly) by the same temperature as that of the dye, $T = 300\,\mathrm{K}$ (Klaers, Schmitt, et al. 2011). In conjunction with the effective mass determined above, this corresponds to a thermal wavelength $\lambda_T \sim 1.6\,\mu\mathrm{m}$.

At this stage, the situation seems similar to that of blackbody radiation, where one considers photons in equilibrium with the walls of an

oven. However, in the case of black-body radiation, we are led to impose a zero chemical potential to the photons. This is because the number of photons, or more precisely the number of excitations in the system, is not conserved. When we consider the dynamics of photons interacting with the oven walls, we can have a process of the type:

$$1 \text{ photon } \rightarrow \text{ 1 wall excitation } \rightarrow \text{ 2 photons} \tag{II.72}$$

resulting in the conversion of one photon of energy $\hbar\omega$ into two photons of energy $\hbar\omega'$ and $\hbar\omega''$, with $\omega = \omega' + \omega''$. The existence of such processes imposes $\mu = 2\mu$ for photons, i.e. $\mu = 0$.

The situation is very different in the Bonn experiment. Although the photons have the same temperature T as the dye, their number in the wavelength range around 570 nm is different from that of a black body at this temperature, since it also depends on the pumping intensity. To understand this point, let us start with the process shown in figure II.6:

$$1 \text{ photon} + \text{one molecule } g \longleftrightarrow \text{one molecule } e. \tag{II.73}$$

In such an elementary process, the number of excitations in the system is constant, unlike in the case of black-body radiation [3]. A simplified version of the equilibrium in the above relationship can be written in terms of the balance equation:

$$\mathcal{N}(\omega)\; N_g(E) = [1 + \mathcal{N}(\omega)]\, N_e(E + \hbar\omega) \tag{II.74}$$

where $\mathcal{N}(\omega)$ represents the number of photons of frequency ω, $N_{g/e}(E)$ the number of molecules of internal energy E. In this equation, we have taken into account the phenomenon of stimulated emission, which is responsible for condensation. In this simple model, we have

$$\frac{N_e(E + \hbar\omega)}{N_g(E)} = Z\, \mathrm{e}^{-\hbar\omega/k_\mathrm{B}T}, \tag{II.75}$$

which implicitly assumes that relaxation within rovirational sublevels guarantees a thermal distribution for each of these two continua. In contrast, the ratio between the global populations of g and e is not thermal,

[3] If we return to the description of elementary processes of molecule-radiation interaction, we may note that this point is the basis of the rotating field approximation (RWA), which consists in keeping in the Hamiltonian only the terms in $\hat{a}^\dagger|g\rangle\langle e| + \text{H.c.}$

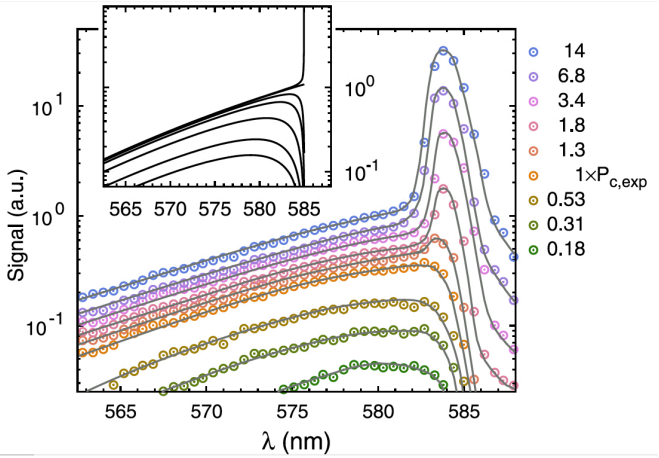

Figure II.7. *Spectrum of light emitted for different pump powers. Continuous lines are fits by Bose–Einstein distributions associated with energy (II.71) and non-zero fugacity. For a pump power above a certain threshold, a macroscopic accumulation of photons occurs in the lowest transverse mode of the cavity. Figure taken from Klaers, Schmitt, et al. (2011).*

but imposed by the pump laser and described by the coefficient Z. The solution to the balance equation is

$$\frac{\mathcal{N}(\omega)}{1 + \mathcal{N}(\omega)} = \frac{N_e(E + \hbar\omega)}{N_g(E)} \qquad \longrightarrow \qquad \mathcal{N}(\omega) = \frac{1}{\frac{1}{Z}\mathrm{e}^{\hbar\omega/k_\mathrm{B}T} - 1} \tag{II.76}$$

i.e. a Bose-Einstein law of fugacity $Z \neq 1$.

3-3 Experimental results

A typical example of experimental spectra is shown in figure II.7. We can see that, over a range of around twenty nanometers, the frequency distribution of photons emitted by the cavity reproduces very well a Bose–Einstein law at temperature $T = 300\,\mathrm{K}$ and with a chemical potential that depends on the pump power. For high enough power, one clearly observes an accumulation of photons in a narrow peak, with a wavelength around

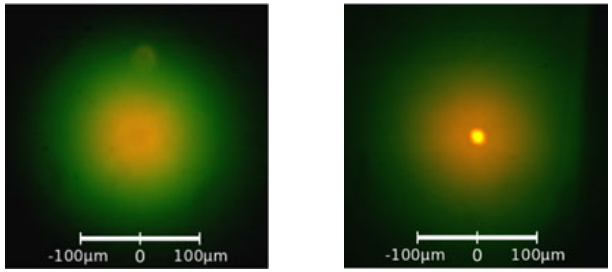

Figure II.8. *Spatial distribution of light emitted by the cavity, below (left) and above (right) the threshold power. Note that the shortest wavelengths (green) are emitted at the edges, confirming the presence of the effective harmonic potential* $m_{\rm ph}\Omega^2 r^2/2$. *Figure taken from Klaers, Schmitt, et al. (2011).*

584 nm. A direct image of the light from the cavity, below and above the threshold, confirms the interpretation of this peak as an accumulation of photons in a central cavity mode (figure II.8). For $\lambda > 585\,\text{nm}$, the number of photons falls, as this region is beyond the cut-off wavelength for the mode under consideration ($N = 7$). The spectrum is then very different from that of a black body, for which $\mathcal{N}(\omega)$ diverges at low frequency. The number of photons in the cavity at the threshold of the transition is of the order of 60,000, in good agreement with the prediction[4] for an ideal gas $\frac{\pi^2}{3}\,(k_{\rm B}T/\hbar\Omega)^2$.

More recent experiments, still carried out by the Bonn group, have focused on studying the statistical distribution of the number of photons present in the condensate at a given time. Schmitt, Damm, et al. (2014) have shown that these fluctuations correspond to those expected for the grand canonical ensemble. This is consistent with the idea that the photon gas exchanges energy and particles with the reservoir formed by the dye molecules. This result was recently confirmed by measuring the phase coherence of the light leaving the cavity (Schmitt, Damm, et al. 2016). Measurement of the specific heat of the photon gas (fig. II.9), with a characteristic variation showing "a λ point", has further confirmed the validity of the interpretation of these phenomena as a Bose–Einstein condensation

[4]This number differs by a factor of 2 from (II.48) because the two possible polarization states for the photons must be taken into account.

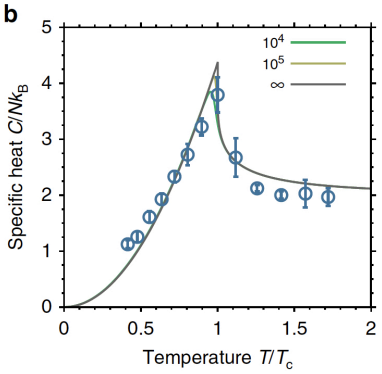

Figure II.9. *Specific heat (per photon) measured as a function of the reduced temperature* T/T_c, *showing the characteristic singularity ("*λ *point") of the Bose–Einstein transition. In the high-temperature regime, the specific heat reaches the classical limit of* $2k_{\rm B}$ *per photon. The solid lines show the prediction for an ideal Bose gas for three different numbers of particles. Figure taken from Damm, Schmitt, et al. (2016).*

(Damm, Schmitt, et al. 2016).

Condensate or laser? The answer to this question depends on the criteria we set to obtain one or the other of the two effects. Firstly, a condensate can be required to appear above a pedestal that can be assimilated to a thermal distribution, which is not the case for a laser. The Bonn experiment satisfies this criterion. Furthermore, most lasers tend to produce light with a Poisson distribution of the number of photons emitted over a given duration. Here, the light leaving the cavity exhibits much larger fluctuations, well described in the grand-canonical ensemble of a Bose gas. It should also be noted that a condensate corresponds to a situation of thermodynamic equilibrium. From this point of view, the Bonn experiment is not really in a state of equilibrium, since the cavity is an open system: energy is continuously injected into it via the pump, and energy escapes when photons leave the cavity. On the other hand, since each photon undergoes multiple "absorption-emission" processes before escaping, a quasi-thermal equilibrium has plenty of time to be reached. In view of these various criteria, all

linked to static properties of the system, it seems legitimate to consider that this experiment has indeed produced a 2D condensate of trapped photons. Finally, we should point out that Chiocchetta, Gambassi, et al. (2015) recently proposed criteria of a different, more restrictive nature, based on the verification of fluctuation-dissipation type relations. To our knowledge, these criteria have not yet been tested on 2D photon condensates.

4 Two-dimensional binary collisions

To go beyond the ideal gas model and arrive at the BKT transition, we need to take particle interactions into account. In the dilute gases of interest here, these interactions are well described by a binary collision model, where the interaction Hamiltonian is described as a sum of two-body terms

$$\hat{H}_{\text{int}} = \frac{1}{2}\sum_{i\neq j} U(\boldsymbol{r}_i - \boldsymbol{r}_j). \tag{II.77}$$

We must therefore begin by describing the two-body problem in the presence of the interaction potential $U(\boldsymbol{r})$. The study is simplified by the following remarks:

- The dominant interactions are spherically symmetric, so that $U(\boldsymbol{r})$ depends only on $r = |\boldsymbol{r}|$. The angular momentum is conserved in a collision, allowing the two-body problem to be treated using the eigenstates of the operator $\hat{\boldsymbol{L}}$. This is the principle of partial wave expansion, identified by the value $\ell \in \mathbb{N}$ of angular momentum. Note that for polarized bosons, symmetrization of the two-body wave function means that only even values of ℓ are allowed.
- Atoms are cold and their thermal wavelength λ_T is large compared to the range of the potential, which will be noted here b. In other words, the relevant wave vectors $\boldsymbol{k}$, which are of the order of $1/\lambda_T$, verify $kb \ll 1$. Furthermore, the potential $U(\boldsymbol{r})$ decreases quite rapidly at infinity. The combination of these two properties ensures that collisions essentially occur in the s-wave channel, i.e. the state corresponding to a relative angular momentum $\ell = 0$ between the two collision partners (figure II.10).

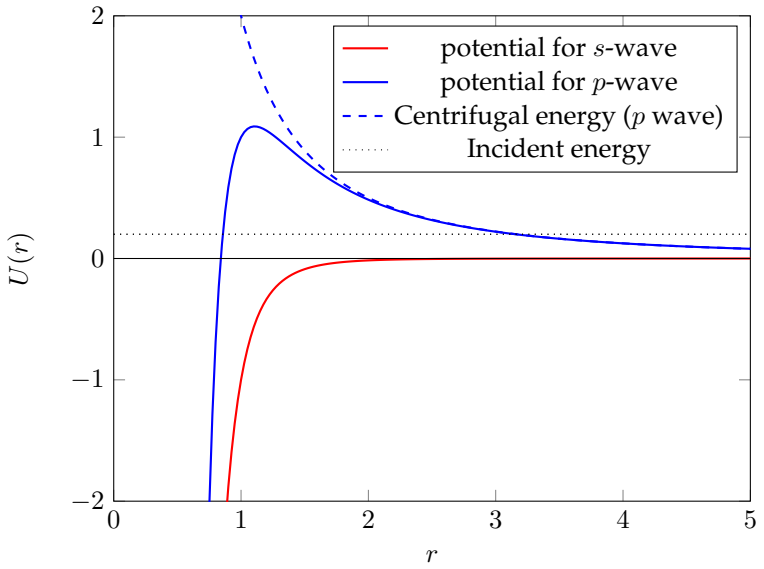

Figure II.10. *$-1/r^6$ radial potential experienced by a particle in the s-wave channel (red, no centrifugal term), and in a partial wave of non-zero angular momentum (blue, with a centrifugal term in $+1/r^2$). Length and energy scales are chosen here as dimensionless.*

The treatment of 3D binary collisions is covered in most quantum physics textbooks. In the case of cold atoms, see for example our subsequent lecture series (2021-22). The aim of this section is to show the important changes brought about by the move to two dimensions, and so set the scene for our study of the BKT transition.

4-1 Separation of variables and scattering amplitude

Consider two identical atoms of mass m and introduce the center-of-mass variables, $\boldsymbol{R}$ and $\boldsymbol{P}$:

$$\boldsymbol{R} = \frac{1}{2}(\boldsymbol{r}_1 + \boldsymbol{r}_2), \qquad \boldsymbol{P} = \boldsymbol{p}_1 + \boldsymbol{p}_2 \tag{II.78}$$

and the relative variables, $\boldsymbol{r}$ and $\boldsymbol{p}$:

$$\boldsymbol{r} = \boldsymbol{r}_1 - \boldsymbol{r}_2, \qquad \boldsymbol{p} = \frac{1}{2}(\boldsymbol{p}_1 - \boldsymbol{p}_2). \tag{II.79}$$

The two-body Hamiltonian splits into two terms

$$\hat{H} = \hat{H}_{\rm CM} + \hat{H}_{\rm rel}, \qquad \hat{H}_{\rm CM} = \frac{\hat{P}^2}{2M}, \qquad \hat{H}_{\rm rel} = \frac{\hat{p}^2}{2m_r} + U(\boldsymbol{r}), \tag{II.80}$$

where we introduced the total mass $M = 2m$ and the relative mass $m_r = m/2$. The binary collision problem therefore boils down to a one-body problem with reduced mass m_r in the external potential $U(\boldsymbol{r})$, described by the Hamiltonian $\hat{H}_{\rm rel}$. This is the problem we are going to study.

We are going to look at the asymptotically free states that describe a scattering process. The formalism of scattering theory relies on the fact that for any plane wave $\mathrm{e}^{\mathrm{i}\boldsymbol{k}\cdot\boldsymbol{r}}$, i.e. any eigenstate of the Hamiltonian

$$\hat{H}_{\rm rel,0} = \frac{\hat{p}^2}{2m_r}, \tag{II.81}$$

with eigenvalue $E_{\boldsymbol{k}} = \hbar^2 k^2/2m_r$, one can associate an eigenstate $\psi_{\boldsymbol{k}}(\boldsymbol{r})$ of $\hat{H}_{\rm rel}$ with the same energy,

$$\hat{H}_{\rm rel}\psi_{\boldsymbol{k}}(\boldsymbol{r}) = E_{\boldsymbol{k}}\ \psi_{\boldsymbol{k}}(\boldsymbol{r}), \tag{II.82}$$

this state being written asymptotically as the sum of the incident plane wave and a spherical (three-dimensional) or cylindrical (two-dimensional) outgoing wave:

$$\text{3D, } 1 \ll kr \quad : \quad \psi_{\boldsymbol{k}}(\boldsymbol{r}) \ \sim\ C_0 \left\{ \mathrm{e}^{\mathrm{i}\boldsymbol{k}\cdot\boldsymbol{r}} + f(k)\frac{\mathrm{e}^{\mathrm{i}kr}}{r} \right\}, \tag{II.83}$$

$$\text{2D, } 1 \ll kr \quad : \quad \psi_{\boldsymbol{k}}(\boldsymbol{r}) \ \sim\ C_0 \left\{ \mathrm{e}^{\mathrm{i}\boldsymbol{k}\cdot\boldsymbol{r}} + f(k)\frac{\mathrm{e}^{\mathrm{i}kr}}{\sqrt{kr}} \left[-\sqrt{\frac{\mathrm{i}}{8\pi}} \right] \right\}, \tag{II.84}$$

where C_0 is a normalization constant. We have taken into account the fact that the scattering process takes place essentially in the channel of zero angular momentum (s-wave), and we have therefore restricted ourselves to the case of an isotropic scattered wave. We also note that the definition of the scattering amplitude $f(k)$ is not exactly the same in three and two dimensions, with the factor $1/\sqrt{k}$ appearing explicitly in (II.84). The definition used here ensures simple analytical properties for $f(k)$ (Adhikari 1986). Finally, the reason for the factor in square brackets in the 2D definition lies in the form found for $f(k)$ in the case of quasi-2D geometry (§4-4), which takes the form $f(k) \approx \tilde{g}$, where the constant $\tilde{g}$ is the parameter commonly used to characterize the strength of interactions in this type of problem.

The scattering amplitude $f(k)$ therefore determines the properties of the binary collision. To calculate it, let us take the angular average of the Schrödinger equation (II.82) by noting $R_k(r) = \frac{1}{4\pi}\int \psi_{\boldsymbol{k}}(r,\theta,\varphi)\ \sin\theta\ \mathrm{d}\theta\ \mathrm{d}\varphi$ at 3D and $R_k(r) = \frac{1}{2\pi}\int \psi_{\boldsymbol{k}}(r,\varphi)\ \mathrm{d}\varphi$ at 2D. We then arrive at the radial Schrödinger equation :

$$\text{3D:} \qquad \frac{\mathrm{d}^2 R_k}{\mathrm{d}r^2} + \frac{2}{r}\frac{\mathrm{d}R_k}{\mathrm{d}r} + \left[k^2 - \frac{2m_r}{\hbar^2}U(r) \right] R_k(r) = 0 \tag{II.85}$$

and

$$\text{2D:} \qquad \frac{\mathrm{d}^2 R_k}{\mathrm{d}r^2} + \frac{1}{r}\frac{\mathrm{d}R_k}{\mathrm{d}r} + \left[k^2 - \frac{2m_r}{\hbar^2}U(r) \right] R_k(r) = 0, \tag{II.86}$$

The difference between the 3D and 2D cases appears minor here, with only a factor of 2 difference for the term with a first derivative in r. We will see, however, that this difference strongly alters the behavior of the radial function $R_k(r)$ and the scattering amplitude $f(k)$. Note that the asymptotic behavior of the radial function $R_k(r)$ is obtained by angular averaging of (II.83-II.84):

$$\text{3D, } 1 \ll kr \quad : \quad R_k(r) \ \sim\ C_0 \left\{ \frac{\sin(kr)}{kr} + f(k)\frac{\mathrm{e}^{\mathrm{i}kr}}{r} \right\}, \tag{II.87}$$

$$\text{2D, } 1 \ll kr \quad : \quad R_k(r) \ \sim\ C_0 \left\{ J_0(kr) + f(k)\frac{\mathrm{e}^{\mathrm{i}kr}}{\sqrt{kr}} \left[-\sqrt{\frac{\mathrm{i}}{8\pi}} \right] \right\}. \tag{II.88}$$

To simplify our analysis, we will assume that the potential $U(\boldsymbol{r})$ cancels out (or takes on negligible values compared to the other energies in the problem) beyond the radius b. We will focus on the low-energy regime $kb \ll 1$, so that there is an intermediate region of space

$$b < r \ll k^{-1} \tag{II.89}$$

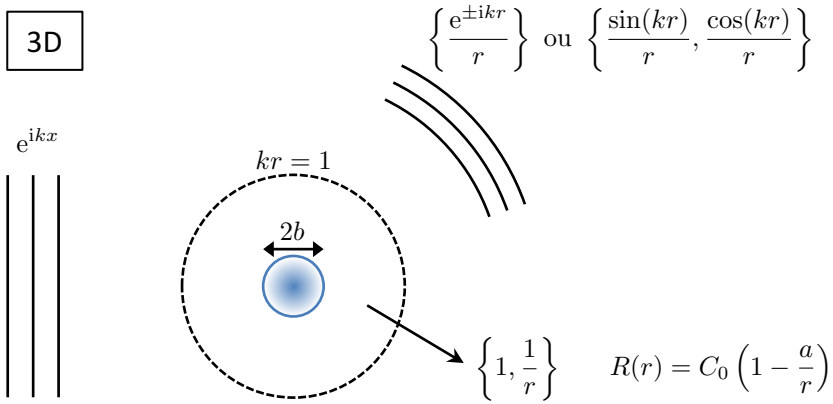

Figure II.11. *Principle of the calculation of the 3D scattering amplitude for low wave vectors $kb \ll 1$. We assume that the scattering potential takes significant values only for $r < b$. For $kr \gg 1$, the superposition of the incident plane wave and the divergent spherical wave can be written after angular averaging as a linear combination of $e^{\pm ikr}/r$. These two basis functions connect in the intermediate region $b < r < k^{-1}$ to the two functions $R^{(I)}(r) = 1$ and $R^{(II)}(r) = 1/r$. The physically relevant linear combination, including the required regularity at $r = 0$, is used to define the scattering length a.*

in which the potential $U(\boldsymbol{r})$ has no influence, and where we can still make an expansion in powers of kr for the scattering states $\psi_{\boldsymbol{k}}(\boldsymbol{r})$. In particular, the incident plane wave is $e^{i\boldsymbol{k}\cdot\boldsymbol{r}} \approx 1$ in this intermediate region.

4-2 Scattering length in 3D

Our aim here is to obtain a solution of the Schrödinger equation with asymptotic behavior (II.87). To do this, we proceed in three steps, which we will then repeat in the two-dimensional case.

Step 1: general solutions in the zone $U = 0$. Consider the zone $r > b$ where U is negligible. The two functions $e^{\pm ikr}/r$ are then exact solutions of the radial equation (II.85) (both for $kr \gg 1$ and for $b < r < k^{-1}$), and the general solution is therefore a linear combination of these two functions. In particular, in the intermediate region $b < r < k^{-1}$, we find (*cf.* figure II.11)

$$\frac{e^{\pm ikr}}{r} \approx \frac{1 \pm ikr}{r} = \frac{1}{r} \pm ik \tag{II.90}$$

which, by linear combination, provides a convenient basis of the solutions in this region:[5]

$$R^{(I)}(r) = 1 \qquad R^{(II)}(r) = 1/r, \tag{II.91}$$

or

$$R(r) = C_1 - \frac{C_2}{r}, \tag{II.92}$$

where C_1 and C_2 are two constants. The asymptotic form (II.87) written in terms of the two functions $e^{\pm ikr}/r$ can be transposed to this intermediate region since these functions are exact solutions as long as the potential U is negligible. We thus end up with the form (II.92) with

$$R_k(r) = C_1\left[1 + \frac{f(k)}{r}\right]. \tag{II.93}$$

Step 2: zero energy solution. Let us take $k = 0$ in the radial Schrödinger equation (II.85) and consider the region $0 < r < b$ where $U(r)$ is no longer negligible. Since this is a second-order linear differential equation, the space of solutions is always of dimension 2. However, it is generally found that only one linear combination of solutions is acceptable if we impose that $R_0(r)$ should be regular in $r = 0$. When we follow this solution up to the point $r = b$ where U becomes negligible and the form (II.92) becomes relevant, this linear combination imposes the ratio C_2/C_1. Let us define the three-dimensional scattering length by $a = C_2/C_1$. The solution for $E = 0$ therefore has the following form for $r > b$:

$$E = 0 : \qquad R_0(r) = C_1\left(1 - \frac{a}{r}\right), \tag{II.94}$$

the scattering length corresponding, by definition, to the point where this asymptotic form vanishes.

[5] This basis can recovered by considering the limit $k \to 0, U \to 0$ of (II.85), $rR'' + 2R' = 0$, which integrates into $R'(r) = C_2/r^2$ where C_2 is a constant, and thus $R(r) = C_1 - C_2/r$ where C_1 is another constant.

Step 3: Matching solutions for low energy. We now consider a low-energy solution $R_k(r)$ ($kb \ll 1$) and we study its behavior in the intermediate zone $b < r \ll k^{-1}$. Comparing the form (II.93) with the solution $R_0(r)$ for $E = 0$ leads immediately to the link between the scattering length and the amplitude $f(k)$:

$$a = -\lim_{k\to 0} f(k). \tag{II.95}$$

The total effective scattering cross-section associated to the potential $U(r)$ is then calculated by balancing the input and output probability currents, and we find $\sigma = 4\pi a^2$. For identical particles obeying Bose-Einstein statistics, quantum statistical effects multiply this result by 2 if the two particles are prepared in the same spin state.

4-3 Scattering length in 2D

We now transpose to the 2D case the various steps of the approach that we outlined above for 3D scattering (see figure II.12).

Step 1: general solutions in the $U = 0$ zone. The 2D case immediately appears more complicated than the 3D case, since the cylindrical waves $\mathrm{e}^{\pm \mathrm{i}kr}/\sqrt{r}$ are not exact solutions of the radial equation (II.86) for $U = 0$. If they were, the low-energy limit would give the basis of functions $\frac{1}{\sqrt{r}} \pm \mathrm{i}k\sqrt{r}$ and thus, by linear combination, $\frac{1}{\sqrt{r}}$ and $\sqrt{r}$. However the limit $k \to 0$ and $U \to 0$ of (II.86) gives $rR'' + R' = 0$ which integrates into $R'(r) = C_1/r$ and thus

$$R^{(\mathrm{I})}(r) = \ln(r) \qquad R^{(\mathrm{II})}(r) = 1, \tag{II.96}$$

and thus the general solution:

$$R(r) = C_1 \ln(r) + C_2. \tag{II.97}$$

To return to this result in a more general context, we note that the equation (II.86) for the radial function in the case $U = 0$ is in fact the equation defining Bessel functions of order 0. Two independent solutions of this equation are the first-order Bessel function, $J_0(kr)$, and the second-order Bessel function, $Y_0(kr)$. The behavior of J_0 and Y_0 is known for both large

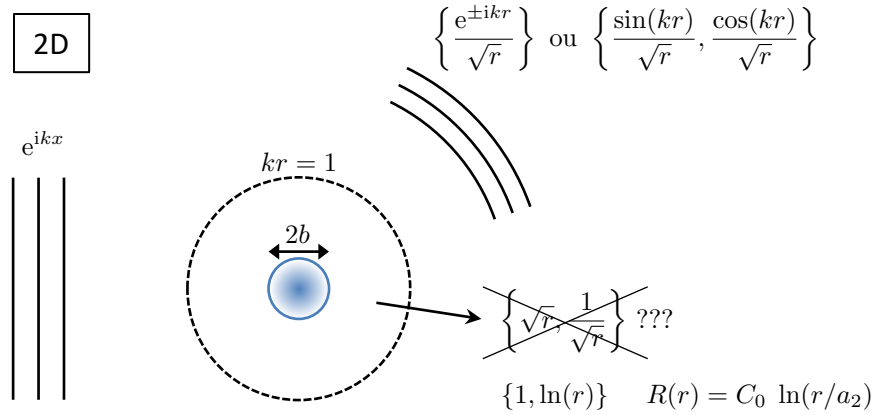

Figure II.12. *Principle of 2D scattering amplitude calculation by a potential taking significant values only for $r < b$ and for low wave vectors $kb \ll 1$. For $kr \gg 1$, the superposition of the incident plane wave and the divergent spherical wave can be written after angular averaging as a linear combination of $\mathrm{e}^{\pm \mathrm{i}kr}/\sqrt{r}$. These two functions are the asymptotic forms of the Bessel functions of the first and second kind. They connect in the intermediate region $b < r < k^{-1}$ to the two functions $R^{(\mathrm{I})}(r) = \ln(r)$ and $R^{(\mathrm{II})}(r) = 1$. The physically relevant linear combination, including the required regularity at $r = 0$, is used to define the 2D scattering length a_2.*

and small values of kr :

$$kr \gg 1 : \qquad J_0(kr) \sim \sqrt{\frac{2}{\pi kr}} \cos\left(kr - \frac{\pi}{4}\right) \tag{II.98}$$

$$Y_0(kr) \sim \sqrt{\frac{2}{\pi kr}} \sin\left(kr - \frac{\pi}{4}\right) \tag{II.99}$$

and

$$kr \ll 1 : \qquad J_0(kr) \sim 1 \tag{II.100}$$

$$Y_0(kr) \sim \frac{2}{\pi} \ln(\eta\, kr) \tag{II.101}$$

where [6] $\eta = 0.89\ldots$. In particular, any linear combination of J_0 and Y_0 for

[6] $\eta = \mathrm{e}^{\gamma}/2$ where $\gamma = 0.5772\ldots$ is Euler's constant.

$kr \ll 1$ is of the form (II.97).

Step 2: zero energy solution. For $k = 0$ and in the presence of the potential $U(r)$, the space of solutions $R_0(r)$ of the radial equation is of dimension 2. The regularity condition of $R_0(r)$ in $r = 0$ selects a particular linear combination of these functions. When extended beyond the radius $r = b$, this linear combination connects to a particular linear combination of the type $C_1 \ln(r) + C_2$ [*cf.* (II.97)], which can still be written as

$$r > b : \qquad R_0(r) = C_1 \ln(r/a_2) \tag{II.102}$$

where $a_2 \equiv \mathrm{e}^{-C_2/C_1}$ is the two-dimensional scattering length.

Step 3: Matching solutions for low energy. Let us move on to the case where k is not zero, but remains very small in front of $1/b$. To form an outgoing cylindrical wave, we see on (II.98-II.99) that we must take a function proportional to the linear combination[7] $J_0 + \mathrm{i}Y_0$. More precisely, we will choose

$$\text{2D, } 1 \ll kr : \qquad \frac{1}{4\mathrm{i}} \left[J_0(kr) + \mathrm{i}Y_0(kr) \right] \sim \frac{\mathrm{i}kr}{\sqrt{kr}} \left[-\sqrt{\frac{\mathrm{i}}{8\pi}} \right], \tag{II.103}$$

where we recognize in square brackets the prefactor of $f(k)$ introduced in (II.88). For $r > b$, the radial function we are looking for is of the type

$$R_k(r) = C_0 \left\{ J_0(kr) + \frac{f(k)}{4\mathrm{i}} \left[J_0(kr) + \mathrm{i}Y_0(kr) \right] \right\}. \tag{II.104}$$

In the intermediate region $b < r < k^{-1}$, this linear combination becomes:

$$R_k(r) = C_0 \left\{ 1 + \frac{f(k)}{4\mathrm{i}} \left[1 + \mathrm{i}\,\frac{2}{\pi} \ln(\eta\, kr) \right] \right\}. \tag{II.105}$$

which leads to the equation in the limit $k \to 0$:

$$f(k) = -4\mathrm{i}\, \frac{1}{1 + \mathrm{i}\,\dfrac{2}{\pi} \ln(\eta\, ka_2)} = \frac{1}{-\dfrac{1}{2\pi} \ln(\eta\, ka_2) + \dfrac{\mathrm{i}}{4}} \tag{II.106}$$

[7] This combination is called the Hankel function of the first kind, denoted $H_0^{(1)}(kr)$. The function of the second kind, $H_0^{(2)}(kr)$, corresponds to $J_0 - \mathrm{i}Y_0$.

to find the form (II.102) in $C_1 \ln(r/a_2)$, with in particular $R_k(r) = 0$ for $r = a_2$ (Petrov & Shlyapnikov 2001; Pricoupenko & Olshanii 2007).

Note in particular that the scattering amplitude $f(k)$ tends towards 0 at small k, contrary to the 3D case where it tended towards a finite limit equal to $-a$. Furthermore, the total effective cross-section of scattering by the potential $U(r)$ can also be calculated by balancing the input and output probability currents. We find $\sigma(k) = |f(k)|^2/(4k)$, a quantity that has the dimension of a length and diverges at small k.

4-4 Collisions in quasi-2D geometry

In an experiment, the reduction of dimensionality is achieved by strongly confining the atoms along an axis, z for example. Confinement is characterized by the residual extension of the gas along this direction. For example, if the confinement is achieved by imposing the harmonic potential $V_{\mathrm{trap}}^{(1\mathrm{D})}(z) = \frac{1}{2} m\omega_z^2 z^2$ and if the temperature is low enough, the atoms will occupy only the ground state $n_z = 0$ of the motion along z,

$$\chi_0(z) = \frac{1}{(\pi a_{\mathrm{oh}}^2)^{1/4}} \mathrm{e}^{-z^2/(2a_{\mathrm{oh}}^2)} \qquad \text{with} \quad a_{\mathrm{oh}} = \sqrt{\frac{\hbar}{m\omega_z}}, \tag{II.107}$$

at least as long as we neglect the interactions between these atoms.

A detailed treatment of the collision between two atoms in the presence of the potential $V_{\mathrm{trap}}^{(1\mathrm{D})}(z)$ has been given by Petrov & Shlyapnikov (2001). Here, we simply report some of the results of that paper. The interaction between two atoms in the absence of potential along the z axis is characterized by the three-dimensional scattering length a. We will concentrate on the case most often encountered in practice:

$$a \ll a_{\mathrm{oh}}, \tag{II.108}$$

so that the energy associated with the interactions, $\hbar^2/(ma^2)$, is greater than $\hbar\omega_z$. In a dynamical view of the collision, this means that even if the atoms enter and leave in the $n_z = 0$ channel, several $n_z \neq 0$ excited states of motion along z are involved during the collision.

Furthermore, since the asymptotic states are those of a gas confined along z in the $n_z = 0$ state, the wave function of the relative variable of the

pair of atoms must be written in the 2D version seen above:

$$1 \ll kr : \qquad \psi_{\boldsymbol{k}}(\boldsymbol{r}, z) \sim \left\{ \mathrm{e}^{\mathrm{i}\boldsymbol{k}\cdot\boldsymbol{r}} + f(k) \frac{\mathrm{e}^{\mathrm{i}kr}}{\sqrt{kr}} \left[-\sqrt{\frac{\mathrm{i}}{8\pi}} \right] \right\} \chi_0(z) \quad \text{(II.109)}$$

where $\boldsymbol{r} \equiv (x, y)$. The scattering amplitude $f(k)$ must remain of the form (II.106) and Petrov & Shlyapnikov (2001) were able to relate the two-dimensional scattering length a_2 to the three-dimensional scattering length a. Their result can be written as follows[8]:

$$a_2 = 2.092\, a_{\mathrm{oh}}\, \exp\left(-\sqrt{\frac{\pi}{2}} \frac{a_{\mathrm{oh}}}{a} \right). \quad \text{(II.110)}$$

In practice, as $a \ll a_{\mathrm{oh}}$, this equation leads to extremely low values of a_2. Let us take the case of rubidium atoms ($a \approx 5\,\mathrm{nm}$) confined by a potential of frequency $\omega_z/2\pi = 10\,\mathrm{kHz}$, which leads to $a_{\mathrm{oh}} \approx 100\,\mathrm{nm}$. We then find $a_2 \approx 3\ 10^{-18}\,\mathrm{m}$. This value, 1000 times smaller than the size of the atomic nucleus, has no particular physical significance. It is actually more interesting to return to the expression for the scattering amplitude (II.106), which can be put in the form:

$$f(k) = \frac{1}{\dfrac{1}{\tilde{g}} - \dfrac{1}{2\pi} \ln(\eta'\, k a_{\mathrm{oh}}) + \dfrac{\mathrm{i}}{4}} \qquad \text{with} \quad \eta' = 1.86. \quad \text{(II.111)}$$

and

$$\tilde{g} = \sqrt{8\pi}\, \frac{a}{a_{\mathrm{oh}}}. \quad \text{(II.112)}$$

The parameter $\tilde{g}$ will play a central role in the following chapters, as it will enable us to characterize the strength of interactions between atoms. To understand this role, let us note that the condition of validity of our treatment, $a \ll a_{\mathrm{oh}}$, entails that $\tilde{g} \ll 1$. The $1/\tilde{g}$ term in the denominator of $f(k)$ is therefore larger than 1. Since the wave vectors describing collisions between atoms are of order $1/a_{\mathrm{oh}}$ (at least, they do not differ from this value by orders of magnitude), the term $\ln(\eta'\, k a_{\mathrm{oh}})$ contributing to the denominator of $f(k)$ is of order 1. It follows that the term $1/\tilde{g}$ is largely dominant

[8] The evaluation of the numerical coefficient 2.092 involved in this equation has been improved by Pricoupenko & Olshanii (2007) and it is therefore the value of the latter that we report here.

Region	allowed		forbidden	
Equation	$rR'' + R' + rk^2 R = 0$		$rR'' + R' - rk^2 R = 0$	
Function	$J_0(kr)$	$Y_0(kr)$	$I_0(kr)$	$K_0(kr)$
$kr \to 0$	$1 - \frac{1}{4}(kr)^2$	$\frac{2}{\pi} \ln(\eta\, kr)$	$1 + \frac{1}{4}(kr)^2$	$-\ln(\eta\, kr)$
$kr \to \infty$	$\sqrt{\frac{2}{\pi kr}} \cos\left(kr - \frac{\pi}{4}\right)$	$\sqrt{\frac{2}{\pi kr}} \sin\left(kr - \frac{\pi}{4}\right)$	$\frac{1}{\sqrt{2\pi kr}} \mathrm{e}^{kr}$	$\sqrt{\frac{\pi}{2kr}} \mathrm{e}^{-kr}$
Derivative	$J_0' = -J_1$	$Y_0' = -Y_1$	$I_0' = I_1$	$K_0' = -K_1$

Table II.1. *Summary of the properties of the Bessel functions used in this chapter to determine the radial function $R(r)$. The constant $\eta \approx 0.8905\ldots$ is defined by $\eta = \mathrm{e}^{\gamma}/2$ where $\gamma = 0.5772\ldots$ is the Euler constant.*

compared to the terms $\frac{1}{2\pi} \ln(\eta'\, k a_{\mathrm{oh}})$ and $\mathrm{i}/4$, at least as long as $\tilde{g}$ remains less than 1. We can then approximate

$$\tilde{g} \lesssim 1 : \quad f(k) \approx \tilde{g} \quad \text{(II.113)}$$

corresponding to a constant scattering amplitude.

We will return to this approximation (II.113) in the next chapter as part of a variational approach, and we will come back to the corrective terms to this approximation in chapter 6. We will then show that these corrections are responsible for a "quantum anomaly", which breaks the scale invariance of the 2D problem treated by a classical field.

Appendix: scattering by a square potential

As an example, we present in this paragraph the problem of the scattering of a particle of mass m_r by a potential well ($U_0 < 0$) or a potential barrier ($U_0 > 0$), each with radius b:

$$U(\boldsymbol{r}) = U_0 \quad \text{if } r < b, \qquad U(\boldsymbol{r}) = 0 \quad \text{if } r > b. \quad \text{(II.114)}$$

We set $k_0 = \sqrt{2m_r|U_0|}/\hbar$. In the zone $r > b$, we know that the radial function is a linear combination of the Bessel functions

$$r > b : \qquad R(r) = C_1\, J_0(kr) + C_2\, Y_0(kr) \quad \text{(II.115)}$$

and that the scattering amplitude is related to the coefficients C_1 and C_2 by [*cf.* (II.104)]

$$\frac{C_1}{C_2} = \frac{1+f(k)/4\mathrm{i}}{f(k)/4} \qquad \Longrightarrow \qquad \frac{1}{f(k)} = \frac{1}{4}\frac{C_1}{C_2} + \frac{\mathrm{i}}{4}. \tag{II.116}$$

We then identify the scattering length from the relationship (II.106):

$$k \to 0 : \qquad \frac{1}{f(k)} \approx -\frac{1}{2\pi}\ln(\eta\, k a_2) + \frac{\mathrm{i}}{4}, \tag{II.117}$$

or

$$k \to 0 : \qquad \ln(\eta\, k a_2) \approx -\frac{\pi}{2}\frac{C_1}{C_2}. \tag{II.118}$$

Case of a potential barrier

We consider the case of low-energy scattering, with $k < k_0$. The central region is therefore classically forbidden, and the radial equation for the function $R(r)$ reads in this zone:

$$rR'' + R' - rk_1^2 R = 0 \qquad \text{with} \quad k_1^2 = k_0^2 - k^2 > 0. \tag{II.119}$$

The solutions to this equation are the modified Bessel functions (also known as hyperbolic Bessel functions) $I_0(k_1 r)$ and $K_0(k_1 r)$. Their behavior in the vicinity of 0 is given by

$$x \to 0 : \qquad I_0(x) \approx 1 + \frac{x^2}{4} \tag{II.120}$$

$$K_0(x) \approx -\ln(\eta x). \tag{II.121}$$

The divergence in $\ln(r)$ eliminates the contribution of K_0:

$$r < b : \qquad R(r) = C_0\, I_0(k_1 r) \tag{II.122}$$

and we need to connect this function in $r = b$ with (II.115), ensuring the continuity of the function itself and its first derivative. This requires

$$k_1 \frac{I_0'(k_1 b)}{I_0(k_1 b)} = k \frac{C_1 J_0'(kb) + C_2 Y_0'(kb)}{C_1 J_0(kb) + C_2 Y_0(kb)}. \tag{II.123}$$

Using $J_0'(x) \approx -x/2$ and $Y_0'(x) \approx 2/(\pi x)$ in the vicinity of 0, we can see that we can neglect the contribution of J_0' in front of that of Y_0' in the numerator of the above expression[9]. Since we are interested in the $k \to 0$ limit, we take $k_1 \approx k_0$, $J_0(kb) \approx 1$ and $Y_0(kb) \approx \frac{2}{\pi}\ln(\eta kb)$, and we arrive at

$$\frac{C_1}{C_2} = -\frac{2}{\pi}\ln(\eta\, kb) + \frac{2}{\pi k_0 b}\frac{I_0(k_0 b)}{I_0'(k_0 b)} \tag{II.124}$$

from which we deduce the scattering length (figure II.13):

$$a_2 = b\, \exp\left[-\frac{1}{k_0 b}\frac{I_0(k_0 b)}{I_0'(k_0 b)}\right]. \tag{II.125}$$

In the limit $U_0 \to \infty$ (hard sphere), the scattering length tends to b. The asymptotic behavior of $I_0(x)$ at infinity is indeed

$$x \to \infty : \qquad I_0(x) \sim \frac{\mathrm{e}^x}{\sqrt{2\pi x}} \tag{II.126}$$

so that $I_0(x)/I_0'(x) \sim 1$. In the inverse limit $U_0 \to 0$, we find $a_2 \approx b\exp[-2/(k_0 b)^2]$ which tends exponentially fast to 0.

Case of a potential well

Search for bound states

A cylindrically symmetric bound state of energy $E = -\hbar^2\kappa^2/2m_r$, with $|E| < |U_0|$, is characterized by a radial function solution of

$$rR'' + R' + rk_1^2 R = 0 \qquad \text{with} \quad k_1^2 = k_0^2 - \kappa^2 > 0 \tag{II.127}$$

inside the well (allowed region) and

$$rR'' + R' - r\kappa^2 R = 0 \tag{II.128}$$

outside (forbidden region).

[9] We can *a posteriori* check that the relative amplitude of C_1 and C_2 we end up with is compatible with this approximation.

In the allowed region, the solutions are linear combinations of $J_0(k_1 r)$ and $Y_0(k_1 r)$. The function $Y_0(k_1 r)$ diverges at $r = 0$ and must therefore be eliminated. This leaves

$$r < b : \qquad R(r) = C_0 \; J_0(k_1 r). \tag{II.129}$$

In the forbidden region, the solution is a linear combination of $I_0(\kappa r)$ and $K_0(\kappa r)$. We have already indicated that $I_0(x)$ diverges as $\mathrm{e}^x/\sqrt{2\pi x}$ at infinity and should therefore be discarded. The function $K_0(x)$, on the other hand, behaves like

$$x \to \infty : \qquad K_0(x) \sim \sqrt{\frac{\pi}{2x}}\, \mathrm{e}^{-x} \tag{II.130}$$

and is acceptable. We therefore take in this region:

$$r > b : \qquad R(r) = C_1 \; K_0(\kappa r). \tag{II.131}$$

The boundary connection in $r = b$ imposes

$$k_1 \frac{J_0'(k_1 b)}{J_0(k_1 b)} = \kappa \frac{K_0'(\kappa b)}{K_0(\kappa b)}, \qquad \kappa^2 + k_1^2 = k_0^2, \tag{II.132}$$

which can be used to determine a discrete set of solutions for a fixed value of k_0.

Let us consider the case of a shallow well $k_0 b \ll 1$. Using the expansions of the functions J_0 and K_0 in the vicinity of 0, we find a unique solution to the problem in this case

$$\eta\, \kappa b \approx \mathrm{e}^{-2/k_0^2 b^2}. \tag{II.133}$$

So there is always al least one bound state in a 2D square potential well, but its binding energy may be very weak since it decreases exponentially fast with the depth $|U_0|$. Remember that in 3D, a bound state exists in a square potential well only above a certain threshold value of the depth $|U_0|$.

As we increase the depth of the well, more bound states appear. At the threshold for the appearance of a bound state, we have $\kappa \approx 0$, so that the right-hand member $\kappa K_0'/K_0$ of (II.132) tends to 0 at this point. The appearance of a new bound state therefore corresponds to a zero of $J_0'(k_0 b)$, or $J_1(k_0 b)$ since $J_1(x) = -J_0'(x)$.

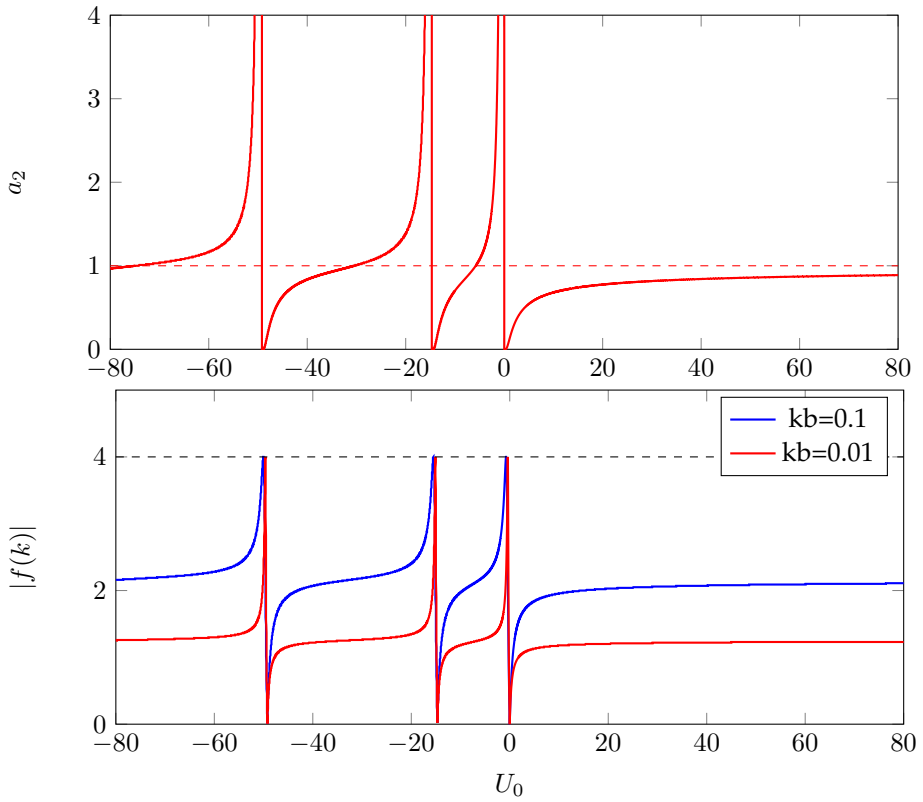

Figure II.13. *Top: variation of the scattering length a_2 (in units of b) as a function of the well depth U_0 (in units of $\hbar^2/(2m_r b^2)$). Bottom: modulus of the scattering amplitude $f(k)$ for two values of the wave vector, $kb = 0.1$ and $kb = 0.01$. This amplitude is calculated directly from (II.116) and (II.123) (or its equivalent when the central region is classically allowed). One can check numerically that this result is very close to the asymptotic expression (II.106).*

Search for scattering states

In the central zone of the well, we keep the form

$$r < b : \qquad R(r) = C_0 \; J_0(k_1 r) \qquad \text{with} \quad k_1^2 = k_0^2 + k^2 \tag{II.134}$$

and we take in the outer zone:

$$r > b : \qquad R(r) = C_1 \, J_0(kr) + C_2 \, Y_0(kr). \tag{II.135}$$

The connection in $r = b$ now imposes for $k \to 0$:

$$\frac{C_1}{C_2} = -\frac{2}{\pi} \, \ln(\eta k b) + \frac{2}{\pi} \, \frac{1}{k_0 b} \, \frac{J_0(k_0 b)}{J_0'(k_0 b)} \tag{II.136}$$

or (figure II.13):

$$a_2 = b \; \exp\left[-\frac{1}{k_0 b} \, \frac{J_0(k_0 b)}{J_0'(k_0 b)} \right]. \tag{II.137}$$

The scattering length therefore diverges at the appearance of each new bound state, since $J_0'(k_0 b)$ cancels out at this point and changes its sign (Levinson's theorem).

For a shallow well ($k_0 b \ll 1$), we find

$$a_2 = b \, \mathrm{e}^{2/(k_0 b)^2} \tag{II.138}$$

which corresponds to a large scattering length. Using (II.133), we find that $\eta \, a_2 \kappa = 1$, so that $\hbar^2/(2 m_r a_2^2)$ is equal (to within a factor of η^2) to the absolute value of the (very low) energy of this bound state.

Chapter III

The quasi-long-range order

We now turn to the description of an interacting two-dimensional gas. We will concentrate on the low-temperature regime, where the state of the gas can be described as a "quasi-condensate", i.e. a condensate with a fluctuating phase (Kagan, Svistunov, et al. 1987; Popov 1987; Petrov, Gangardt, et al. 2004).

We will adopt a classical field description of the atomic fluid, which leads to significant simplifications compared with the quantum description. We will show that this description in terms of the classical field still contains an important quantum element, the quantization of velocity circulation. The latter will play a central role in the following chapter, where we will look at the physics of vortices.

In this chapter, we will be concentrating on the low energy excitations of the gas, i.e. phonons, which dominate at low temperatures. Our key result will be to show that the repulsive interactions between atoms that underlie phonon physics induce quasi-long-range order in the gas, with an algebraic decay of the one-body correlation function $G_1(r)$. This result is radically different from that found for an ideal gas in the previous chapter, where we showed that $G_1(r)$ always decays exponentially with distance in the absence of interactions.

1 The classical field approach

1-1 Optical analogy

Bose-condensed or superfluid states are quantum states of matter. To describe them theoretically, we need to go beyond Boltzmann statistics and take into account the indistinguishability of particles. The Bose–Einstein or Fermi–Dirac quantum statistics that appear in this case make it possible to explain the emergence of the superfluid or superconducting states when particle interactions are taken into account.

From this point of view, the approach we are going to adopt in this chapter and the next one may seem paradoxical: we are going to describe the assembly of N interacting particles by a classical field. Hence the immediate question: isn't this classical field approach contradictory to the quantum phenomenon we are trying to describe? The aim of this first section is to show that this is not the case. One should not confuse the classical treatment of the particles (which we will not do) with the treatment of this gas by a classical field (which we will do). In a sense that we will soon clarify, these two concepts – although both qualified as "classical" – correspond to two opposite limiting cases of the Bose–Einstein distribution.

An optical analogy may be useful at this point. The classical field treatment simply corresponds to solving Maxwell's equations for the electric $\boldsymbol{E}(\boldsymbol{r},t)$ and magnetic fields $\boldsymbol{B}(\boldsymbol{r},t)$. We know that this treatment can be

used to describe a wide range of optical phenomena, including those we might be tempted to describe as "non-classical", such as the operation of a laser. Phenomena that are not describable by this treatment are those where the granularity of light plays an important role, such as the phenomenon of spontaneous emission. Another limitation of the classical field approach originates from the blackbody problem: the energy of the classical field diverges due to the contribution of high-energy, and therefore weakly populated, modes. But for situations where the number of photons in the relevant modes is greater than 1, this restriction is not essential.

1-2 Simplification of the many-body quantum problem

The state of a many-body quantum system is described by its wave function $\Phi(\boldsymbol{r}_1, \ldots, \boldsymbol{r}_N)$ or, more generally, by its density operator $\hat{\rho}$. The idea of the *classical field* treatment is to approximate this quantum state by a statistical mixture of one-body states characterized by a field $\psi(\boldsymbol{r})$, common to the N particles and denoted :

$$|N:\psi\rangle \quad \text{or equivalently} \quad \psi(\boldsymbol{r}_1)\ldots\psi(\boldsymbol{r}_N), \tag{III.1}$$

and called a *Hartree function*. The problem is to find a probability distribution $\mathcal{P}[\psi]$ that reproduces as faithfully as possible the state Φ or the density matrix $\hat{\rho}$. Ideally, for any physical quantity A described by the observable $\hat{A}$, using the functional integral formalism for the field ψ, we would like to have

$$\mathrm{Tr}\left(\hat{A}\,\hat{\rho}\right) = \int \langle N:\psi|\hat{A}|N:\psi\rangle\, \mathcal{P}[\psi]\, \mathrm{d}[\psi]. \tag{III.2}$$

As we will show below on a simple example, it is not always possible to find a function $\mathcal{P}[\psi]$ satisfying all the properties required for a probability distribution, such as positivity and regularity. Rather, for a given problem, one has to find the distribution $\mathcal{P}[\psi]$ that best approximates the many-body quantum state Φ or the density operator $\hat{\rho}$. This search has been the subject of numerous works in quantum optics for photons, using for example the Wigner, Glauber–Sudarshan or Husimi representations (Gardiner & Zoller 2004).

The impossibility of finding a distribution $\mathcal{P}[\psi]$ to represent any state $|\Phi\rangle$ is shown by the following counterexample. We take a system composed of two identical particles, each with two possible states $\uparrow$ and $\downarrow$, and we consider the Bell state

$$|\Phi\rangle = \frac{1}{\sqrt{2}}\left(|1:\uparrow\,;\,2:\downarrow\rangle + |1:\downarrow\,;\,2:\uparrow\rangle\right). \tag{III.3}$$

We are interested in[1] the probability $P_\uparrow$ of finding both particles in the $\uparrow$ state and the probability $P_\downarrow$ of finding both particles in the $\downarrow$ state. These two probabilities are clearly zero for the state $|\Phi\rangle$, whereas they cannot be simultaneously zero if we consider a statistical mixture of one-body functions $|\psi\rangle$. Indeed, these functions can be parameterized by the two angles θ and φ:

$$|\psi\rangle = \cos\theta\,|\uparrow\rangle + \sin\theta\,\mathrm{e}^{\mathrm{i}\varphi}\,|\downarrow\rangle. \tag{III.4}$$

and we find $P_{\uparrow\uparrow} = \langle\cos^4\theta\rangle$, $P_{\downarrow\downarrow} = \langle\sin^4\theta\rangle$. So we have

$$P_{\uparrow\uparrow} + P_{\downarrow\downarrow} = \frac{3}{4} + \frac{1}{4}\langle\cos(4\theta)\rangle \qquad \rightarrow \qquad P_{\uparrow\uparrow} + P_{\downarrow\downarrow} \geq \frac{1}{2}. \tag{III.5}$$

This counter-example is instructive. In the second quantization framework, the vanishing of the probability $P_{\uparrow\uparrow}$ comes from the fact that we have to calculate the mean value of the operator $\hat{a}^\dagger_\uparrow\hat{a}^\dagger_\uparrow\hat{a}_\uparrow\hat{a}_\uparrow$, which is null because we cannot destroy two particles in $\uparrow$ for the state $|\Phi\rangle$. On the other hand, if we consider $\hat{a}^\dagger_\uparrow\hat{a}_\uparrow\hat{a}^\dagger_\uparrow\hat{a}_\uparrow$, we find a non-zero mean value compatible with a classical field representation. This counter-example is thus based on the fact that the commutator $[\hat{a}^\dagger_\uparrow, \hat{a}_\uparrow]$ is non-zero.

This remark gives us the main validity criterion for the classical field representation. As long as we are interested in modes with individual populations much larger than 1, the difference between $\hat{a}^\dagger_\uparrow\hat{a}_\uparrow$ and $\hat{a}_\uparrow\hat{a}^\dagger_\uparrow$, i.e. the commutator $[\hat{a}_\uparrow, \hat{a}^\dagger_\uparrow] = 1$, will not play an important role and the approximation will be relevant. On the other hand, for modes with a population of the order of or smaller than 1, "quantum granularity" effects will be essential and the approximation will be invalid.

1-3 Back to statistical distributions

To explain how the classical field approach is radically different from the classical Boltzmann treatment of particles, it is useful to go back over the

[1] Associated operators: $\hat{A} = |1:\uparrow\,;\,2:\uparrow\rangle\langle 1:\uparrow\,;\,2:\uparrow|$ and $\hat{B} = |1:\downarrow\,;\,2:\downarrow\rangle\langle 1:\downarrow\,;\,2:\downarrow|$.

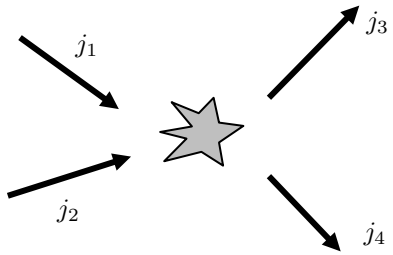

Figure III.1. *Elastic collision between two particles to ensure thermal equilibrium. Energy conservation imposes that* $E_1 + E_2 = E_3 + E_4$.

assumptions underlying the different statistical distributions. Here, we will take up the main lines of an argument we have already presented in the 2015-16 lecture series.

Boltzmann statistics. Implicit in the statistical laws for an ideal gas is an equilibrium balance between different collision processes. Consider a pair of particles in states j_1 and j_2, of energies E_1 and E_2 respectively. These particles can enter into an elastic collision (figure III.1) and exit the collision in two other states, j_3 and j_4, assuming the total energy is conserved:

$$j_1 + j_2 \longrightarrow j_3 + j_4 \quad \text{if} \quad E_1 + E_2 = E_3 + E_4. \tag{III.6}$$

The reverse process $j_3 + j_4 \longrightarrow j_1 + j_2$ is also possible, and at equilibrium the *detailed balance* condition imposes equality between the rates of the two processes:

$$N_{j_1}\, N_{j_2} = N_{j_3}\, N_{j_4} \quad \text{if} \quad E_1 + E_2 = E_3 + E_4. \tag{III.7}$$

Let us assume for simplicity that the population of a state j depends only on the energy E_j of this state, $N_j = N(E_j)$, so the detailed balance relation is written:

$$N(E_1)\, N(E_2) = N(E_3)\, N(E_4) \quad \text{if} \quad E_1 + E_2 = E_3 + E_4. \tag{III.8}$$

A simple mathematical analysis (see course 2015-16) shows that the functions $N(E)$ satisfying this equation are the exponentials of an affine function $aE + b$:

$$N(E) = \mathrm{e}^{aE+b} \equiv \mathrm{e}^{(\mu-E)/k_{\mathrm{B}}T} \qquad \text{with} \quad a = -1/k_{\mathrm{B}}T, \quad b = \mu/k_{\mathrm{B}}T. \tag{III.9}$$

We recover in this way Maxwell-Boltzmann statistics.

Bose-Einstein statistics. The difference with the Boltzmann gas case is that transition probabilities are increased by stimulated emission if the final states are already occupied. The detailed equation is therefore as follows

$$N_{j_1}\, N_{j_2}\, [1 + N_{j_3}]\, [1 + N_{j_4}] = N_{j_3}\, N_{j_4}\, [1 + N_{j_1}]\, [1 + N_{j_2}], \tag{III.10}$$

which can be rewritten as

$$\frac{N_{j_1}}{1 + N_{j_1}}\, \frac{N_{j_2}}{1 + N_{j_2}} = \frac{N_{j_3}}{1 + N_{j_3}}\, \frac{N_{j_4}}{1 + N_{j_4}} \tag{III.11}$$

for any quadruplet of states such that $E_1 + E_2 = E_3 + E_4$. Again we assume that N_j depends only on the energy E_j of state j, and we define

$$G(E) = \frac{N(E)}{1 + N(E)}. \tag{III.12}$$

The function $G(E)$ satisfies an equation identical to that found for Boltzmann statistics

$$G(E_1)\, G(E_2) = G(E_3)\, G(E_4) \quad \text{if} \quad E_1 + E_2 = E_3 + E_4. \tag{III.13}$$

The solutions are $G(E) = \mathrm{e}^{(\mu-E)/k_{\mathrm{B}}T}$, which leads to

$$N(E) = \frac{1}{\frac{1}{G(E)} - 1} = \frac{1}{\mathrm{e}^{(E-\mu)/k_{\mathrm{B}}T} - 1}. \tag{III.14}$$

We have thus recovered Bose-Einstein statistics.

Before moving on to the case of a classical field, it is interesting to distinguish two regimes for Bose–Einstein statistics, depending on the relative values of $E - \mu$ and $k_{\mathrm{B}}T$ [*cf.* figure III.2]:

- If $E - \mu \gg k_{\mathrm{B}}T$, the exponential dominates the denominator of $N(E)$ and we can neglect the "- 1" in front of this exponential. We then find

$$N(E) \approx \mathrm{e}^{-(E-\mu)/k_{\mathrm{B}}T}, \tag{III.15}$$

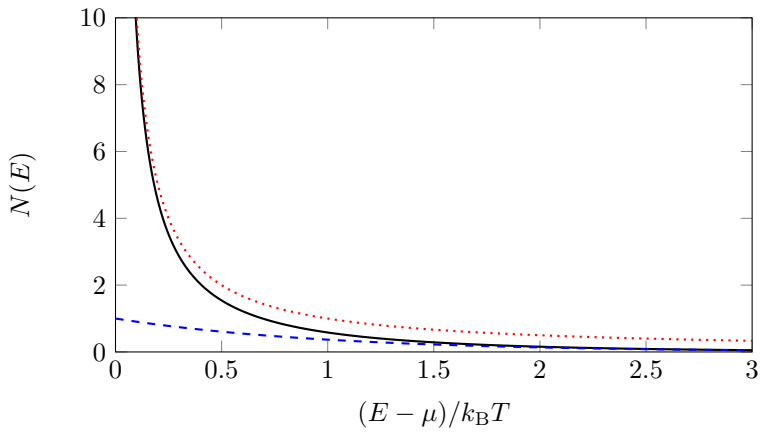

Figure III.2. *Black solid line: Bose-Einstein distribution* $N(E) = 1/[\mathrm{e}^{(E-\mu)/k_{\rm B}T} - 1]$. *Blue dashed line: Maxwell-Boltzmann distribution* $N(E) = \mathrm{e}^{-(E-\mu)/k_{\rm B}T}$. *Red dotted line: distribution for a classical field* $N(E) = \frac{k_{\rm B}T}{E-\mu}$.

i.e. the Boltzmann result. This result is by construction valid if and only if $N(E) < 1$, since we have required the exponential to be dominant in the denominator.

- In the opposite case, $E - \mu \ll k_{\rm B}T$, we can expand the exponential, $\mathrm{e}^{(E-\mu)/k_{\rm B}T} \approx 1 + (E-\mu)/k_{\rm B}T$, similar to the approximation used in the previous chapter in the case of the ideal gas, and we find

$$N(E) \approx \frac{k_{\rm B}T}{E-\mu}. \tag{III.16}$$

This result is by construction valid only if $N(E) > 1$.

We therefore have two approximations of the Bose–Einstein law, depending on whether the mean occupation of a single-particle state is small or large in front of 1. In the first case, we find the result for classical particles à la Boltzmann. The second case, as we have already indicated, corresponds to the domain of validity of the *classical field* approach.

Classical field statistics. As the classical field will play a central role in what follows, it may be useful to show how the approximation (III.16) can be recovered directly from the detailed balance equation obtained for bosons

$$N_{j_1}\ N_{j_2}\ [1+N_{j_3}]\ [1+N_{j_4}] = N_{j_3}\ N_{j_4}\ [1+N_{j_1}]\ [1+N_{j_2}] \tag{III.17}$$

when N_j are greater than 1. If we neglect all the "1 "s in this equation, we get the trivial result that $N_{j_1}N_{j_2}N_{j_3}N_{j_4}$ must be equal to itself. Let us go to the next order, which gives

$$N_{j_1}\ N_{j_2}\ [N_{j_3}+N_{j_4}] = N_{j_3}\ N_{j_4}\ [N_{j_1}+N_{j_2}] \tag{III.18}$$

or

$$\frac{1}{N_{j_1}} + \frac{1}{N_{j_2}} = \frac{1}{N_{j_3}} + \frac{1}{N_{j_4}} \quad \text{if} \quad E_1 + E_2 = E_3 + E_4. \tag{III.19}$$

The solution to this equation is simple: the function $1/N(E)$ must be an affine function of E and can therefore be written as

$$\frac{1}{N(E)} = \frac{E-\mu}{k_{\rm B}T} \quad \rightarrow \quad N(E) = \frac{k_{\rm B}T}{E-\mu}. \tag{III.20}$$

This brings us back to the "high-occupancy" limit of the Bose-Einstein distribution found above. This $N(E) \propto 1/E$ behavior for large enough energies will be characteristic of the equilibrium state of the classical field we will find in this chapter.

Now that we have verified that the classical field approximation correctly describes highly populated, i.e. low-energy modes, the relevance of this approximation to the problem addressed in this year's lecture series becomes clear. We have seen in the preceding chapters that the specificity of the two-dimensional case, with the Mermin-Wagner-Hohenberg theorem, lies in the system's behavior at long wavelengths. These wavelengths are associated with low-energy modes, which will therefore be well described by a classical field. The same applies to the study of Bose-Einstein condensation in the three-dimensional case.

1-4 What is quantum in this problem?

As we have already indicated, the classical field approach amounts to forget about the granularity of matter, by neglecting the commutator $[\hat{a}, \hat{a}^\dagger]$,

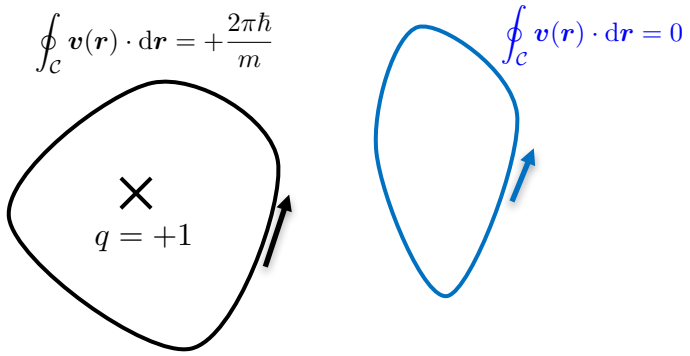

Figure III.3. *Quantification of the circulation of the velocity $\boldsymbol{v}(\boldsymbol{r}) = \frac{\hbar}{m}\boldsymbol{\nabla}\theta$ associated with the classical field $\psi(\boldsymbol{r}) = \sqrt{\rho(\boldsymbol{r})}\,\mathrm{e}^{\mathrm{i}\theta(\boldsymbol{r})}$. The value of the circulation can change only if the contour $\mathcal{C}$ passes over a vortex, i.e. a point where $\rho(\boldsymbol{r})$ cancels out.*

where $\hat{a}$ is the destruction operator of a given mode. Nevertheless, there remains a quantum aspect to the description of the state of the assembly of atoms by a field $\psi(\boldsymbol{r})$. For a two-dimensional gas, the complex field $\psi(\boldsymbol{r})$ is characterized by its amplitude and its phase: $\psi(\boldsymbol{r}) = \sqrt{\rho(\boldsymbol{r})}\,\mathrm{e}^{\mathrm{i}\theta(\boldsymbol{r})}$. This field is associated with a velocity at any point where the phase is defined, i.e. where the density is non-zero:

$$\boldsymbol{v}(\boldsymbol{r}) = \frac{\hbar}{m}\boldsymbol{\nabla}\theta. \tag{III.21}$$

As explained by Svistunov, Babaev, et al. (2015), this equation highlights the relevant parameter $\hbar/m$ of the classical field approach. The mass m of an atom has lost its physical meaning since the granularity of matter has been erased. The same applies to $\hbar$ taken individually. On the other hand, the ratio $\hbar/m$ plays a central role in linking the field ψ to the flow of observable matter.

Once this point has been established, the quantum aspect that remains is clear. It is about *the quantization of the circulation of velocity* on any closed contour not passing through a point where $\rho(\boldsymbol{r})$ vanishes (figure III.3):

$$\oint \boldsymbol{v}(\boldsymbol{r}) \cdot \mathrm{d}\boldsymbol{r} = n\frac{2\pi\hbar}{m}, \qquad n \in \mathbb{Z}. \tag{III.22}$$

This quantification follows directly from the fact that the velocity is proportional to the gradient of a phase. It is essential for the emergence of the notion of topological defects, the vortices, which will constitute the building blocks of the BKT mechanism.

2 The Gross-Pitaevskii Functional

2-1 From quantum to classical fields

Here we consider a fluid composed of identical particles (bosons) with a binary interaction described by the potential $U(\boldsymbol{r}_i - \boldsymbol{r}_j)$. These particles are also trapped by the external potential

$$V_{\mathrm{trap}}^{(3\mathrm{D})}(\boldsymbol{r}) = V_{\mathrm{trap}}^{(1\mathrm{D})}(z) + V_{\mathrm{trap}}^{(2\mathrm{D})}(x, y) \tag{III.23}$$

which induces:

- a strong confinement along the z axis, freezing the corresponding motion and making the gas two-dimensional.
- a weaker confinement in the xy plane, for example in the form of a harmonic potential or a box of size $L \times L$. In this chapter, we will take the box case and assume periodic boundary conditions in the xy plane.

The Hamiltonian of the fluid is:

$$\hat{H} = \sum_{j=1}^{N}\left(\frac{\hat{\boldsymbol{p}}_j^2}{2m} + V_{\mathrm{trap}}^{(3\mathrm{D})}(\hat{\boldsymbol{r}}_j)\right) + \frac{1}{2}\sum_{i\neq j} U(\hat{\boldsymbol{r}}_i - \hat{\boldsymbol{r}}_j). \tag{III.24}$$

It can also be written in second quantization formalism, introducing the operator $\hat{\Psi}(\boldsymbol{r})$, which destroys a particle at point $\boldsymbol{r}$, and its conjugate her-

mitian $\hat{\Psi}^\dagger(\boldsymbol{r})$, which creates a particle at this point:

$$\begin{aligned}\hat{H} &= \int \left(\frac{1}{2m} \boldsymbol{\nabla}\hat{\Psi}^\dagger(\boldsymbol{r}) \cdot \boldsymbol{\nabla}\hat{\Psi}(\boldsymbol{r}) + \hat{\Psi}^\dagger(\boldsymbol{r}) V_{\text{trap}}^{(3\text{D})}(\boldsymbol{r}) \hat{\Psi}(\boldsymbol{r}) \right) \mathrm{d}^3 r \\ &+ \frac{1}{2} \iint \hat{\Psi}^\dagger(\boldsymbol{r}) \hat{\Psi}^\dagger(\boldsymbol{r}')\, U(\boldsymbol{r}-\boldsymbol{r}') \hat{\Psi}(\boldsymbol{r}') \hat{\Psi}(\boldsymbol{r})\, \mathrm{d}^3 r\, \mathrm{d}^3 r'.\end{aligned}$$

The exact treatment of this Hamiltonian is complicated as soon as the interaction potential U is non-zero. In two and three dimensions, for example, it is not possible to simply replace this potential by a contact interaction $U(\boldsymbol{r}) = U_0\, \delta(\boldsymbol{r})$, as this leads to mathematical inconsistencies. On the other hand, this is not a problem in the classical field formalism we described in the first paragraph and which we will now use.

As explained above, a simple way of approaching the bosonic many-body problem (whatever the dimensionality) is to take a Hartree *ansatz* as a class of possible functions:

$$\Phi(\boldsymbol{r}_1, \ldots, \boldsymbol{r}_N) \propto \phi(\boldsymbol{r}_1) \ldots \phi(\boldsymbol{r}_N), \tag{III.25}$$

the function ϕ being normalized here by the number of particles[2]:

$$\int |\phi(\boldsymbol{r})|^2\, \mathrm{d}^3 r = N. \tag{III.26}$$

This *ansatz* is of course inspired by the concept of Bose–Einstein condensation, since all particles are placed in the same state. But the function ϕ here does not correspond to the minimum energy state; it simply provides a possible sampling of the fluid at a given instant. In what follows, this function will have its own dynamics, with amplitude and phase fluctuations playing an important role. These fluctuations can be used to assign a temperature to the fluid and highlight the desired phase transition.

The energy $E(\phi)$ associated with a given function ϕ is calculated from $\langle \Phi | \hat{H} | \Phi \rangle$ by injecting the Hartree ansatz:

$$E(\phi) = \int \left(\frac{\hbar^2}{2m} |\boldsymbol{\nabla}\phi|^2 + V_{\text{trap}}^{(3D)}(\boldsymbol{r}) |\phi(\boldsymbol{r})|^2 \right) \mathrm{d}^3 r \tag{III.27}$$

$$+ \frac{1}{2} \int U(\boldsymbol{r}-\boldsymbol{r}')\, |\phi(\boldsymbol{r})|^2\, |\phi(\boldsymbol{r}')|^2\, \mathrm{d}^3 r\, \mathrm{d}^3 r' \tag{III.28}$$

[2] In the 2015-16 lecture series, we normalized ϕ to unity.

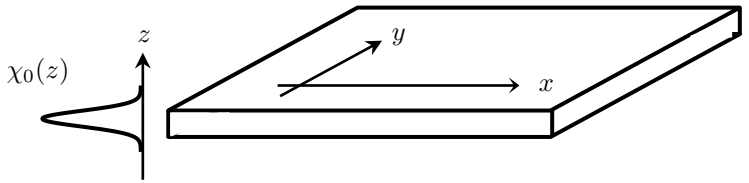

Figure III.4. *Wave function $\chi_0(z)$ corresponding to the freezing of motion in the z direction.*

where we have taken $N - 1 \approx N$.

In this "classical field" approach, there is no problem in modeling the interaction between atoms by a contact interaction

$$U(\boldsymbol{r}-\boldsymbol{r}') = g\, \delta(\boldsymbol{r}-\boldsymbol{r}') \qquad \text{with} \quad g = \frac{4\pi\hbar^2 a}{m}, \tag{III.29}$$

where a is the scattering length associated with the initial potential U. The energy functional (still in 3D for now) is therefore:

$$E(\phi) = \int \left(\frac{\hbar^2}{2m} |\boldsymbol{\nabla}\phi|^2 + V_{\text{trap}}^{(3\text{D})}(\boldsymbol{r}) |\phi(\boldsymbol{r})|^2 + \frac{g}{2} |\phi(\boldsymbol{r})|^4 \right) \mathrm{d}^3 r. \tag{III.30}$$

2-2 Factorization of the frozen degree-of-freedom

We have to take into account the fact that the motion along the z direction is frozen by the strongly confining potential along this axis (figure III.4). We therefore make an additional *ansatz*, which consists in writing the function $\phi(\boldsymbol{r})$ in the factorized form:

$$\phi(x, y, z) = \psi(x, y)\, \chi_0(z) \tag{III.31}$$

where $\chi_0(z)$ is the ground state of the one-particle motion along z:

$$-\frac{\hbar^2}{2m} \frac{\mathrm{d}^2 \chi_0}{\mathrm{d}z^2} + V_{\text{trap}}^{(1\text{D})}(z)\, \chi_0(z) = \epsilon_0\, \chi_0(z), \tag{III.32}$$

which we normalize to unity:

$$\int |\chi_0(z)|^2 \, \mathrm{d}z = 1. \tag{III.33}$$

This factorization assumption is valid if the energy associated with particle interactions and the thermal energy $k_\mathrm{B}T$ are both small compared to the difference between the energy of the ground state of this motion along z and that of its first excited state.

Up to an unimportant additive constant, we arrive at the energy associated with $\psi(x, y)$:

$$E(\psi) = \int \left(\frac{\hbar^2}{2m} |\boldsymbol{\nabla}\psi|^2 + V_\mathrm{trap}^{(2\mathrm{D})}(\boldsymbol{r}) |\psi(\boldsymbol{r})|^2 + \frac{\hbar^2}{2m} \, \tilde{g} \, |\psi(\boldsymbol{r})|^4 \right) \mathrm{d}^2 r, \tag{III.34}$$

where we have introduced the dimensionless number $\tilde{g}$ which characterizes the strength of interactions in this 2D problem:

$$\tilde{g} = 4\pi \, a \int |\chi_0(z)|^4 \, \mathrm{d}z. \tag{III.35}$$

For harmonic confinement of frequency ω_z along the z axis, the state χ_0 is:

$$\chi_0(z) = \frac{1}{(\pi a_\mathrm{oh}^2)^{1/4}} \mathrm{e}^{-z^2 \, / \, (2a_\mathrm{oh}^2)} \qquad \text{with} \quad a_\mathrm{oh} = \sqrt{\frac{\hbar}{m\omega_z}}, \tag{III.36}$$

which leads to

$$\tilde{g} = \sqrt{8\pi} \, \frac{a}{a_\mathrm{oh}}. \tag{III.37}$$

We are back to the dimensionless parameter characteristic of two-dimensional interactions that we already introduced in the previous chapter.

At this stage, it is interesting to write the equation of motion of the field $\psi(\boldsymbol{r})$, i.e. the time-dependent Gross–Pitaevskii equation[3]. Taking isotropic harmonic trapping of frequency ω in the xy plane, we arrive at:

$$\mathrm{i}\frac{\partial \psi}{\partial t} = -\frac{\hbar}{2m} \, \boldsymbol{\nabla}^2 \psi \; + \frac{m}{2\hbar} \omega^2 r^2 \psi \; + \; \frac{\hbar}{m} \, \tilde{g} \, |\psi|^2 \psi \tag{III.40}$$

[3]This equation can also be obtained using the Lagrangian approach, with [cf. lecture series 2015-16]

$$L(\psi) = \int \mathcal{L}_\mathrm{dyn}[\psi(\boldsymbol{r})] \, \mathrm{d}^2 r - E(\psi) \tag{III.38}$$

where the dynamical part of the Lagrangian is, within one total derivative with respect to time:

$$\mathcal{L}_\mathrm{dyn}[\psi(\boldsymbol{r})] = \frac{\mathrm{i}\hbar}{2} \left(\psi^* \dot{\psi} - \dot{\psi}^* \psi \right). \tag{III.39}$$

As announced above, we can verify that the relevant parameter in this equation is $\hbar/m$, together with the trap frequency ω and the interaction parameter $\tilde{g}$. Furthermore, we can check that the total number of particles $N(\psi) = \int |\psi|^2$ and the total energy $E(\psi)$ are conserved quantities for this equation of evolution.

For the sake of simplicity, let us now consider the case of a gas confined in a box of size $L \times L$ with periodic boundary conditions. The total energy (III.34) is the sum of the kinetic energy and the interaction energy:

$$E_\mathrm{kin} = \frac{\hbar^2}{2m} \int |\boldsymbol{\nabla}\psi|^2 \, \mathrm{d}^2 r \qquad\qquad E_\mathrm{int} = \frac{\hbar^2}{2m} \, \tilde{g} \int \rho^2(\boldsymbol{r}) \, \mathrm{d}^2 r \tag{III.41}$$

where we have introduced the surface density at the $\boldsymbol{r}$ point

$$\rho(\boldsymbol{r}) = |\psi(\boldsymbol{r})|^2 \qquad \text{with} \quad \int \rho(\boldsymbol{r}) \, \mathrm{d}^2 r = N. \tag{III.42}$$

The ground state of the system corresponds to the uniform wave function:

$$\psi(\boldsymbol{r}) = \sqrt{\rho} \qquad \text{with} \quad \rho = \frac{N}{L^2}, \tag{III.43}$$

for which only the interaction energy is non-zero:

$$E_\mathrm{int} = \frac{\hbar^2}{2m} \, \tilde{g} \, \rho N. \tag{III.44}$$

To gain some intuition regarding the value of $\tilde{g}$ corresponding to a "strong interaction", we can compare the interaction energy of the ground state with the kinetic energy of the gas if we arrange the N particles on the first N energy states of the box, ranging from energy $E = 0$ to energy E_max (a "fermionized" state[4]). Using the (constant) density of states $D(E)$ determined in Chapter 2, we first determine the value of E_max:

$$N = \int_0^{E_\mathrm{max}} D(E) \, \mathrm{d}E \qquad \text{with} \quad D(E) = \frac{mL^2}{2\pi\hbar^2} \qquad \Longrightarrow \qquad E_\mathrm{max} = \frac{2\pi\hbar^2}{m} \, \rho. \tag{III.45}$$

[4]This is the type of state that appears in the quantum Hall effect (Laughlin state) or in 1D problems (Tonks-Girardeau state).

We deduce the kinetic energy of this fermionized gas:

$$E_{\text{kin, fermion.}} = \int_0^{E_{\max}} E\, D(E)\, \mathrm{d}E = \frac{\pi\hbar^2}{m}\, \rho N. \qquad \text{(III.46)}$$

According to this somewhat arbitrary criterion, we can see that a "strong" interaction corresponds to

$$E_{\text{int}} \sim E_{\text{kin, fermion.}} \qquad \longrightarrow \qquad \tilde{g} \sim 2\pi. \qquad \text{(III.47)}$$

For such a value of $\tilde{g}$, the classical field approach developed here will no longer apply, as the correlations between particles created by interactions are too strong: they are likely to prevent any accumulation of several particles in the same quantum state. In experiments with cold atoms, the value of $\tilde{g}$ is significantly less than 1; for rubidium atoms confined along z by a potential frequency $\omega_z/(2\pi) = 10\,\text{kHz}$, we find $\tilde{g} = 0.24$.

2-3 Ultraviolet cutoff and healing length

Like all classical field theories, modeling the fluid in terms of a wave function $\psi(\boldsymbol{r})$ suffers from a problem of ultra-violet divergence. This is the famous "black body" problem: there are modes of arbitrarily high wave vector $\boldsymbol{q}$, and the equipartition of energy applied to each of these modes leads to a divergence of the physical quantities calculated by summing over $\boldsymbol{q}$. Indeed, as we saw in (III.20), the population of these modes $N(E)$ decays "softly" as $1/E_{\boldsymbol{q}}$, and this soft decay associated with the constant density of states $D(E)$ (for free particles) causes the integral $\int E\ N(E)\ D(E)\ \mathrm{d}E$ to diverge. This problem can only be solved exactly by quantizing the field, which introduces an effective cutoff for modes of frequency $\omega_{\boldsymbol{q}}$ greater than $k_{\mathrm{B}}T/\hbar$ [more precisely, by introducing an exponential decay for $N(E)$, *cf.* (III.15)].

In practice, this divergence will not be a major difficulty for us: we are interested in the long-range behavior of our fluid's correlation functions, which are associated with small wave vectors. Precise knowledge of the physical quantities of interest in the ultraviolet will therefore not be necessary. To eliminate discrepancies, it will be sufficient to establish a cutoff at a wavenumber $\boldsymbol{q}_{\text{cut}}$ given by

$$q_{\text{cut}} \sim \frac{1}{\lambda_T} \qquad \leftrightarrow \qquad \hbar\omega_{\text{cut}} \approx \frac{\hbar^2 q_{\text{cut}}}{2m} \sim k_{\mathrm{B}}T, \qquad \text{(III.48)}$$

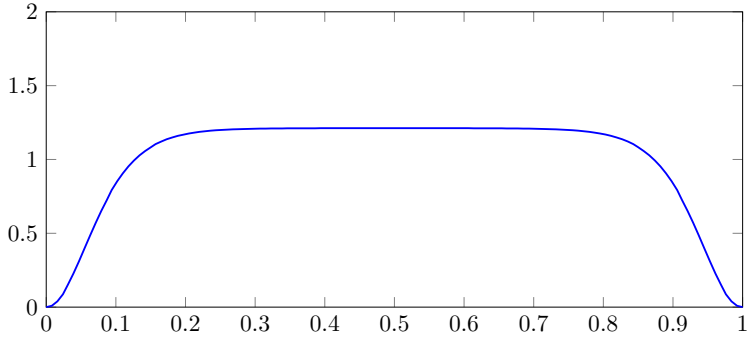

Figure III.5. *The healing length is the characteristic distance required for the density to return to its mean value, when the wave function is forced to cancel at a given point (here, the two ends of the segment).*

at least in the "usual" regime where $k_{\mathrm{B}}T$ is greater than the interaction energy per particle E_{int}/N.

Precise knowledge of fluid behavior on length scales shorter than λ_T would require a treatment beyond our classical approach, but will not be necessary to study the macroscopic phases (superfluid or not) likely to appear. Note that a "semi-classical method" not requiring the introduction of a UV cutoff has been proposed and applied to the case of two-dimensional Bose gas by Giorgetti, Carusotto, et al. (2007). Alternatively, to obtain a more complete theory at least in the regime where the interactions are not strong, we can connect classical field theory for $q < q_{\text{cut}}$ to quantum perfect gas theory for $q > q_{\text{cut}}$ [see for example Prokof'ev & Svistunov (2002)].

The length λ_T therefore does not appear as such in classic field processing, other than in the form of a short distance cut-off put by hand. This is to be expected, since $\lambda_T \propto \hbar/\sqrt{m}$ is not a function of our $\hbar/m$ parameter alone. The other characteristic distance of a quantum gas is the healing length, which can be accessed in this classical field approach. Recall that the healing length is the length scale associated with the interaction energy per particle:

$$\frac{\hbar^2}{2m\xi^2} = \frac{\hbar^2}{m}\,\tilde{g}\rho \qquad \rightarrow \qquad \xi = \frac{1}{\sqrt{2\tilde{g}\rho}}. \qquad \text{(III.49)}$$

It gives the length scale over which the fluid density returns to its normal

value, if we force it to cancel at a point (figure III.5). This point may be the location of a potential bump or the center of a vortex. It is interesting to evaluate the number of missing atoms around this point:

$$\delta N \approx \pi \xi^2 \rho = \frac{\pi}{2\tilde{g}} \tag{III.50}$$

The larger the interaction parameter $\tilde{g}$, the smaller the missing number. For strong enough interactions ($\tilde{g} \gtrsim 1$), this number becomes less than one atom. This defect can then no longer be detected by *in situ* imaging of the gas; it is simply a point where a mathematical singularity occurs.

As we wrote in the previous paragraph, the usual regime for experiments with atomic gases corresponds to an interaction energy per particle that is lower than the thermal energy $k_{\mathrm{B}}T$, which leads to[5]:

$$E_{\mathrm{int}}/N \; < \; k_{\mathrm{B}}T \qquad \rightarrow \qquad \xi > \lambda_T, \tag{III.52}$$

which confirms that ξ can be calculated from classical field simulation, while λ_T corresponds to the cutoff distance, associated with the cutoff energy $\sim k_{\mathrm{B}}T$.

2-4 The "non-linear optics" version

The classical field formalism developed above to describe a macroscopic matter wave applies almost unchanged to the propagation of an intense light field in a nonlinear medium. This basic problem in optics has been the subject of recent experimental research in connection with condensation or quasi-condensation [let us cite in particular Sun, Jia, et al. (2012), as well as a private communication by Robin Kaiser from April 2017].

It should be noted at the outset that this is a different problem from that of photon condensation studied at Bonn, and which we discussed in the previous chapter (Klaers, Schmitt, et al. 2010). In the Bonn experiments, a Fabry-Perot cavity was used to freeze the degree of freedom along z. In what we describe here, the beam propagates freely along the z axis, this

[5] More precisely:

$$\frac{\xi^2}{\lambda_T^2} = \frac{1}{8\pi} \frac{k_{\mathrm{B}}T}{E_{\mathrm{int}}/N}. \tag{III.51}$$

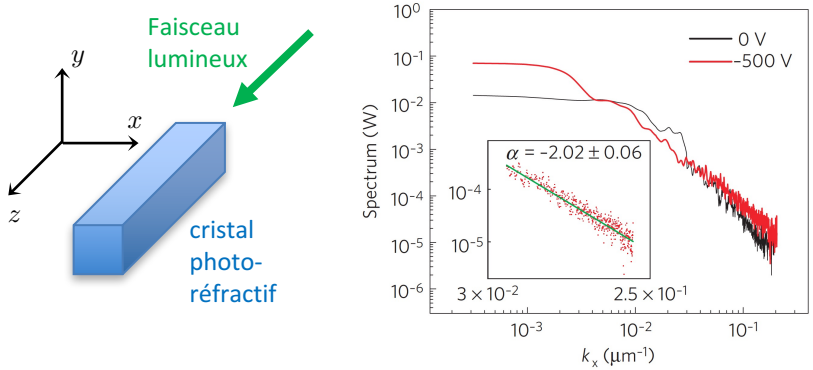

Figure III.6. *Principle of the condensation of classical light waves: a laser beam with a certain disorder in amplitude and phase is sent into a photo-refractive crystal. For a sufficiently long interaction length, the non-linear evolution of the light field leads to a quasi-thermal distribution of the light beam's transverse modes. This distribution is characterized by a decay of the mode population as $1/k_\perp^2$. Figure taken from Sun, Jia, et al. (2012).*

propagation playing the role of time in an effective Schrödinger equation, describing the dynamics of the field in the xy plane perpendicular to the propagation axis.

Let us start with the wave equation for a component $u(\boldsymbol{r}, t)$ of the electric or magnetic field vector in a medium of index n_0. Starting from Maxwell's equations, this equation can be written as:

$$\boldsymbol{\nabla}^2 u - \frac{n_0^2}{c^2} \frac{\partial^2 u}{\partial t^2} = 0. \tag{III.53}$$

A well-known category of solutions is formed by plane waves, such as those propagating along the z axis, $u(\boldsymbol{r}, t) = u_0 \mathrm{e}^{\mathrm{i}(kz - \omega t)}$, with the dispersion relation $\omega = ck/n_0$. Let us look at solutions deduced from these plane waves, written in the form

$$u(\boldsymbol{r}, t) = \psi(\boldsymbol{r}) \; \mathrm{e}^{\mathrm{i}(kz - \omega t)} \tag{III.54}$$

where $\psi(\boldsymbol{r})$ is assumed to be "slowly variable" in space, i.e.

$$\left|\frac{\partial^2\psi}{\partial z^2}\right| \ll k\left|\frac{\partial\psi}{\partial z}\right|. \tag{III.55}$$

By injecting this form for $u(\boldsymbol{r},t)$ into the wave equation (III.53) and neglecting the terms involving $\partial^2\psi/\partial z^2$, we arrive at

$$\mathrm{i}\frac{\partial\psi}{\partial z} = -\frac{1}{2k}\boldsymbol{\nabla}_\perp^2\psi \tag{III.56}$$

where the transverse Laplacian $\boldsymbol{\nabla}_\perp^2$ corresponds to the operator $\partial_x^2+\partial_y^2$. This equation is formally identical to the Schrödinger equation for a two-dimensional free particle, with time replaced by the z coordinate along the axis of propagation. In fact, we can switch to a true time coordinate by introducing $\tau = n_0 z/c$, which parameters the propagation time for a given distance z. The equation (III.56) then becomes

$$\mathrm{i}\frac{\partial\psi}{\partial\tau} = -\frac{\hbar}{2m_{\mathrm{phot}}}\boldsymbol{\nabla}_\perp^2\psi \tag{III.57}$$

where, as in the previous chapter, the effective photon mass $m_{\mathrm{phot}} = n_0^2\,\hbar\omega/c^2$ has been introduced.

For the evolution of ψ to be similar to that of the matter field studied above, we use an optically non-linear medium so that the index n_0 must be replaced by $n_0+n_2|\psi|^2/k^2$. Note that ψ has the dimension of the inverse of a length so that $\int|\psi|^2\,\mathrm{d}^2r$ is dimensionless, so that n_2 is also dimensionless. Injecting this expression into (III.53) and restricting ourselves to the first non-zero term in n_2, we arrive at:

$$\mathrm{i}\frac{\partial\psi}{\partial z} = -\frac{1}{2k}\boldsymbol{\nabla}_\perp^2\psi - \frac{n_2}{n_0 k}\,|\psi|^2\psi \tag{III.58}$$

which has exactly the structure of the Gross–Pitaevskii equation (III.40) in the absence of a trap.

In the experiment by Sun, Jia, et al. (2012), a controlled disorder is imparted to the light beam at the entrance to the nonlinear medium. During propagation, two independent conserved quantities can be defined, the equivalent of the particle number N given by the integral of $|\psi|^2$, and the energy E given by the Gross–Pitaevskii functional. If the interaction length along the z axis is sufficient, the equivalent of a microcanonical ensemble is realized, the output field configuration being a sampling of this ensemble for the chosen pair (N,E). The greater the initial disorder, the greater the energy, and therefore the temperature.

We saw at the beginning of this chapter that for a weakly interacting classical field, thermodynamic equilibrium corresponds to a population of the wave-vector modes $k_\perp$ varying as $T/[E(k_\perp)-\mu]$, with $E(k_\perp)\propto k_\perp^2$ in the paraxial approximation (Connaughton, Josserand, et al. 2005; Picozzi, Garnier, et al. 2014). Remember that this distribution is only valid over a finite interval of $k_\perp$ values, due to the ultraviolet divergence inherent in the classical field theory. In practice, this $k_\perp^{-2}$ distribution is experimentally verified over more than a decade [figure III.6 from Sun, Jia, et al. (2012)]. Furthermore, finite-size effects in this experiment lead to a macroscopic population in the central mode $\boldsymbol{k}_\perp = 0$ (hence the terminology "light-wave condensation").

3 Phase fluctuations and quasi-order

At strictly zero temperature, a relatively weakly interacting 2D Bose gas has the energy of the functional (III.34) and is therefore condensed: it is described by the spatially uniform wave function $\psi = \sqrt{\rho}\,\mathrm{e}^{\mathrm{i}\theta}$, where the density $\rho = N/L^2$ and the phase θ are also uniform, with θ arbitrarily chosen between 0 and 2π (gauge invariance). Its kinetic energy is zero and its interaction energy is:

$$E_{\mathrm{kin}} = 0 \qquad E_{\mathrm{int}} = \frac{\hbar^2}{2m}\,\tilde{g}\,L^2\,\rho^2. \tag{III.59}$$

At non-zero temperature, $\rho(\boldsymbol{r})$ and $\theta(\boldsymbol{r})$ will be functions varying in space under the effect of thermal fluctuations. Characterizing these fluctuations in terms of correlation functions between two points $\boldsymbol{r}$ and $\boldsymbol{r}'$ will allow us to specify the type of order present in the fluid.

3-1 Suppression of density fluctuations

An important point in what follows, at least for the low-temperature region, is the reduction in density fluctuations compared to the ideal gas case, due to repulsive interactions between particles. The link between energy considerations and the reduction of these fluctuations is immediate if we note that the interaction energy (III.41) can be written as

$$E_{\rm int} = \frac{\hbar^2}{2m}\,\tilde{g}\,L^2\,\langle\rho^2(\boldsymbol{r})\rangle \tag{III.60}$$

so that the extra cost in interaction energy compared the zero temperature case is directly proportional to the density fluctuations characterized by (Cohen-Tannoudji & Robilliard 2001)

$$(\Delta\rho)^2 = \langle\rho^2(\boldsymbol{r})\rangle - \rho^2 = [g_2(0)-1]\;\rho^2, \tag{III.61}$$

where $g_2(\boldsymbol{r}) = \langle\rho(\boldsymbol{r})\rho(0)\rangle/\rho^2$ is the density-density correlation function. For a gas described by a classical field $\psi(\boldsymbol{r})$, the quantity $(\Delta\rho)^2$ is always positive, i.e. $g_2(0)\geq 1$, due to the Cauchy-Schwarz inequality:

$$L^2\int\rho^2(\boldsymbol{r})\,{\rm d}^2r \geq \left(\int\rho(\boldsymbol{r})\,{\rm d}^2r\right)^2 \tag{III.62}$$

so that the interaction energy is always greater in the presence of thermal fluctuations than at zero temperature.

For an ideal Bose gas in the absence of a condensate, which is the case at 2D if $T\neq 0$, we always have $g_2(0)=2$. This result is obtained by expressing the operator $\hat\rho(\boldsymbol{r})$ in terms of the field operator, developed on the basis of 2D plane waves:

$$\hat\rho(\boldsymbol{r}) = \hat\Psi^\dagger(\boldsymbol{r})\hat\Psi(\boldsymbol{r}) \qquad \text{with} \quad \hat\Psi(\boldsymbol{r}) = \frac{1}{L}\sum_{\boldsymbol{p}} {\rm e}^{{\rm i}\boldsymbol{p}\cdot\boldsymbol{r}/\hbar}\hat a_{\boldsymbol{p}}. \tag{III.63}$$

For example, choosing the point $\boldsymbol{r}=0$, we obtain:

$$\langle\hat\rho^2(0)\rangle = \frac{1}{L^4}\sum_{\boldsymbol{p}_1,\boldsymbol{p}_2,\boldsymbol{p}_3,\boldsymbol{p}_4}\langle\hat a^\dagger_{\boldsymbol{p}_1}\hat a^\dagger_{\boldsymbol{p}_2}\hat a_{\boldsymbol{p}_3}\hat a_{\boldsymbol{p}_4}\rangle. \tag{III.64}$$

If there is no macroscopically populated state, we can neglect in this sum the contribution of terms where $\boldsymbol{p}_1=\boldsymbol{p}_2$, $\boldsymbol{p}_3=\boldsymbol{p}_4$. For the other terms, using the fact that the density operator at thermal equilibrium is diagonal in the $\boldsymbol{p}$ basis, we note that a term of the type $\langle\hat a^\dagger_{\boldsymbol{p}_1}\hat a^\dagger_{\boldsymbol{p}_2}\hat a_{\boldsymbol{p}_3}\hat a_{\boldsymbol{p}_4}\rangle$ is non-zero if and only if

$$\{\boldsymbol{p}_1=\boldsymbol{p}_3 \text{ and } \boldsymbol{p}_2=\boldsymbol{p}_4\} \qquad \text{or} \qquad \{\boldsymbol{p}_1=\boldsymbol{p}_4 \text{ and } \boldsymbol{p}_2=\boldsymbol{p}_3\}, \tag{III.65}$$

each of the two options having the same contribution. We thus have:

$$\langle\hat\rho^2(0)\rangle \approx 2\sum_{\boldsymbol{p}_1,\boldsymbol{p}_2}\langle\hat a^\dagger_{\boldsymbol{p}_1}\hat a_{\boldsymbol{p}_1}\rangle\langle\hat a^\dagger_{\boldsymbol{p}_2}\hat a_{\boldsymbol{p}_2}\rangle = 2\left(\langle\hat\rho(0)\rangle\right)^2. \tag{III.66}$$

For an interacting gas, on the other hand, the energy $E_{\rm int}$ always ends up dominating if we go to a sufficiently low temperature. The interaction energy per particle, which is of the order of $\frac{\hbar^2}{2m}\tilde g\,\rho$, in fact always becomes greater than $k_{\rm B}T$ if T is sufficiently low. More precisely:

$$\frac{\frac{\hbar^2}{2m}\tilde g\,\rho}{k_{\rm B}T} = \frac{\tilde g}{4\pi}\,\mathcal{D} \tag{III.67}$$

where we have introduced the phase-space density

$$\mathcal{D} = \rho\lambda_T^2 \qquad \text{with} \quad \lambda_T = \frac{\hbar\sqrt{2\pi}}{\sqrt{mk_{\rm B}T}}. \tag{III.68}$$

Therefore, for a phase-space density such that

$$\mathcal{D} \gg \frac{4\pi}{\tilde g}, \tag{III.69}$$

any significant change in density from its mean value, leading to a value of $g_2(0)$ significantly greater than 1, will be prohibitively expensive compared to $k_{\rm B}T$.

3-2 Effective Hamiltonian at low energy

In the limit where density fluctuations can be neglected, the gradient of the wave function $\psi(\boldsymbol{r})$ involved in the kinetic energy term is

$$\boldsymbol{\nabla}\psi = \boldsymbol{\nabla}\left(\sqrt{\rho(\boldsymbol{r})}\,{\rm e}^{{\rm i}\theta(\boldsymbol{r})}\right) \approx \sqrt{\rho}\;({\rm i}\,\boldsymbol{\nabla}\theta)\;{\rm e}^{{\rm i}\theta(\boldsymbol{r})} \tag{III.70}$$

so that the kinetic energy term becomes

$$E_{\rm kin} \approx \frac{\hbar^2}{2m}\,\rho\int (\boldsymbol{\nabla}\theta)^2\ {\rm d}^2r. \qquad \text{(III.71)}$$

This expression for energy reflects the phase rigidity of the system: the relevant excitations are the phase fluctuations, and their energy is related to the price to be paid for "twisting" this phase between two zones of the sample.

We showed in the 2015-16 course that this notion of phase rigidity can be used to rigorously define the superfluid density in a homogeneous gas. From this point of view, the expression (III.71) shows that implicitly, a 2D system described by the Gross–Pitaevskii energy functional is superfluid if its density fluctuations are totally neglected. Moreover, its superfluid density ρ_s – i.e. the coefficient in front of $(\boldsymbol{\nabla}\theta)^2$ – is equal to the total density ρ.

This point of view using (III.71) and leading to $\rho_s = \rho$ is certainly valid at very low temperatures, but does not account for the observed decrease in superfluid density with increasing temperature. To account for this decrease rigorously, we need to

- perform a coupled treatment of phase and density fluctuations, which we will do using Bogoliubov method later on;
- take into account vortices which, as we will see in the next chapter, can exist in the superfluid part in the form of pairs of vortices of opposite signs.

We can also proceed phenomenologically, by introducing "by hand" a superfluid density ρ_s, which depends on temperature, and which leads to the energy

$$E_{\rm kin} \approx \frac{\hbar^2}{2m}\,\rho_s(T)\int (\boldsymbol{\nabla}\theta)^2\ {\rm d}^2r. \qquad \text{(III.72)}$$

This renormalization of ρ to ρ_s is a simple way of absorbing all non-essential thermal fluctuations, including density fluctuations over short distances, in order to concentrate on long-distance physics and the long-range quasi-order likely to emerge.

It should be clear that the energy $E_{\rm kin}$ given in (III.72) cannot be considered as a microscopic Hamiltonian, if only because it depends on temperature via ρ_s. This quantity describes in fact the increase of the free energy of the gas if we impose the superfluid current $(\hbar/m)\ \boldsymbol{\nabla}\theta$ [see, for example, the discussion in the appendix to the article by Bloch, Dalibard, et al. 2008].

3-3 Fourier analysis of phase fluctuations

Based on the phenomenological expression (III.72) for the energy associated with a phase fluctuation $\theta(\boldsymbol{r})$, we want to evaluate the function $G_1(r)$ describing the correlations between two points in the system:

$$G_1(\boldsymbol{r}) = \langle\psi(\boldsymbol{r})\ \psi^*(0)\rangle = \rho\ \langle {\rm e}^{{\rm i}[\theta(\boldsymbol{r})-\theta(0)]}\rangle. \qquad \text{(III.73)}$$

We first need to determine the fluctuations of $\theta(\boldsymbol{r})-\theta(0)$, which we will do by expanding the function $\theta(\boldsymbol{r})$ in Fourier series and applying the energy equipartition theorem.

Let us start by writing the phase $\theta(\boldsymbol{r})$ in the form

$$\theta(\boldsymbol{r}) = \sum_{\boldsymbol{q}} c_{\boldsymbol{q}}\, e^{i\boldsymbol{q}\cdot\boldsymbol{r}} \qquad \text{(III.74)}$$

where the reality of θ results in

$$c^*_{\boldsymbol{q}} = c_{-\boldsymbol{q}}. \qquad \text{(III.75)}$$

Note that such an expansion, however natural it may seem given the periodic boundary conditions, is not trivial: it does not account for the periodicity of the function ${\rm e}^{{\rm i}\theta}$ when $\theta \to \theta + 2\pi$. This is not a problem if we restrict ourselves to situations where θ varies smoothly and regularly over the sample, but it neglects vortices from the outset, which are points around which the phase varies from 0 to 2π over arbitrarily short distances.

We inject the expansion (III.74) into the energy (III.72) and obtain:

$$E_{\rm kin} = \rho_s L^2 \sum_{\boldsymbol{q}} \frac{\hbar^2 q^2}{2m}\,|c_{\boldsymbol{q}}|^2. \qquad \text{(III.76)}$$

To take account of the fact that the modes $\boldsymbol{q}$ and $-\boldsymbol{q}$ are linked by (III.75), we can restrict the sum on $\boldsymbol{q}$ to $q_x > 0$ and write:

$$E_{\rm kin} = \sum_{\boldsymbol{q},q_x>0} \epsilon_{\boldsymbol{q}} \, |c_{\boldsymbol{q}}|^2 \qquad \text{with} \quad \epsilon_{\boldsymbol{q}} = \rho_s L^2 \, \frac{\hbar^2 q^2}{m}. \tag{III.77}$$

The probability of occurrence of a configuration corresponding to a given $\{c_{\boldsymbol{q}}\}$ given is given by Boltzmann's law:

$$\mathcal{P}[\{c_{\boldsymbol{q}}\}] \propto \prod_{\boldsymbol{q}} \mathrm{e}^{-\epsilon_{\boldsymbol{q}}|c_{\boldsymbol{q}}|^2/k_{\rm B}T}. \tag{III.78}$$

The $c_{\boldsymbol{q}}$ with $q_x > 0$ are therefore complex independent Gaussian variables. By decomposing them into real and imaginary parts,

$$c_{\boldsymbol{q}} = c'_{\boldsymbol{q}} + \mathrm{i}c''_{\boldsymbol{q}} \qquad \text{with} \quad c'_{\boldsymbol{q}} = c'_{-\boldsymbol{q}} \quad \text{and} \quad c''_{\boldsymbol{q}} = -c''_{-\boldsymbol{q}} \tag{III.79}$$

we find at thermal equilibrium :

$$\langle (c'_{\boldsymbol{q}})^2 \rangle = \langle (c''_{\boldsymbol{q}})^2 \rangle = \frac{k_{\rm B}T}{2\epsilon_{\boldsymbol{q}}}. \tag{III.80}$$

Note that we find here that the average population $\langle |c_{\boldsymbol{q}}|^2 \rangle$ of a given mode $\boldsymbol{q}$ is equal to $k_{\rm B}T/\epsilon_q$, as we announced in (III.20) when laying the foundations of classical field theory.

3-4 Phase correlations at thermal equilibrium

We consider now the phase difference $\theta(\boldsymbol{r}) - \theta(0)$ that appears in (III.73). We have :

$$\begin{aligned} \theta(\boldsymbol{r}) - \theta(0) &= \sum_{\boldsymbol{q}} \left(c'_{\boldsymbol{q}} + \mathrm{i}c''_{\boldsymbol{q}}\right) \left(\mathrm{e}^{\mathrm{i}\boldsymbol{q}\cdot\boldsymbol{r}} - 1\right) \\ &= -2 \sum_{\boldsymbol{q},q_x>0} \left\{ c'_{\boldsymbol{q}} \left[1 - \cos(\boldsymbol{q}\cdot r)\right] + c''_{\boldsymbol{q}} \sin(\boldsymbol{q}\cdot\boldsymbol{r}) \right\} \end{aligned} \tag{III.81}$$

which, when averaged over the square of this expression at thermal equilibrium, gives

$$\begin{aligned} \langle [\theta(\boldsymbol{r}) - \theta(0)]^2 \rangle &= 4 \sum_{\boldsymbol{q},q_x>0} \langle (c'_{\boldsymbol{q}})^2 \rangle \left[1 - \cos(\boldsymbol{q}cdot\boldsymbol{r})\right]^2 + \langle (c''_{\boldsymbol{q}})^2 \rangle \sin^2(\boldsymbol{q}\cdot\boldsymbol{r}) \\ &= 4 \sum_{\boldsymbol{q},q_x>0} \frac{k_{\rm B}T}{\epsilon_{\boldsymbol{q}}} \left[1 - \cos(\boldsymbol{q}\cdot\boldsymbol{r})\right] \\ &= 2 \sum_{\boldsymbol{q}} \frac{k_{\rm B}T}{\epsilon_{\boldsymbol{q}}} \left[1 - \cos(\boldsymbol{q}\cdot\boldsymbol{r})\right] \end{aligned} \tag{III.82}$$

where we relaxed the $q_x > 0$ constraint in the last line by dividing by a factor 2. By transforming this discrete sum into an integral, we arrive at

$$\begin{aligned} \langle [\theta(\boldsymbol{r}) - \theta(0)]^2 \rangle &= 2 \, \frac{L^2}{4\pi^2} \int \frac{k_{\rm B}T}{\epsilon(\boldsymbol{q})} \left[1 - \cos(\boldsymbol{q}\cdot\boldsymbol{r})\right] \, \mathrm{d}^2 q \\ &= \frac{1}{\pi} \, \frac{1}{\rho_s \lambda_T^2} \int \frac{1 - \cos(\boldsymbol{q}\cdot\boldsymbol{r})}{q^2} \, \mathrm{d}^2 q. \end{aligned} \tag{III.83}$$

The function

$$f(\boldsymbol{r}) = \frac{1}{(2\pi)^2} \int \frac{1 - \cos(\boldsymbol{q}\cdot\boldsymbol{r})}{q^2} \, \mathrm{d}^2 q \tag{III.84}$$

can be estimated by noting that its Laplacian has a simple expression:

$$\nabla^2 f(\boldsymbol{r}) = \frac{1}{(2\pi)^2} \int \cos(\boldsymbol{q}\cdot\boldsymbol{r}) \, \mathrm{d}^2 q = \frac{1}{(2\pi)^2} \int \mathrm{e}^{\mathrm{i}\boldsymbol{q}\cdot\boldsymbol{r}} \, \mathrm{d}^2 q = \delta(\boldsymbol{r}) \tag{III.85}$$

which can be integrated in two dimensions[6] in

$$f(\boldsymbol{r}) = \frac{1}{2\pi} \, \ln(r) + \text{constant}. \tag{III.87}$$

However, it is not immediate to fix the relevant value of the constant, since this function admits no finite limit at either short or long distance.

[6] This is the two-dimensional equivalent of

$$\text{3D}: \qquad \nabla^2 f(\boldsymbol{r}) = \delta(\boldsymbol{r}) \qquad \Rightarrow \qquad f(\boldsymbol{r}) = \frac{1}{4\pi r} + \text{constant}. \tag{III.86}$$

For what follows, it is instructive to evaluate this integral "by hand", by cutting – for a given value of r – the space of wave vectors into two parts, as we did in the first chapter when studying a crystal:

$$(2\pi)^2\ f(\boldsymbol{r}) \;=\; \int_{|\boldsymbol{q}|<\pi/r} \frac{1-\cos(\boldsymbol{q}\cdot\boldsymbol{r})}{q^2}\,\mathrm{d}^2q + \int_{|\boldsymbol{q}|>\pi/r} \frac{1-\cos(\boldsymbol{q}\cdot\boldsymbol{r})}{q^2}\,\mathrm{d}^2q \tag{III.88}$$

$$\approx \int_{|\boldsymbol{q}|<\pi/r} \frac{(\boldsymbol{q}\cdot\boldsymbol{r})^2/2}{q^2}\,\mathrm{d}^2q \;+\; \int_{|\boldsymbol{q}|>\pi/r} \frac{1}{q^2}\,\mathrm{d}^2q \tag{III.89}$$

The first part, in which we have replaced the cosine by its approximation in the vicinity of 0, gives a constant contribution after integration, equal to $\pi/4$. The second part, in which we have taken a zero mean for the cosine, diverges on the side of large values of q. As explained above, we put a cutoff at the wave vector π/λ_T and arrive at

$$f(\boldsymbol{r}) \approx \frac{\pi}{16} + \frac{1}{2\pi}\ln(r/\lambda_T). \tag{III.90}$$

or, neglecting the constant term in front of the logarithm, which is *a priori* large in front of 1 if we are interested in large values of r:

$$f(\boldsymbol{r}) \approx \frac{1}{2\pi}\ln(r/\lambda_T). \tag{III.91}$$

We now have all the ingredients we need to evaluate the phase correlation function. First, we find:

$$\langle[\theta(\boldsymbol{r})-\theta(0)]^2\rangle \approx \frac{2}{\rho_s\lambda_T^2}\ln(r/\lambda_T) \tag{III.92}$$

then by injecting this result into the G_1 function and using the result $\langle \mathrm{e}^{\mathrm{i}u}\rangle = \mathrm{e}^{-\langle u^2\rangle/2}$ for a Gaussian variable u:

$$\begin{aligned} G_1(r) &= \langle\psi(\boldsymbol{r})\,\psi^*(0)\rangle \\ &\approx \rho\,\langle \mathrm{e}^{\mathrm{i}[\theta(\boldsymbol{r})-\theta(0)]}\rangle \\ &\approx \rho\,\mathrm{e}^{-\langle[\theta(\boldsymbol{r})-\theta(0)]^2\rangle/2} \\ &\approx \rho\left(\frac{\lambda_T}{r}\right)^{\alpha} \qquad \text{with} \quad \alpha = \frac{1}{\rho_s\lambda_T^2}. \end{aligned} \tag{III.93}$$

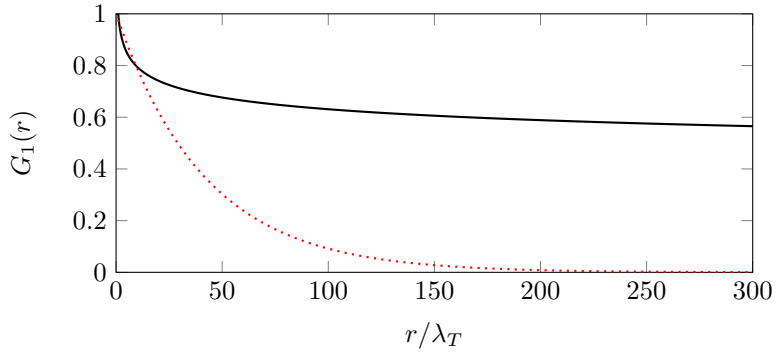

Figure III.7. *Black solid line: variation of G_1 for a phase-space density $\mathcal{D} = 10$ for the algebraic case (in the presence of interactions), $G_1(r) \sim (\lambda_T/r)^{1/\mathcal{D}}$. Red dotted line: non-interacting case, $G_1(r) \sim \mathrm{e}^{-r/\ell}$ with $\ell = (\lambda_T/\sqrt{4\pi})\ \mathrm{e}^{\mathcal{D}/2} \approx 40\,\lambda_T$.*

We therefore find an algebraic decay for the function $G_1(r)$ when $r \to \infty$. This conclusion is compatible with the Mermin-Wagner-Hohenberg theorem, which is reassuring. But we note that this decay is much slower than that found for the ideal gas in the previous chapter, which was exponential in $\mathrm{e}^{-r/\ell}$ with $\ell = (\lambda_T/\sqrt{4\pi})\ \mathrm{e}^{\rho\lambda_T^2/2}$. Moreover, we will see in the next chapter that the superfluid phase, when it exists, always verifies $\rho_s\lambda_T^2 > 4$, which means that the decay (III.93) is always slower than $r^{-1/4}$.

Practical Example. At this point, it is useful to look at a realistic example to see how the case of the interacting gas differs from that of the ideal gas. To simplify, let us take $\rho = \rho_s$ and consider a phase-space density $\mathcal{D} = \rho\lambda_T^2 = 10$, corresponding to a fairly strongly degenerate gas (figure III.7).

- For the ideal gas, we find a characteristic decay distance $\ell \approx 40\lambda_T$. For a sample of size $L = 300\,\lambda_T$, the function $G_1(r)$ decreases by a factor > 1000 from one edge of the sample to the other: there is no appreciable phase coherence at this distance.
- Let us move on to an interacting gas, for which the algebraic decay

(III.93) tells us that the function $G_1(r)$ decreases between $r = \lambda_T$ and $r = L$ by the factor $(300)^{1/10} < 2$: there remains a strong phase coherence between the two edges of the sample, comparable to what we would expect for a true condensate.

This example shows how the change in decay type, from exponential to algebraic, radically alters the phase coherence of this system. This coherence is induced by repulsive interactions, which are responsible for freezing density fluctuations. In systems of reasonable finite size, it is also responsible for a significant condensed fraction. The condensed fraction in a system of size L can indeed be defined as the value of $G_1(L)$ [*cf.* lecture series 2015-16] and the example above shows us that for the parameters considered, the condensed fraction is greater than 50 %, once the repulsive interactions have played their role as "density smoother".

More generally, these considerations show just how tricky the notion of a thermodynamic limit can be for a system reduced-dimension. If, in accordance with the Mermin-Wagner theorem, we define this limit as a gas whose condensed fraction $G_1(L)$ does not exceed 1 % (arbitrary, but meaningful value), we see that the size L to be taken is

$$\left(\frac{\lambda_T}{L}\right)^{\alpha} = 0.01 \quad \rightarrow \quad L = \frac{\lambda_T}{(0.01)^{1/\alpha}} = 10^{20}\ \lambda_T. \tag{III.94}$$

Here we return to the famous argument of Bramwell & Holdsworth (1994) who, in the context of the magnetization of 2D systems, showed that samples the size of the "state of Texas" would be needed to reach the thermodynamic limit.

We are therefore in a subtle situation where Mermin–Wagner's theorem precludes long–range order and the appearance of a condensate at the thermodynamic limit, but where interactions between atoms make it possible to establish a quasi-order which, in many realistic cases of finite size, "simulates" the existence of a true condensate.

3-5 The xy model and its implementation with atoms

The effective Hamiltonian we have studied in this section, $\hat{H} \propto \int (\boldsymbol{\nabla}\theta)^2$, has a discrete version which is a model widely used in statistical physics,

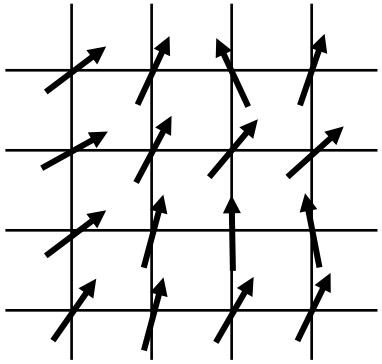

Figure III.8. *The two-dimensional xy model, which can be considered as the discretized version of the Bose gas whose density fluctuations have been frozen.*

the xy model [see for example Kardar (2007)]. We consider a regular lattice with a unit vector $\boldsymbol{S_j}$ at each site $\boldsymbol{j}$ of the lattice. This vector evolves in a fictitious two-dimensional space (hence the name xy model). This vector can be parameterized by the angle $\theta_{\boldsymbol{j}}$ it makes with a reference direction (θ_j is defined modulo 2π). In the 2D problem we are interested in, the regular lattice is itself of dimension 2; it can be a square lattice, as shown in figure III.8, or a triangular lattice.

In the simplest version of the xy model, we restrict ourselves to an interaction between neighboring sites, written as follows

$$\hat{H} = -J \sum_{\langle \boldsymbol{i},\boldsymbol{j}\rangle} \boldsymbol{S_i} \cdot \boldsymbol{S}_j = -J \sum_{\langle \boldsymbol{i},\boldsymbol{j}\rangle} \cos\left(\theta_{\boldsymbol{j}} - \theta_{\boldsymbol{j}}\right). \tag{III.95}$$

The choice $J > 0$ leads to a ground state where all $\theta_{\boldsymbol{j}}$ are equal. Low-energy excitations correspond to slow variations of the $\theta_{\boldsymbol{j}}$'s, so that an expansion of the cosine yields the Hamiltonian $\int (\boldsymbol{\nabla}\theta)^2$ after passing to the continuous limit. The xy model thus leads to a behavior similar to the continuous model we studied: at low temperatures, algebraic decay of the one-body correlation function as seen above; above a critical temperature, BKT transition to a completely disordered state similar to what we will see in the next course. The advantage of this lattice-based model is that it naturally

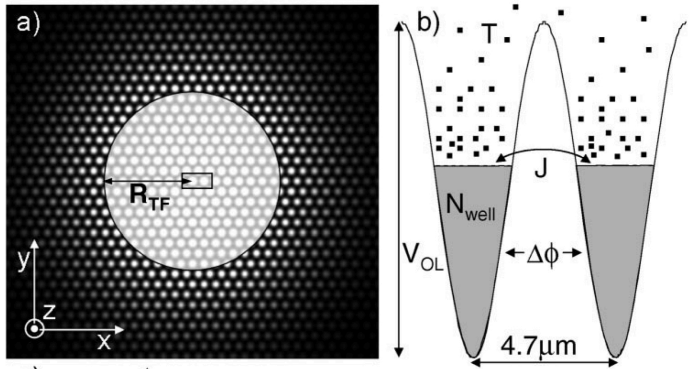

Figure III.9. *A triangular array of micro-condensates trapped at the nodes of an optical lattice, with tunnel coupling between close neighbors. Each site contains around 7,000 atoms, ensuring that the phase of a micro-condensate is well defined. This experiment is a practical implementation of the xy model. Figure taken from Schweikhard, Tung, et al. (2007).*

provides a high-energy cutoff that avoids ultraviolet divergences, and allows the use of resolution methods specific to periodic models, such as transfer matrices.

This xy model was realized experimentally with a gas of cold atoms by Schweikhard, Tung, et al. (2007). Starting with a 3D condensate of approximately spherical shape, the Boulder researchers used an optical lattice to cut out around 200 vertical tubes forming a triangular lattice in a horizontal plane (figure III.9). Each tube contains around 7,000 atoms; this number is sufficiently large for each tube to constitute a micro-condensate of well-defined phase, which plays the role of the θ_j variable in the xy model. Each tube is tunnel-coupled to its six neighbors, creating the equivalent of Josephson junctions. The tunnel matrix element plays the role of the coupling J of the xy Hamiltonian. We will not go any further for the moment in describing this experiment; let us just note that, like those carried out on continuous gases, it enabled one to observe the BKT mechanism by detecting, above a critical value of the J/T parameter, the proliferation of vortices when all the micro-condensates are fused together.

4 The Bogoliubov approach

We now go beyond the "frozen density" approach developed in the previous paragraph, to gain a more complete view of the dynamics of the fluid in the low-temperature regime. To this end, we are going to use the Bogoliubov formalism, in a version adapted to the case of quasi-condensates by Mora & Castin (2003) and Castin (2004)[7]. The idea is not to write, as in 3D, $\psi(\boldsymbol{r}) = \psi_0 + \delta\psi(\boldsymbol{r})$ with $\psi_0 = \sqrt{\rho_0}\, \mathrm{e}^{\mathrm{i}\theta_0}$, where $\delta\psi$ would be at any point smaller than ψ_0; indeed, there is no homogeneous phase θ_0 in our 2D fluid. Our approach will be to expand the density fluctuations and allow the phase to vary significantly over the sample area (while remaining expandable in a Fourier series, which excludes vortices as before).

4-1 Equations of motion for the amplitude and the phase

Starting from the expression $\psi(\boldsymbol{r},t) = \sqrt{\rho(\boldsymbol{r},t)}\, \mathrm{e}^{\mathrm{i}\theta(\boldsymbol{r},t)}$, we assume that the phase θ varies slowly in space and can be developed as a Fourier series, as in the previous paragraph:

$$\theta(\boldsymbol{r},t) = \sum_{\boldsymbol{q}} c_{\boldsymbol{q}}(t)\, e^{i\boldsymbol{q}\cdot\boldsymbol{r}}\,. \tag{III.96}$$

We also assume that relative density fluctuations are small. As indicated above [*cf.* (III.69)], this assumption is valid provided the phase-space density is sufficiently large. The density can then be written as

$$\rho(\boldsymbol{r},t) = \rho_0\,(1\,+\,2\eta(\boldsymbol{r},t)) \qquad \text{with} \quad \rho_0 = \frac{N}{L^2} \quad \text{et} \quad \eta \ll 1. \tag{III.97}$$

The function η can also be expanded into a Fourier series:

$$\eta(\boldsymbol{r},t) = \sum_{\boldsymbol{q}} d_{\boldsymbol{q}}(t)\, e^{i\boldsymbol{q}\cdot\boldsymbol{r}}. \tag{III.98}$$

[7] The program of Mora & Castin (2003) is in fact more ambitious than ours, since it involves giving meaning to the density and phase operators within the framework of quantum field theory. This is possible in an approximate way by discretizing space and ensuring that each lattice site contains on average a sufficiently large number of particles.

The functions θ and η are real, which implies $c^*_{\boldsymbol{q}} = c_{-\boldsymbol{q}}$ and $d^*_{\boldsymbol{q}} = d_{-\boldsymbol{q}}$. The conservation of the norm leads to

$$\int \eta \, d^3r = 0 \qquad \rightarrow \qquad d_0 = 0. \tag{III.99}$$

The energy functional (III.34)

$$\begin{aligned} E[\psi] &= \frac{\hbar^2}{2m} \int \left(|\boldsymbol{\nabla}\psi|^2 + \tilde{g}|\psi|^4 \right) \, \mathrm{d}^2 r \\ &= \frac{\hbar^2}{2m} \int \left(\rho (\boldsymbol{\nabla}\theta)^2 \, + \, \frac{(\boldsymbol{\nabla}\rho)^2}{4\rho} \, + \, \tilde{g}\rho^2 \right) \, \mathrm{d}^2 r \end{aligned} \tag{III.100}$$

is written with this setting:

$$\begin{aligned} E[\psi] &= \frac{\hbar^2}{2m} \tilde{g}\rho_0 N \, + \, \frac{\hbar^2}{2m} \rho_0 \int \left[(\boldsymbol{\nabla}\theta)^2 + (\boldsymbol{\nabla}\eta)^2 + 4\,\tilde{g}\rho_0\,\eta^2(\boldsymbol{r}) \right] \mathrm{d}^2 r, \\ &= \frac{\hbar^2}{2m} \tilde{g}\rho_0 N \, + \, \frac{\hbar^2}{2m} N \sum_{\boldsymbol{q}} \left[q^2 \, |c_{\boldsymbol{q}}|^2 + \left(q^2 + 4\tilde{g}\rho_0 \right) \, |d_{\boldsymbol{q}}|^2 \right]. \end{aligned} \tag{III.101}$$

The time-dependent Gross–Pitaevskii equation (III.40) then leads to the two coupled equations[8]

$$\left(\frac{2m}{\hbar} \right) \frac{\partial \theta}{\partial t} = \nabla^2 \eta \, - \, 4\,\tilde{g}\rho_0\,\eta \, , \tag{III.102}$$

$$\left(\frac{2m}{\hbar} \right) \frac{\partial \eta}{\partial t} = - \, \nabla^2 \theta. \tag{III.103}$$

The evolution of the coefficients $c_{\boldsymbol{q}}$ and $d_{\boldsymbol{q}}$ deduced from (III.102–III.103) is:

$$\left(\frac{2m}{\hbar} \right) \dot{c}_{\boldsymbol{q}} = - \left(q^2 + 4\,\tilde{g}\rho_0 \right) \, d_{\boldsymbol{q}} \, , \tag{III.104}$$

$$\left(\frac{2m}{\hbar} \right) \dot{d}_{\boldsymbol{q}} = q^2 \, c_{\boldsymbol{q}} \, . \tag{III.105}$$

[8] With the variables adopted here, the dynamic Lagrangian can be taken $\mathcal{L}_{\mathrm{dyn}}[\psi(\boldsymbol{r})] = -2\hbar\rho_0\,\dot{\theta}\,\eta$.

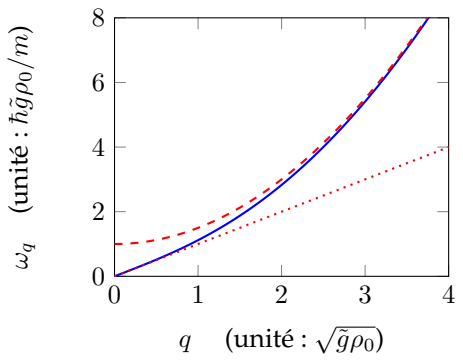

Figure III.10. *Bogoliubov dispersion relation (III.107). The dotted line corresponds to the linear approximation (III.109) at small values of q determining the phonon regime. The dashed parabolic curve corresponds to large values of q, where we recover the free particle regime (III.111).*

For $\boldsymbol{q} = 0$, we obtain $\dot{c}_0 = 0$, which reflects the fact that the global phase of the gas does not evolve since the energy of the ground state of (III.101) is 0.

By eliminating one of the two variables ($c_{\boldsymbol{q}}$ or $d_{\boldsymbol{q}}$) in favor of the other, we obtain the evolution

$$\ddot{c}_{\boldsymbol{q}} + \omega_q^2 c_{\boldsymbol{q}} = 0, \qquad \ddot{d}_{\boldsymbol{q}} + \omega_q^2 d_{\boldsymbol{q}} = 0, \tag{III.106}$$

with the frequency ω_q given by

$$\omega_q = \frac{\hbar}{2m} \left[q^2 \left(q^2 + 4\,\tilde{g}\rho_0 \right) \right]^{1/2}, \tag{III.107}$$

which is the well-known Bogoliubov spectrum, a few properties of which are described below.

4-2 Bogoliubov spectrum and sound waves

Bogoliubov formula provides the dispersion relation between the wave vector $\boldsymbol{q}$ of a plane-wave perturbation and its frequency ω_q. Given the form (III.107), it is natural to separate two regimes (figure III.10):

- The small wave-vector sector:

$$q^2 \ll 4\,\tilde{g}\rho_0 \tag{III.108}$$

for which we find a spectrum of sound waves (phonons):

$$\omega_q = c_0 q \qquad \text{with} \quad c_0 = \frac{\hbar}{m}\sqrt{\tilde{g}\rho_0}. \tag{III.109}$$

- The large wave-vector sector:

$$q^2 \gg 4\tilde{g}\rho_0 \tag{III.110}$$

for which we recover the free particle spectrum, shifted by the interaction energy $\epsilon_{\rm int}$.

$$\hbar\omega_q = \frac{\hbar^2 q^2}{2m} + \epsilon_{\rm int} \qquad \text{with} \quad \epsilon_{\rm int} = \frac{\hbar^2}{m}\,\tilde{g}\rho_0. \tag{III.111}$$

The shape of the Bogoliubov excitation spectrum, starting linearly at low wavevectors, is often presented as a sufficient condition for superfluidity. Indeed, using Landau's criterion, we deduce that an impurity moving sufficiently slowly cannot excite the fluid and is therefore not slowed down. However, a more complete definition of a superfluid state involves the notion of current metastability and phase rigidity [see, for example, Ma (1985) as well as the 2015-16 lecture series]. We have already mentioned that the Bose gas described by the energy functional (III.72) exhibits this rigidity and is therefore indeed superfluid. We will come back to this point and generalize it in the next course.

Observation of sound waves at 2D. The propagation of sound waves in degenerate atomic gases has been the subject of numerous studies. These are often carried out in harmonic traps, so that the density varies along the direction of propagation. This inhomogeneity can of course be taken into account in the theoretical description, but nevertheless complicates comparison with experimental results. Recently the team of LKB-Collège de France[9] has measured the propagation of sound waves in a uniform 2D gas. This gas is trapped in a rectangular "box" whose walls are formed by light. The atomic density on one side of the rectangle is temporally modulated using an additional light beam, generating a wave packet that propagates through the gas over a fairly long period (several tens of milliseconds), bouncing off the walls of the box. This makes it possible to accurately measure the speed of sound in the gas. The experiment shown in figure III.11 gives $c_0 = 2.0\,\mathrm{mm/s}$, in good agreement with the prediction made above ($\tilde{g} = 0.15$, $\rho_0 = 50\,\mu\mathrm{m}^{-2}$).

[9]This experiment was carried out by Monika Aidelsburger, Jérôme Beugnon, Sylvain Nascimbene, Raphaël Saint-Jalm and Jean-Loup Ville.

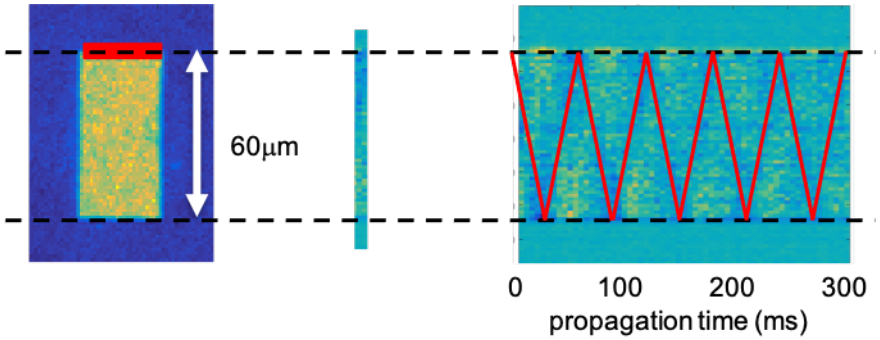

Figure III.11. *Demonstration of sound waves in a 2D gas of rubidium atoms. The gas is confined in a rectangular box and the sound wave is generated by briefly modulating the atomic density on one side of the box.*

The study we have just made is valid at low temperatures, where we are interested in the motion of the fluid as a whole. At higher temperatures, the situation is more complex, as one has to consider the independent motions of the superfluid and normal components. The general formalism is presented for the two-dimensional case by Ozawa & Stringari (2014).

4-3 Phase fluctuations and density fluctuations

We consider a Bogoliubov mode characterized by the amplitudes $\bar{c}_q$ and $\bar{d}_q$ of the phase and density modulations. From the system (III.105) we get:

$$\frac{\bar{d}_q}{\bar{c}_q} = \frac{q}{\sqrt{q^2 + 4\,\tilde{g}\rho_0}}. \tag{III.112}$$

For q small, more precisely when $q^2 \ll 4\tilde{g}\rho_0$ i.e. $q \ll \frac{1}{\xi}$, we find $\bar{d}_q \ll \bar{c}_q$, which means that the modes consist essentially of phase oscillation, with density almost unaffected. This validates the approach followed in § 3, where we focused on phase fluctuations to find the behavior of the fluid on large spatial scales, i.e. at small wave vectors.

We have already characterized the main effect of phase fluctuations, namely the emergence of a quasi-long-range order. Let us now turn our attention to density fluctuations at thermal equilibrium, in order to check that the assumption of linearization of these fluctuations, via the function $\eta(\boldsymbol{r})$, is consistent with the final result. We start from:

$$\frac{\Delta\rho^2}{\rho_0^2} = \frac{\langle\rho^2(0)\rangle}{\rho_0^2} - 1 = 4\sum_{\boldsymbol{q}}\langle|d_{\boldsymbol{q}}|^2\rangle. \tag{III.113}$$

To evaluate this quantity, we use the equipartition theorem for the classical field $\eta(\boldsymbol{r})$. As explained above, we avoid UV divergences by assigning an average energy $k_{\mathrm{B}}T/2$ to all modes of energy $\hbar\omega_q$ less than $k_{\mathrm{B}}T$, and assuming that higher-energy modes are unpopulated. This leads to :

$$\frac{\hbar^2}{m}N\left(q^2 + 4\tilde{g}\rho_0\right)\ \langle|d_{\boldsymbol{q}}|^2\rangle = \begin{cases} k_{\mathrm{B}}T & \text{if } \hbar\omega_q < k_{\mathrm{B}}T\,, \\ 0 & \text{if } \hbar\omega_q > k_{\mathrm{B}}T\,. \end{cases} \tag{III.114}$$

Density fluctuations can then be calculated explicitly from (III.113):

$$\frac{\Delta\rho^2}{\rho_0^2} = \frac{2}{\pi\rho_0\lambda_T^2}\int\frac{1}{q^2+4\tilde{g}\rho_0}\mathrm{d}^2q \approx \frac{2}{\rho_0\lambda_T^2}\log\left(\frac{k_{\mathrm{B}}T}{E_{\mathrm{int}}/N}.\right) \tag{III.115}$$

As mentioned above, the thermal energy $k_{\mathrm{B}}T$ is generally greater than the interaction energy per particle E_{int}/N. In practice, the ratio between these two quantities can reach a value of the order of a few tens, so that the logarithm itself is between 1 and 3. The denominator of the above expression is equal to the phase-space density, which must be at least a few tens for the superfluid transition to be reached (*cf.* chapter 4); in practice, it can be as high as a hundred for cold and dense samples. We deduce that $\Delta\rho \ll \rho_0$ for these cold samples, which justifies the approximation of small density fluctuations used in this section.

Chapter IV

The critical point of the BKT transition

In the previous chapter, we described the role played by phonons in a 2D Bose gas at thermodynamic equilibrium. We showed that, in accordance with the Mermin–Wagner–Hohenberg theorem, these phonons cause the long-range order to disappear for $T \neq 0$, replacing it by a quasi-order: the one-body correlation function decreases algebraically, $G_1(r) \propto r^{-\alpha}$, where $\alpha = 1/\mathcal{D}_s$ is related to the superfluid phase-space density $\mathcal{D}_s = \rho_s \lambda_T^2$. We also found via Landau's criterion that this quasi-order was indeed sufficient to maintain a superfluid state.

The aim of this chapter is to go beyond the purely phononic model and take vortices into account. The influence of vortices can be understood intuitively (figure IV.1): suppose we have – after taking phonons into account – a certain phase coherence between two points A and B, characterized by the probability law for the phase difference ϕ; if a vortex with its phase winding of 2π can be randomly inserted on the segment AB, the phase difference will switch between ϕ and $\phi + \pi$. This random phase shift will cause A and B to lose all coherence, and the quasi-phase order that may have existed between these two points will be destroyed.

In what follows, we will look successively at the role of an isolated vortex, then at a pair of vortices with opposite circulations, before turning to the thermodynamics of a vortex assembly. Finally, we will look at the role of vortices via a renormalization group approach. This will enable us to establish a clear criterion for superfluidity; in particular, we will see that $\mathcal{D}_s$ is either zero or greater than 4.

1 Threshold of appearance of an isolated vortex

1-1 Vortex appearance and disappearance

In the context of our gas of atoms described by a classical wave function $\psi(\boldsymbol{r})$, a vortex is a zero of this function. Around this zero, the phase winding[1] is $\pm 2\pi$. This is referred to as a $Q = \pm 1$ vortex.

A simple mathematical way of representing vortex emergence in this context is to consider the two functions $\mathrm{Re}[\psi(\boldsymbol{r})]$ and $\mathrm{Im}[\psi(\boldsymbol{r})]$. Each of these two functions fluctuates in space under the effect of thermal excitations; $\mathrm{Re}[\psi(\boldsymbol{r})]$, for example, takes on positive values in some regions of the plane and negative values in others. The boundaries between these regions are lines along which $\mathrm{Re}[\psi(\boldsymbol{r})]$ cancels out. The same applies to $\mathrm{Im}[\psi(\boldsymbol{r})]$. There may therefore be discrete points $\boldsymbol{r}_j$ in the plane where these lines intersect, i.e.

$$\mathrm{Re}[\psi(\boldsymbol{r}_j)] = 0 \qquad \text{and} \qquad \mathrm{Im}[\psi(\boldsymbol{r}_j)] = 0. \tag{IV.1}$$

It is easy to check that a simple zero of ψ corresponds to a vortex with topological charge $Q_j = \pm 1$ (figure IV.2).

[1] Other situations can be considered, but they all boil down to superpositions of the two $\pm 2\pi$ cases. For example, if the winding is zero, this density zero can be seen as the superposition of vortices with opposite topological charges. If the winding is $2n\pi$, this corresponds to the superposition of n vortices of unit charge.

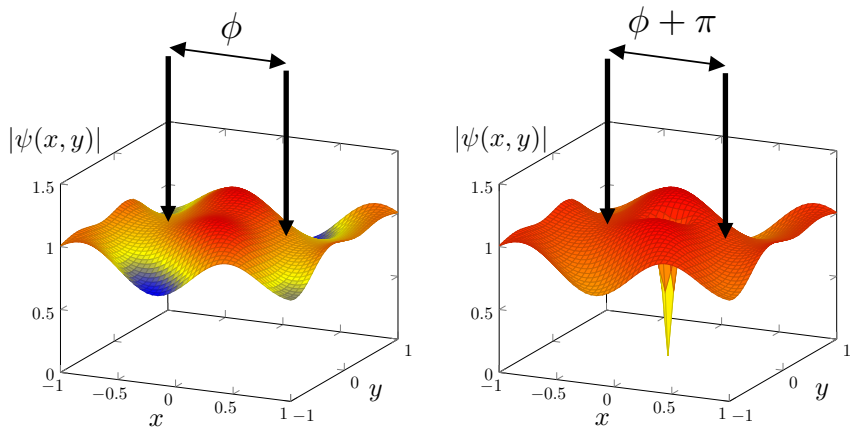

Figure IV.1. *Isolated vortices and phase coherence: if an isolated vortex is inserted between two points, the relative phase between these two points changes from ϕ to $\phi+\pi$. Consequently, in a fluid where isolated vortices can be randomly distributed, phase coherence cannot exceed a length of the order of the average distance between vortices.*

The phase winding of a vortex constitutes a topological "protection". A vortex of charge $Q \neq 0$ cannot be spontaneously generated within a sample, nor can it be eliminated. There are two possible ways for vortices to appear or disappear:

- The vortex is created or annihilated individually at the edge of the sample, where the wave function $\psi(\boldsymbol{r})$ cancels out;

- A pair of oppositely-charged vortices appears or disappears by passing through the intermediate state of a double zero of $\psi(\boldsymbol{r})$, corresponding to zero phase winding (figure IV.3). This intermediate state can be seen as the superposition of two oppositely-charged vortices.

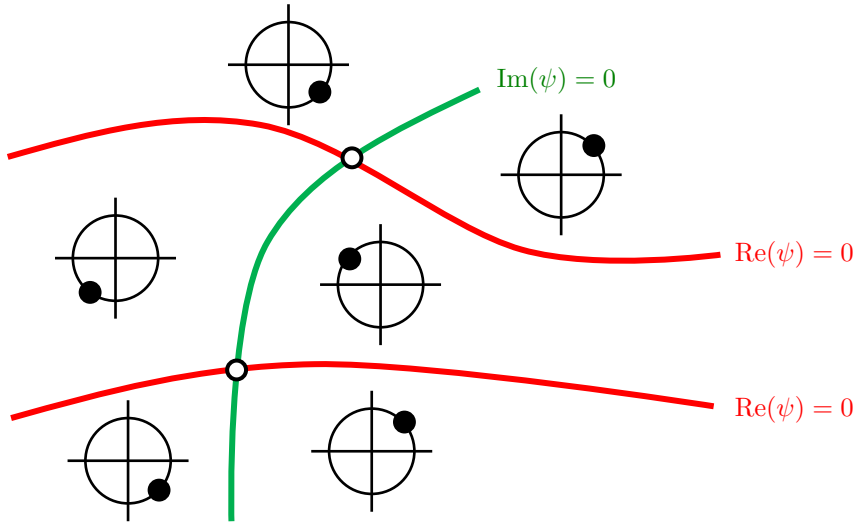

Figure IV.2. *Lines on which $\mathrm{Re}[\psi(\boldsymbol{r})] = 0$ (in red) and $\mathrm{Im}[\psi(\boldsymbol{r})] = 0$ in green. The points of intersection $\boldsymbol{r}_j$ are (generally) simple zeros of $\psi(\boldsymbol{r})$ and correspond to a phase winding of $\pm 2\pi$, i.e. a vortex of topological charge $Q = \pm 1$. A representation of the phase of ψ on the trigonometric circle is shown in each area of the plane, enabling the phase winding of the vortex to be determined.*

1-2 The energy of a vortex

Energy and entropy arguments will play a central role in what follows to determine whether a vortex has a significantly non-zero probability of being present in a quantum fluid. We will start by assessing the energy of an isolated vortex by considering the simplest possible situation, that of a circular sample with a vortex located at its center.

The velocity field created by the vortex is orthoradial and such that circulation along a circle centered on the origin is always equal to h/m, which gives (figure IV.4)

$$\boldsymbol{v}(\boldsymbol{r}) = \frac{\hbar}{mr}\boldsymbol{u}_\varphi \qquad \text{with} \quad \boldsymbol{u}_\varphi = \boldsymbol{u}_z \times \frac{\boldsymbol{r}}{r}. \tag{IV.2}$$

The density cancels at the point $\boldsymbol{r} = 0$ and returns to its asymptotic value

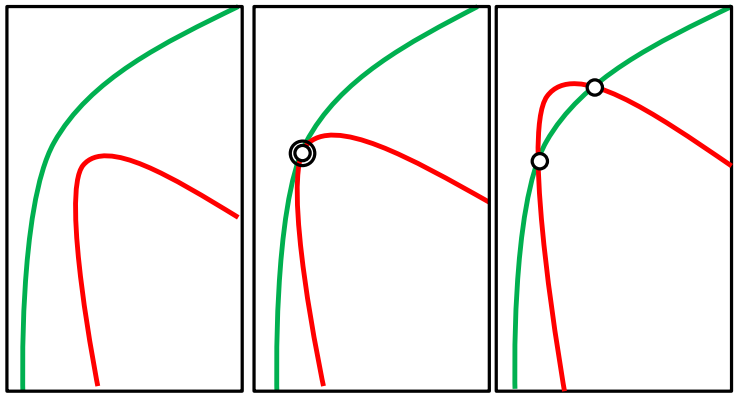

Figure IV.3. *Emergence of a vortex pair due to thermal fluctuations in the gas. Under the effect of a fluctuation, the line corresponding to $Re[\psi(\boldsymbol{r})] = 0$ (in red), initially disjoint from the line $Im[\psi(\boldsymbol{r})] = 0$ (in green) [drawing on the left], crosses it to form a double zero [central drawing], then into two single zeros of opposite windings [drawing on the right]. The result is a pair of vortices with charges $Q_1 = +1$ and $Q_2 = -1$. The reverse process is also possible, leading to the annihilation of the vortex pair.*

over a distance of the order of the healing length defined in the previous chapter:

$$\xi = \frac{1}{\sqrt{2\tilde{g}\rho}}. \tag{IV.3}$$

For the sake of simplicity, we will model the density profile as a staircase function:

$$\begin{aligned} \rho(\boldsymbol{r}) &= 0 \quad \text{if } r < \xi, \\ \rho(\boldsymbol{r}) &= \rho \quad \text{if } r > \xi. \end{aligned} \tag{IV.4}$$

The kinetic energy of the fluid is therefore:

$$\begin{aligned} E_{\rm kin} &= \frac{1}{2}m\int \rho(\boldsymbol{r})\,\boldsymbol{v}^2(\boldsymbol{r})\,\mathrm{d}^2r \approx \frac{1}{2}m\rho\frac{\hbar^2}{m^2}\int_\xi^R \frac{1}{r^2}\,2\pi r\,\mathrm{d}r \\ &= \frac{\pi\hbar^2\rho}{m}\ln(R/\xi). \end{aligned} \tag{IV.5}$$

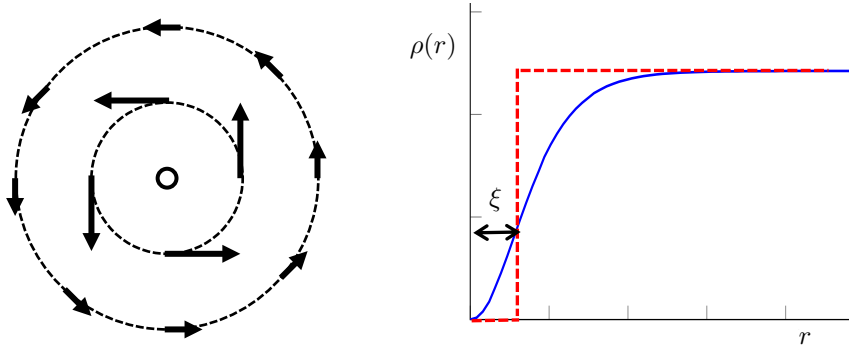

Figure IV.4. *Left: velocity field created by a vortex, decreasing as $1/r$. Right: density profile in the vicinity of the vortex core. The size of the core is of the order of the healing length $\xi = 1/\sqrt{2\tilde{g}\rho}$. Dotted line shows the staircase function given in (IV.4).*

The essential point of this result is that the energy of a single vortex, i.e. a "microscopic" object, tends towards infinity when the size of the system itself tends towards infinity. Of course, the divergence is only logarithmic, but this is enough to make the thermodynamic limit singular with respect to isolated vortices. Note that in this expression, the prefactor $\pi\hbar^2\rho/m$ in front of the logarithm is "robust": it does not depend on the model chosen for the density profile. The precise form of this model only plays a role in the argument of the logarithm, and therefore contributes via a constant that is added to the dominant term in $\ln(R)$.

There is also an increase in the interaction energy of the fluid, as we go from a uniform density $N/(\pi R^2)$ to the density $\rho = N/[\pi(R^2 - \xi^2)]$. Starting from the general expression for the interaction energy seen in the previous chapter,

$$E_{\rm int} = \frac{\hbar^2}{2m}\tilde{g}\int \rho^2(\boldsymbol{r})\,\mathrm{d}^2r, \tag{IV.6}$$

this increase is written:

$$\begin{aligned}\epsilon_0 &= \frac{\hbar^2}{2m}\tilde{g}\left\{\left[\frac{N}{\pi(R^2-\xi^2)}\right]^2\pi(R^2-\xi^2)-\left[\frac{N}{\pi R^2}\right]^2\pi R^2\right\}\\ &\approx \frac{\pi}{2}\,\frac{\hbar^2\rho}{m}.\end{aligned} \tag{IV.7}$$

This energy remains constant as the disk size tends towards infinity, and is therefore much smaller than the kinetic energy, which diverges as $\ln(R)$. For an isolated vortex, this energy ϵ_0 can therefore be neglected, but this will no longer be the case when we are interested in a vortex-antivortex pair, as the kinetic energy will then be greatly reduced. The value $\pi/2$ of the prefactor is only indicative, since it depends on the model chosen to describe the cancellation of density at the vortex center.

Total and superfluid densities. In the foregoing, the density ρ represents the total density of the sample, which is assumed to be at zero temperature. In this case, the total density ρ and the superfluid density ρ_s coincide. If the temperature is not zero, the superfluid density is reduced, due to short-scale density fluctuations. To evaluate the kinetic energy of the vortex, which involves the phase gradient of $\psi(\boldsymbol{r})$ over a large length scale, it is then necessary to involve only the superfluid density, which leads to

$$E_{\rm kin} \approx \frac{\pi\hbar^2\rho_s}{m}\ln(R/\xi) \qquad\qquad \epsilon_0 \sim \frac{\hbar^2\rho_s}{m}. \tag{IV.8}$$

Let us emphasize that this superfluid density ρ_s is a quantity dependent on the temperature and the spatial scale a at which the system is considered. Density-phase fluctuations with wavelengths shorter than a (and, as we will see later, vortex pairs separated by less than a) are absorbed into the definition of ρ_s. This remark plays a central role in the treatment of the transition by the renormalization group approach.

Off-centered vortex. The above analysis assumes that the vortex is centered on the sample, which means that the calculations can be carried out analytically. In the case of an off-centered vortex, an exact treatment is more delicate, but the result is only slightly altered since the energy depends on the radius only via a logarithm.

1-3 Is the observation of an isolated vortex likely?

As mentioned above, a vortex can appear in the sample by being nucleated on the walls, then drifting towards the central region. The state of a gas with a vortex is determined by knowledge of the vortex position. Since the core of the vortex has an extent $\pi\xi^2$, we can consider that we have

$$W \approx \frac{\pi R^2}{\pi\xi^2} \tag{IV.9}$$

independent states for an individual vortex in the disk of radius R.

The probability of a given state occurring is given by Boltzmann's law

$$p \approx \mathrm{e}^{-E_{\rm kin}/k_{\rm B}T}, \tag{IV.10}$$

where we have neglected the contribution of the interaction energy ϵ_0 in front of the kinetic energy. Introducing the thermal wavelength λ_T and the phase-space density $\mathcal{D}_s$ associated with the superfluid fraction

$$\lambda_T = \frac{\hbar\sqrt{2\pi}}{\sqrt{mk_{\rm B}T}}, \qquad \mathcal{D}_s = \rho_s\lambda_T^2, \tag{IV.11}$$

this probability is written using (IV.8)

$$p \approx \exp\left[-\frac{\mathcal{D}_s}{2}\ln\left(\frac{R}{\xi}\right)\right] = \left(\frac{\xi}{R}\right)^{\mathcal{D}_s/2}. \tag{IV.12}$$

For a "macroscopic" sample such as $R \gg \xi$, this probability is small in front of 1 as soon as $\mathcal{D}_s$ is significantly non-zero.

Now let us look at the probability of a vortex being present in the sample, regardless of its position (figure IV.5). Since there are W possible states, this probability is $\approx Wp$, at least as long as $Wp \ll 1$:

$$Wp = \frac{R^2}{\xi^2}p \approx \left(\frac{\xi}{R}\right)^{-2+\mathcal{D}_s/2}. \tag{IV.13}$$

There are two possible scenarios, depending on the value of the exponent $-2+\mathcal{D}_s/2$:

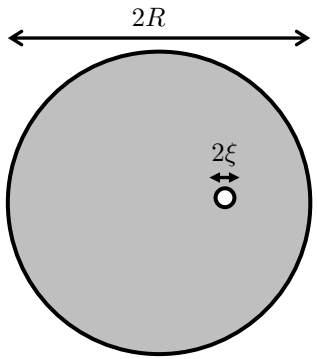

Figure IV.5. *A vortex of radius $\approx \xi$ in a disk of radius R.*

- If this exponent is positive, i.e. if the superfluid density $\mathcal{D}_s$ verifies

$$\mathcal{D}_s > 4, \tag{IV.14}$$

  the probability Wp tends towards 0 at the thermodynamic limit. For large enough samples, an isolated vortex is extremely unlikely.

- On the contrary, if $\mathcal{D}_s < 4$, the quantity Wp diverges at the thermodynamic limit. This quantity can then no longer be interpreted as a probability, but the message is clear: it is very likely that the gas will contain a large number of vortices (of random charge). As we will see later (§ 1-4), this proliferation of individual vortices is enough to eliminate superfluidity. For the sake of consistency, let us take $\mathcal{D}_s = 0$.

The conclusion of this preliminary study is that superfluidity can only exist in this two-dimensional system if the superfluid density is greater than 4, in which case no isolated vortex is present in the system at thermodynamic equilibrium. Remarkably, this conclusion reached from elementary considerations and with a very crude modeling of the gas (a single vortex!) is quantitatively accurate: as we will see in § 4, the critical point of the BKT transition, corresponding to the normal-superfluid transition, corresponds exactly to the point where the superfluid density is such that $\mathcal{D}_s = 4$.

Equally remarkable is the fact that this conclusion does not depend on the strength of the interactions characterized by the parameter $\tilde{g}$. This parameter plays a part in the size of the vortex core, but not in the long-distance velocity field that is the essential element of the previous reasoning. It is therefore a universal result.

"Free energy" approach. A very similar approach, leading to an identical conclusion, is to evaluate the free energy of the one-vortex configuration (Kosterlitz & Thouless 1973),

$$F = E - TS, \tag{IV.15}$$

where E is the energy of a vortex, essentially the kinetic energy (IV.8), and S the entropy associated with this configuration, i.e.

$$S = k_B \ln(W) \tag{IV.16}$$

where W is the number of possible independent states given in (IV.9). We then find:

$$F = \left(\frac{\pi \hbar^2 \rho_s}{m} - 2k_{\mathrm{B}}T \right) \ln(R/\xi) \tag{IV.17}$$

or

$$\frac{F}{k_{\mathrm{B}}T} = \frac{1}{2} \left(\mathcal{D}_s - 4 \right) \ln(R/\xi). \tag{IV.18}$$

This brings us back to the result of the previous discussion. If $\mathcal{D}_s > 4$, the free energy is positive and very large compared to $k_{\mathrm{B}}T$ at the thermodynamic limit: it is extremely unlikely that a free vortex will appear in the sample. On the other hand, if $\mathcal{D}_s < 4$, the free energy is large in absolute value, but negative, indicating that this process – and the appearance of other vortices – is very likely.

1-4 Isolated vortices and non-superfluidity

To understand why the possibility of having an isolated vortex within a 2D gas inhibits superfluidity, the simplest way is to consider a ring-shaped geometry, such as that shown in figure IV.6. If large enough, this ring is a two-dimensional gas with periodic boundary conditions in one direction and Dirichlet boundary conditions in the other.

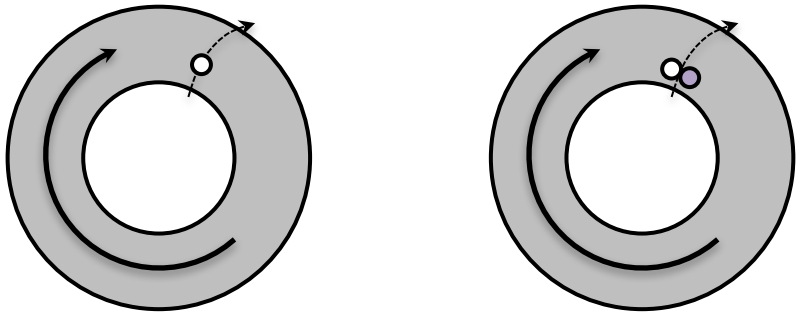

Figure IV.6. *Left: when a two-dimensional fluid ring is traversed by an isolated vortex, the (quantized) current in the ring is modified. There can be no permanent current - a necessary condition for superfluidity - as soon as isolated vortices have a significant probability of being present in the fluid. Right: the crossing of a linked pair of two vortices of opposite charge, on the other hand, has no effect on the permanent current.*

Superfluidity manifests itself as the possibility of a metastable permanent current in this ring, i.e. a phase winding $2\pi N$, where N is an integer. Let us now assume that the temperature is high enough for an isolated vortex, initially present on the inner or outer edge of the ring, to migrate into the high-density zone. We saw above that this can happen if $\mathcal{D}_s < 4$. It may well happen that this vortex crosses the ring and exits at the opposite edge. When this happens, the phase winding is modified:

$$\text{Crossing an isolated vortex:} \quad N \to N \pm 1. \tag{IV.19}$$

If isolated vortices have an appreciable probability of crossing the ring, the current intensity will perform Brownian motion and its mean value will relax towards 0: the current is therefore not metastable and the superfluid density is zero.

Note that the above argument does not apply to pairs formed by two vortices of opposite sign, with a (microscopic) distance between the members of the pair small compared to the (macroscopic) size of the ring. In this case, no change in phase winding accompanies the crossing of the pair:

$$\text{traversée d'une paire de vortex:} \quad N \to N, \tag{IV.20}$$

and the presence of these pairs with non-zero density does not inhibit superfluidity. It can, however, reduce phase rigidity, and hence the superfluid fraction, as we will see a little later.

2 A "vortex – antivortex" pair

The argument of the previous section immediately extends to any "unbalanced" vortex configuration, i.e. with more positive than negative charges, or vice versa. The resulting velocity field will vary over long distances as

$$Q_{\rm tot}\frac{\hbar}{mr} \qquad \text{where} \quad Q_{\rm tot} = \sum_j Q_j, \tag{IV.21}$$

which will lead to a logarithmic divergence of the kinetic energy with sample size, with a multiplicative factor $Q_{\rm tot}^2$.

On the other hand, balanced configurations with $Q_{\rm tot} = 0$ do not exhibit this pathology. Each of these balanced configurations therefore has a non-infinitesimal probability of appearing if the gas temperature is not strictly zero. We will take a look here at the simple case of a pair of vortices, one positively charged, the other negatively charged, which we will call a "vortex – antivortex" pair; this name is justified insofar as the two members of the pair can annihilate each other (figure IV.3), as would an electron and a positron. The next section will focus on the general case, where we take a statistical average over all configurations.

2-1 Velocity field and energy of a vortex pair

Let us consider a pair of vortices with opposite charges, separated by a distance ℓ, these two vortices being located, for example, at $x = \pm\ell/2, y = 0$ (figure IV.7). We will assume that the global velocity field is the sum of the velocity fields created by each of the two vortices, this point being justified in the rest of this chapter [see equation (IV.46)] :

$$\boldsymbol{v}_\pm = \pm\frac{\hbar}{mr_\pm^2}\begin{pmatrix} -y \\ x \pm \ell/2 \end{pmatrix} \qquad \text{with} \quad r_\pm = \left[(x \pm \ell/2)^2 + y^2\right]^{1/2}. \tag{IV.22}$$

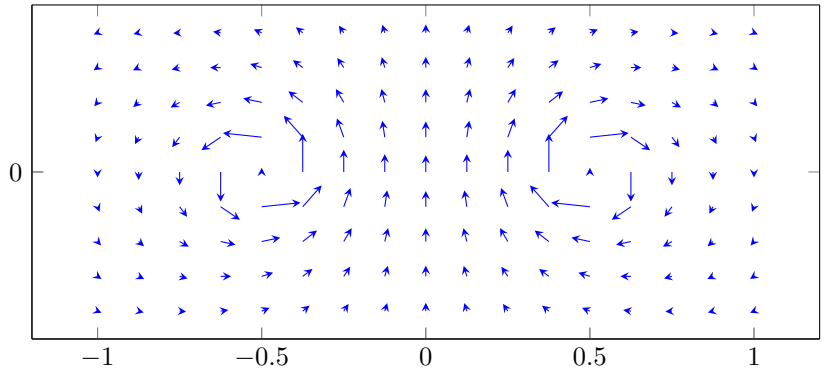

Figure IV.7. *The velocity field created by a pair of oppositely-charged vortices. This velocity field decreases as $1/r^2$ at infinity and the associated kinetic energy is therefore bounded as the sample size tends towards infinity, in contrast to the case of an isolated vortex.*

The calculation of the corresponding kinetic energy is presented by Nozières & Pines (1990) and will be taken up in a general way a little further on [*cf.* (IV.52)]. We therefore give the result without demonstration:

$$E_{\rm kin}(\ell) \approx \frac{2\pi\hbar^2\,\rho_s}{m}\ln\left(\frac{\ell}{\xi}\right). \tag{IV.23}$$

This result has a structure apparently similar to that obtained for an isolated vortex, but it no longer diverges with the sample size R. This size is replaced here by the distance ℓ between the two vortices, as the contributions of the two velocity fields to the kinetic energy compensate for distances to the origin that are larger than ℓ (this velocity field decreases as $1/r^2$ at infinity).

To this kinetic energy must be added the increase in interaction energy linked to the creation of two ξ-sized holes in the fluid, i.e. $2\epsilon_0$, where the energy ϵ_0 was evaluated in (IV.8). For a separation ℓ between the two vortices of a few ξ, kinetic energy and interaction energy are comparable. The Boltzmann weight associated with the appearance of a pair of vortices is therefore:

$$\mathcal{P}(\ell) = \exp\left\{-\frac{2\epsilon_0 + E_{\rm kin}(\ell)}{k_{\rm B}T}\right\} \tag{IV.24}$$

or

$$\mathcal{P}(\ell) \approx y_0^2\,\mathrm{e}^{-\mathcal{D}_s\ln(\ell/\xi)} = y_0^2\left(\frac{\xi}{\ell}\right)^{\mathcal{D}_s}, \tag{IV.25}$$

where we introduce the factor coming from the interaction energy of each vortex, called *vortex fugacity*:

$$y_0 \equiv \exp\left(-\frac{\epsilon_0}{k_{\rm B}T}\right). \tag{IV.26}$$

When modeling the density by a staircase function, the result (IV.7) leads to $y_0 \approx \exp(-\mathcal{D}_s/4)$.

The result (IV.25) is non-negligible in front of 1, at least for close pairs ($\ell \lesssim$ a few ξ) and for a weakly or moderately degenerate gas (superfluid phase-space density $\mathcal{D}_s$ not very large in front of 1).

2-2 Average size of a vortex pair

Using the Boltzmann weight $\mathcal{P}(\ell)$ for the distance between the two vortices in the pair, we can now evaluate several features of the pair statistical distribution. In this paragraph, we focus on the mean size of the pair, i.e. the mean $\langle(\boldsymbol{r}_i - \boldsymbol{r}_j)^2\rangle$ of the square of the distance ℓ.

Starting from

$$\langle\ell^2\rangle = \frac{\int_\xi^{+\infty}\ell^2\mathcal{P}(\ell)\,2\pi\ell\,\mathrm{d}\ell}{\int_\xi^{+\infty}\mathcal{P}(\ell)\,2\pi\ell\,\mathrm{d}\ell} \tag{IV.27}$$

we find (Kosterlitz & Thouless 1973)

$$\langle\ell^2\rangle = \xi^2\,\frac{\mathcal{D}_s - 2}{\mathcal{D}_s - 4}. \tag{IV.28}$$

This quantity plotted on figure IV.8 is only defined for $\mathcal{D}_s > 4$: we saw in the previous section that this is the condition that must be met if a free vortex is not to appear at thermodynamic equilibrium. In other words, it is on this condition that pairs do not dissociate and remain effectively bound, with a finite value of their size.

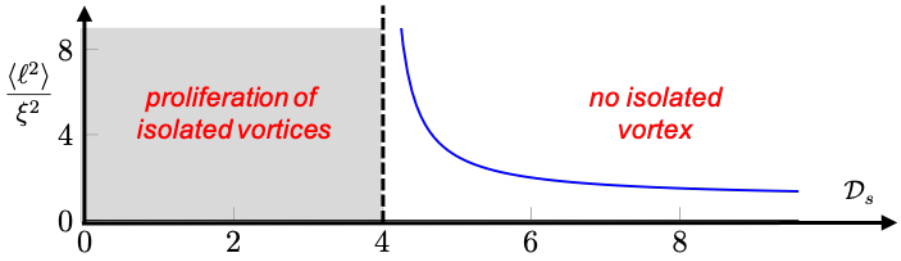

Figure IV.8. *Variation of the average size of a vortex pair as a function of the phase-space density associated with the superfluid fraction* [cf. *eq. (IV.28)*].

For a phase-space density $\mathcal{D}_s$ significantly greater than 4, the mean size is of order ξ, corresponding to a kinetic energy of the order of the interaction energy $2\epsilon_0$. As $\mathcal{D}_s$ decreases and approaches 4, the pairs are less and less bound, the size increases and finally diverges at $\mathcal{D}_s = 4$.

2-3 Density of pairs

We can also use the Boltzmann weight $\mathcal{P}(\ell)$ given in (IV.25) to evaluate the average distance between two pairs in the two-dimensional gas. Let us start with a sample of area πR^2 and define the position of each vortex to within $\pi\xi^2$, as we did for a single vortex in § 1. The probability of the sample containing a vortex pair is

$$\begin{aligned} p(R) &= \iint \mathcal{P}\left(|\boldsymbol{r}_a - \boldsymbol{r}_b|\right) \frac{\mathrm{d}^2 r_a}{\pi\xi^2} \frac{\mathrm{d}^2 r_b}{\pi\xi^2} \\ &= \frac{\pi R^2}{(\pi\xi^2)^2} \int_\xi^R \mathcal{P}(\ell)\, 2\pi\ell\, \mathrm{d}\ell \\ &\approx \frac{2}{\mathcal{D}_s - 2} \frac{R^2}{\xi^2}\, y_0^2. \end{aligned} \qquad \text{(IV.29)}$$

To estimate the average distance d between pairs, we take $d = R$, where R is the radius for which the probability of presence $p(R)$ calculated above becomes of order 1. This gives

$$\frac{2}{\mathcal{D}_s - 2} \frac{d^2}{\xi^2}\, y_0^2 \sim 1 \qquad \longrightarrow \qquad d \approx \xi\, \mathrm{e}^{\epsilon_0/k_\mathrm{B}T} \sqrt{\mathcal{D}_s}. \qquad \text{(IV.30)}$$

For $\mathcal{D}_s \gg 1$, the pairs – which we have seen have an elongation $\sim \xi$ – are distant from each other by the amount $d \gg \xi$; they therefore form a very dilute gaz. On the other hand, as $\mathcal{D}_s$ approaches the value 4 at which the pairs dissociate, the distance d becomes of the order of the average size of a pair. This means that the pairs overlap, rendering our treatment incomplete. The aim of the next section is to present the main tools for studying the neighborhood of the critical point in greater detail.

3 Energy of a vortex assembly

3-1 Longitudinal and transverse velocity fields

In the previous chapter, we started with a wave function $\psi(\boldsymbol{r}) = \sqrt{\rho(\boldsymbol{r})}\, \mathrm{e}^{\mathrm{i}\theta(\boldsymbol{r})}$ to which we associated the superfluid velocity field $\frac{\hbar}{m}\boldsymbol{\nabla}\theta$. We also assumed that the phase could be developed as a Fourier series,

$$\theta(\boldsymbol{r}) = \sum_{\boldsymbol{q}} c_{\boldsymbol{q}}\, \mathrm{e}^{\mathrm{i}\boldsymbol{q}\cdot\boldsymbol{r}} \quad \rightarrow \quad \boldsymbol{v}_s^{\parallel}(\boldsymbol{r}) = \mathrm{i}\frac{\hbar}{m} \sum_{\boldsymbol{q}} \boldsymbol{q}\, c_{\boldsymbol{q}}\, \mathrm{e}^{\mathrm{i}\boldsymbol{q}\cdot\boldsymbol{r}}. \qquad \text{(IV.31)}$$

These relations can also be written as

$$\theta(\boldsymbol{r}) = \frac{1}{2\pi} \int \hat{\theta}(\boldsymbol{q})\, \mathrm{e}^{\mathrm{i}\boldsymbol{q}\cdot\boldsymbol{r}}\, \mathrm{d}^2 q, \qquad v_s^{\parallel}(\boldsymbol{r}) = \mathrm{i}\frac{\hbar}{m} \int \boldsymbol{q}\, \hat{\theta}(\boldsymbol{q})\, \mathrm{e}^{\mathrm{i}\boldsymbol{q}\cdot\boldsymbol{r}}\, \mathrm{d}^2 q \quad \text{(IV.32)}$$

if we treat $\boldsymbol{q}$ as a continuous variable.

The word $\parallel$ added to $\boldsymbol{v}_s$ comes from the fact that the velocity field defined in this way is longitudinal, i.e. parallel to $\boldsymbol{q}$ at any point in Fourier space:

$$\hat{\boldsymbol{v}}_s^{\parallel}(\boldsymbol{q}) = \mathrm{i}\frac{\hbar}{m}\, \boldsymbol{q}\, \hat{\theta}(\boldsymbol{q}). \qquad \text{(IV.33)}$$

It is clear that vortices, with their $\pm 2\pi$ phase winding around a point, escape the previous description: a function $\theta(\boldsymbol{r})$ developable in Fourier

series as (IV.31) verifies $\oint \boldsymbol{\nabla}\theta \cdot \mathrm{d}\boldsymbol{r} = 0$ for any closed contour and therefore cannot exhibit a non-zero phase winding.

To describe both smooth phase fluctuations and vortices, we need to remember that an arbitrary velocity field $\boldsymbol{v}_s(\boldsymbol{r})$ is not necessarily longitudinal. In the general case, it can be written as the sum of a longitudinal and a transverse field:

$$\boldsymbol{v}_s(\boldsymbol{r}) = \boldsymbol{v}_s^{\parallel}(\boldsymbol{r}) + \boldsymbol{v}_s^{\perp}(\boldsymbol{r}) \qquad \hat{\boldsymbol{v}}_s(\boldsymbol{q}) = \hat{\boldsymbol{v}}_s^{\parallel}(\boldsymbol{q}) + \hat{\boldsymbol{v}}_s^{\perp}(\boldsymbol{q}), \tag{IV.34}$$

with

$$\boldsymbol{q} \times \hat{\boldsymbol{v}}_s^{\parallel}(\boldsymbol{q}) = 0 \qquad \boldsymbol{q} \cdot \hat{\boldsymbol{v}}_s^{\perp}(\boldsymbol{q}) = 0, \tag{IV.35}$$

or by returning to the position space:

$$\boldsymbol{\nabla} \times \boldsymbol{v}_s^{\parallel}(\boldsymbol{r}) = 0 \qquad \boldsymbol{\nabla} \cdot \boldsymbol{v}_s^{\perp}(\boldsymbol{r}) = 0. \tag{IV.36}$$

The phonons we studied in the previous chapter are fully described by the longitudinal part of the velocity field. Vortices, on the other hand, are taken into account via the transverse component of the velocity field. For example, for an isolated vortex centered at 0, the velocity field (IV.2) is written in Fourier space

$$\hat{\boldsymbol{v}}_s^{\parallel}(\boldsymbol{q}) = 0 \qquad \hat{\boldsymbol{v}}_s^{\perp}(\boldsymbol{q}) = \mathrm{i}\,\frac{\hbar}{mq^2}\,\boldsymbol{q} \times \boldsymbol{u}_z. \tag{IV.37}$$

To simplify the analysis in the general case, we will approximate a complete decoupling of the two velocity fields. This means, for example, neglecting the influence of density holes created by vortices on phonon propagation. In the following paragraph, starting from a set of given positions $\{\boldsymbol{r}_j\}$ and charges $\{Q_j\}$ of the vortices, we will determine the associated velocity field $\boldsymbol{v}_s^{\perp}(\boldsymbol{r})$ assuming no phonon excitation of the system.

3-2 Velocity field of a vortex assembly

Let us start from a situation where we are given the positions $\{\boldsymbol{r}_j\}$ and charges $\{Q_j\}$ of the vortices and look for the velocity field that minimizes the kinetic energy functional

$$E_{\mathrm{kin}} = \frac{\hbar^2 \rho_s}{2m} \int [\boldsymbol{\nabla}\theta(\boldsymbol{r})]^2 \ \mathrm{d}^2 r. \tag{IV.38}$$

A standard functional derivation method indicates that the minimizing functions $\theta(\boldsymbol{r})$ must satisfy Laplace's equation

$$\nabla^2 \theta = 0 \tag{IV.39}$$

at any point where the phase is well defined, i.e. outside the $\boldsymbol{r}_j$. The associated velocity field $\boldsymbol{v}_s = \frac{\hbar}{m}\boldsymbol{\nabla}\theta$ verifies

$$\boldsymbol{\nabla} \cdot \boldsymbol{v}_s = \frac{\hbar}{m}\,\nabla^2\theta = 0 \qquad \rightarrow \qquad \boldsymbol{q} \cdot \hat{\boldsymbol{v}}_s(\boldsymbol{q}) = 0. \tag{IV.40}$$

This is a purely transverse velocity field, as previously announced. From now on, we will denote it $\boldsymbol{v}_s^{\perp}$.

To solve the Laplace equation, note that in two dimensions, the result (IV.40) indicates that there exists a scalar function $\hat{\Phi}(\boldsymbol{q})$ such that

$$\hat{\boldsymbol{v}}_s^{\perp}(\boldsymbol{q}) = \mathrm{i}\,\boldsymbol{q} \times \Big[\boldsymbol{u}_z\ \hat{\Phi}(\boldsymbol{q})\Big] \tag{IV.41}$$

which is written in real space:

$$\begin{aligned} \boldsymbol{v}_s^{\perp}(\boldsymbol{r}) &= \boldsymbol{\nabla} \times [\boldsymbol{u}_z\ \Phi(\boldsymbol{r})] = [\boldsymbol{\nabla}\Phi(\boldsymbol{r})] \times \boldsymbol{u}_z \\ &= \begin{pmatrix} +\partial_y \Phi \\ -\partial_x \Phi \end{pmatrix}. \end{aligned} \tag{IV.42}$$

We now need to take into account the constraints specific to a superfluid velocity field, for which the velocity circulation on a closed circuit is quantified in multiples of $2\pi\hbar/m$, with a value that depends on the vortex charge inside the contour. Let us use Stokes' formula to express this constraint in terms of Φ:

$$\begin{aligned} \oint \boldsymbol{v}_s^{\perp}(\boldsymbol{r}) \cdot \mathrm{d}\boldsymbol{r} &= \oint \boldsymbol{\nabla} \times [\boldsymbol{u}_z\ \Phi(\boldsymbol{r})] \cdot \mathrm{d}\boldsymbol{r} \\ &= \iint \boldsymbol{u}_z \cdot \boldsymbol{\nabla} \times \{\times [\boldsymbol{u}_z\ \Phi(\boldsymbol{r})]\}\ \mathrm{d}^2 r \\ &= -\iint \nabla^2 \Phi\ \mathrm{d}^2 r. \end{aligned} \tag{IV.43}$$

It is then immediate to obtain the desired quantization by taking

$$\nabla^2 \Phi(\boldsymbol{r}) = \frac{2\pi\hbar}{m} \sum_j Q_j\ \delta(\boldsymbol{r} - \boldsymbol{r}_j). \tag{IV.44}$$

In the previous chapter, we encountered the equation $\nabla^2\Phi \propto \delta(\boldsymbol{r})$ and indicated that its solution is written:

$$\Phi(\boldsymbol{r}) = -\frac{\hbar}{m} \sum_j Q_j \ln|\boldsymbol{r}-\boldsymbol{r}_j| \,, \tag{IV.45}$$

up to the addition of a function of zero Laplacian. The velocity field is then obtained by taking the gradient of the Φ function [*cf.* (IV.42)]:

$$\boldsymbol{v}_s^{\perp}(\boldsymbol{r}) = \frac{\hbar}{m} \sum_j \frac{Q_j}{|\boldsymbol{r}-\boldsymbol{r}_j|^2} \begin{pmatrix} -y+y_j \\ \\ x-x_j \end{pmatrix}. \tag{IV.46}$$

We simply find the sum of the individual velocity fields of each of the vortices, which justifies the calculation made in § 2 for a pair of vortices.

In the following, it will be useful to have an expression for Φ and $\boldsymbol{v}_s^{\perp}$ in terms of the vortex density

$$\rho_v(\boldsymbol{r}) = \sum_j Q_j \, \delta(\boldsymbol{r}-\boldsymbol{r}_j). \tag{IV.47}$$

The expressions (IV.42) and (IV.45) can be rewritten as follows

$$\Phi(\boldsymbol{r}) = -\frac{\hbar}{m} \int \ln|\boldsymbol{r}-\boldsymbol{r}'| \, \rho_v(\boldsymbol{r}') \, \mathrm{d}^2 r' \tag{IV.48}$$

and

$$\boldsymbol{v}_s^{\perp}(\boldsymbol{r}) = \frac{\hbar}{m} \, \boldsymbol{u}_z \times \boldsymbol{\nabla} \left[\int \ln|\boldsymbol{r}-\boldsymbol{r}'| \, \rho_v(\boldsymbol{r}') \mathrm{d}^2 r' \right]. \tag{IV.49}$$

3-3 Energy of the vortices

Before turning to the thermodynamics of the gas, we need to evaluate the kinetic energy associated with the vortex velocity field. Expressing the velocity in terms of the function Φ [*cf.* (IV.42)], we obtain:

$$\begin{aligned} E_{\mathrm{kin}} &= \frac{1}{2} m\rho_s \int (\boldsymbol{v}_s^{\perp})^2(\boldsymbol{r}) \, \mathrm{d}^2 r \\ &= \frac{1}{2} m\rho_s \int \left[(\partial_x\Phi)^2 + (\partial_y\Phi)^2 \right] \mathrm{d}^2 r \\ &= -\frac{1}{2} m\rho_s \int \Phi(\boldsymbol{r}) \, \nabla^2\Phi(\boldsymbol{r}) \, \mathrm{d}^2 r \end{aligned} \tag{IV.50}$$

Magnetostatic	**Vortex**
current I_j	topological charges Q_j
magnetic field $\boldsymbol{B}(\boldsymbol{r})$	velocity field $\boldsymbol{v}_s(\boldsymbol{r})$
vector potential $\boldsymbol{A}(\boldsymbol{r})$	function $\Phi(\boldsymbol{r})\,\boldsymbol{u}_z$
$\boldsymbol{B} = \boldsymbol{\nabla} \times \boldsymbol{A}$	$\boldsymbol{v}_s = \boldsymbol{\nabla} \times [\Phi \, \boldsymbol{u}_z]$
magnetostatic energy $\frac{1}{2\mu_0} \int \boldsymbol{B}^2(\boldsymbol{r}) \, \mathrm{d}^2 r$	kinetic energy $\frac{\hbar^2 \rho_s}{2m} \int \boldsymbol{v}_s^2(\boldsymbol{r}) \, \mathrm{d}^2 r$

Table IV.1. *Analogy between the magnetic field created by a lattice of wires parallel to the z axis and the velocity field created by an assembly of vortices.*

where the integration by part of the last line is only possible if Φ tends to 0 at infinity, which imposes that the total topological charge of the vortices cancels out:

$$Q_{\mathrm{tot}} = \sum_j Q_j = 0. \tag{IV.51}$$

We had already noted in § 1 that this cancellation was a necessary condition for having a superfluid, so this restriction is not a problem.

Using now that $\nabla^2\Phi$ is a sum of Dirac distributions [*cf.* (IV.44)], the previous result simplifies to

$$E \approx N_v \epsilon_0 \; - \; \frac{2\pi\,\hbar^2\,\rho_s}{m} \sum_{i<j} Q_i Q_j \, \ln\left(\frac{|\boldsymbol{r}_i - \boldsymbol{r}_j|}{\xi} \right). \tag{IV.52}$$

The divergence in $\ln(R)$ that was present in the energy (IV.8) of an isolated vortex has disappeared due to the assumption (IV.51) of zero total topological charge. The velocity field decreases at least as fast as $1/r^2$ at infinity, so there is no problem of convergence of the integral defining the kinetic energy.

Magnetostatic analogy. The above results are formally identical to the well-known results for the magnetic field created by wires carrying constant currents I_j. More precisely, the situation envisaged here can be identified with the case of straight wires, all parallel to the z axis and crossing the xy plane at points r_j. The table IV.1 details the various elements of this identification.

4 Superfluid density in a 2D fluid

Superfluidity is a phenomenon characterized by (at least) two distinct properties:

- A superfluid state has a certain phase rigidity. For example, if the superfluid is contained in a bucket that is set in rotation at angular speed Ω, the superfluid will remain at rest in the laboratory reference frame – assumed to be Galilean – at least for low rotation speeds. A normal fluid, on the other hand, rotates for any choice of Ω and acquires the velocity field $\mathbf{\Omega} \times \boldsymbol{r}$ corresponding to rigid rotation.
- A current in a superfluid can be metastable. If the superfluid is set in motion inside a bucket that is immobile in the laboratory reference frame, this motion may last for a very long time. The criterion for metastability is that the relative motion of the superfluid and the roughnesses present on the container walls must have a velocity below a certain critical speed.

In what follows, we will focus on the first criterion, and attempt to calculate the phase rigidity of the two-dimensional superfluid when the contribution of vortices is taken into account.

4-1 Phase rigidity and twisted boundary conditions

The superfluid fraction of a quantum gas can be defined from the cost in free-energy of a slight distortion of the boundary conditions. Let us recall the physical origin of this definition: as mentioned above, the superfluid component corresponds to the fraction of the gas that refuses to move when the container containing the fluid is rotated at speed Ω. Seen from the rotating frame of reference, the normal fluid is at rest, while the superfluid rotates at speed $-\Omega$. In this frame of reference, the superfluid therefore possesses additional kinetic energy compared with the $\Omega = 0$ case.

The transition to the non-galilean rotating frame of reference can be made by replacing the usual periodic boundary conditions with twisted ones. In the change $x \to x + L$, the phase of the admissible wave functions is increased by a quantity Θ, where Θ depends linearly on Ω. The quantity $F(\Theta) - F(0)$ thus corresponds to the kinetic energy of the superfluid in the rotating frame of reference, given that this superfluid has in fact remained at rest in the laboratory frame of reference. For a completely normal fluid, the entire gas is at rest in the rotating frame of reference, so there is no cost associated with twisting the boundary conditions: $\rho_{\rm s} = 0$.

More precisely, we start with a fluid described by the classical field $\psi(\boldsymbol{r})$, for which we assume that the free energy $F(0)$ is known for periodic boundary conditions:

$$\psi(x + L, y) = \psi(x, y + L) = \psi(x, y). \tag{IV.53}$$

We now require the accessible states of the fluid to satisfy

$$\psi(x + L, y) = \mathrm{e}^{\mathrm{i}\Theta}\, \psi(x, y), \qquad \psi(x, y + L) = \psi(x, y), \qquad \Theta \ll 1, \tag{IV.54}$$

which corresponds to a distortion of the boundary conditions along the x axis. By symmetry, the free energy is an even function of Θ and we assume that it can be developed as a series in powers of Θ in the vicinity of $\Theta = 0$. The superfluid density $\rho_{\rm s}$ is defined by

$$F(\Theta) = F(0) + \frac{\hbar^2 \Theta^2}{2m} \rho_{\rm s} + \mathcal{O}(\Theta^4), \qquad \text{i.e.,} \quad \rho_{\rm s} = \frac{m}{\hbar^2} \left.\frac{\partial^2 F}{\partial \Theta^2}\right|_{\Theta=0}. \tag{IV.55}$$

For our 2D gas described by $\psi(\boldsymbol{r}) = \sqrt{\rho}_s\, \mathrm{e}^{\mathrm{i}\theta(\boldsymbol{r})}$ in the presence of twisted boundary conditions, the velocity field can be decomposed into three parts:

$$\boldsymbol{v} = \boldsymbol{v}_s^{\parallel} + \boldsymbol{v}_s^{\perp} + \boldsymbol{v}_\Theta. \tag{IV.56}$$

The longitudinal and transverse components have already been explained. The component $\boldsymbol{v}_\Theta$ reflects the fact that the phase of the wave function is

"twisted" by Θ over a distance L; we will assume here a linear variation:

$$\theta_{\rm twisted}(x) = \Theta \frac{x}{L} \qquad \rightarrow \qquad \boldsymbol{v}_\Theta = \frac{\hbar \Theta}{mL} \boldsymbol{u}_x. \tag{IV.57}$$

We will now evaluate the kinetic energy associated with this velocity field at the lowest non-zero order in Θ, to deduce the desired value of ρ_s. Our approach is similar to that described by Minnhagen & Warren (1981) [see also Chaikin & Lubensky (2000)].

4-2 Superfluid density and velocity correlations

Let us start with a gas of superfluid density $\rho_s^{(0)}$; at zero temperature, $\rho_s^{(0)}$ is equal to the total density ρ; at non-zero temperature, on the other hand, $\rho_s^{(0)} < \rho$. More precisely, the definition of superfluid density requires a minimum distance scale a. All density and phase fluctuations - including vortex pairs - whose length scale is less than a are assumed to be implicitly taken into account by the reduction $\rho \rightarrow \rho_s^{(0)}$. The principle of the renormalization group analysis discussed in the next paragraph is to study the behavior of $\rho_s^{(0)}$ as we increase the distance scale a to absorb more and more fluctuations.

In the presence of long-wavelength phonons and vortices, and with twisted boundary conditions, the kinetic energy is written:

$$\begin{aligned} E_{\rm kin}[\Theta, \boldsymbol{v}_s] &= \frac{m\rho_s^{(0)}}{2} \int (\boldsymbol{v}_\Theta + \boldsymbol{v}_s)^2 \ {\rm d}^2 r \\ &= \frac{mL^2 \rho_s^{(0)}}{2} v_\Theta^2 \ + \frac{m\rho_s^{(0)}}{2} \int \boldsymbol{v}_s^2 \ {\rm d}^2 r + m\rho_s^{(0)} \boldsymbol{v}_\Theta \cdot \int \boldsymbol{v}_s \ {\rm d}^2 r. \end{aligned} \tag{IV.58}$$

The Boltzmann weight ${\rm e}^{-E_{\rm kin}/k_{\rm B}T}$ entering the partition function and thermodynamic averages at equilibrium can then be written

$$\begin{aligned} \exp\left(-\frac{E_{\rm kin}[\Theta, \boldsymbol{v}_s]}{k_{\rm B}T}\right) &= \exp\left(-\frac{mL^2\rho_s^{(0)}}{2k_{\rm B}T} v_\Theta^2\right) \times \exp\left(-\frac{E_c[0, \boldsymbol{v}_s]}{k_{\rm B}T}\right) \\ &\times \exp\left(-\frac{m\rho_s^{(0)}}{k_{\rm B}T} \boldsymbol{v}_\Theta \cdot \int \boldsymbol{v}_s \ {\rm d}^2 r\right) \end{aligned} \tag{IV.59}$$

We will now inject this result into the partition function

$$\mathcal{Z}(\Theta) = \sum_{\{\boldsymbol{v}_s\}} \exp\left(-\frac{E[\Theta, \boldsymbol{v}_s]}{k_{\rm B}T}\right). \tag{IV.60}$$

This sum is to be understood as a functional integral. The energy in this expression is *a priori* the total energy, but the essential contribution comes from the kinetic energy to which we will add in due course the core energy ϵ_0 of each vortex, which will contribute via the fugacity of a vortex $y_0 = {\rm e}^{-\epsilon_0/k_{\rm B}T}$.

Once the partition function is known, we can deduce the free energy $F(\Theta) = -k_{\rm B}T \ln[\mathcal{Z}(\Theta)]$ and the superfluid density via:

$$\rho_s = \frac{m}{\hbar^2} \left.\frac{\partial^2 F}{\partial \Theta^2}\right|_{\Theta=0} = \frac{1}{mL^2} \left.\frac{\partial^2 F}{\partial v_\Theta^2}\right|_{v_\Theta=0}. \tag{IV.61}$$

Note that in the sum (IV.60) defining the partition function, the first term of the right-hand member of (IV.59) can be put as a global factor since it does not depend on the velocity field $\boldsymbol{v}_s$.

To evaluate $\mathcal{Z}(\Theta)$, let us use the fact that we are interested in arbitrarily small values of Θ. We can then use the expansion:

$$\begin{aligned} \exp\left(-\frac{m\rho_s^{(0)}}{k_{\rm B}T} \boldsymbol{v}_\Theta \cdot \int \boldsymbol{v}_s \ {\rm d}^2 r\right) &\approx 1 - \frac{m\rho_s^{(0)}}{k_{\rm B}T} v_\Theta \int v_{s,x} \ {\rm d}^2 r \\ &+ \frac{1}{2}\left(\frac{m\rho_s^{(0)}}{k_{\rm B}T}\right)^2 v_\Theta^2 \iint v_{s,x}(\boldsymbol{r}) \ v_{s,x}(\boldsymbol{r}') \ {\rm d}^2 r \ {\rm d}^2 r' \end{aligned} \tag{IV.62}$$

where we have taken the vector $\boldsymbol{v}_\Theta$ parallel to the x direction, as explained in (IV.57).

From this result, when we multiply by the weight $\exp(-E_{\rm kin}[0, \boldsymbol{v}_s]/k_{\rm B}T)$ given in (IV.59) and integrate over $\boldsymbol{v}_s$, we see that the contribution of the linear term in v_Θ has by symmetry a zero mean

and we are left with

$$\mathcal{Z}(\Theta) \approx \exp\left(-\frac{mL^2\rho_s^{(0)}}{2k_{\rm B}T}v_\Theta^2\right)\times\mathcal{Z}(0) \quad \text{(IV.63)}$$

$$\times \left(1+\frac{1}{2}\left(\frac{m\rho_s^{(0)}}{k_{\rm B}T}\right)^2 v_\Theta^2 \iint \langle v_{s,x}(\boldsymbol{r})\, v_{s,x}(\boldsymbol{r}')\rangle\, {\rm d}^2r\, {\rm d}^2r'\right) \quad \text{(IV.64)}$$

This gives us the free energy $F(\Theta) = -k_{\rm B}T\ln[\mathcal{Z}(\Theta)]$.

$$F(\Theta) \approx \frac{1}{2}mL^2\rho_s^{(0)}v_\Theta^2 + F(0) - \frac{1}{2}\frac{(m\rho_s^{(0)})^2}{k_{\rm B}T}v_\Theta^2 \iint \langle v_{s,x}(\boldsymbol{r})\, v_{s,x}(\boldsymbol{r}')\rangle\, {\rm d}^2r\, {\rm d}^2r'. \quad \text{(IV.65)}$$

We have therefore linked the free energy $F(\Theta)$ at second-order included in Θ to the correlation function of the velocity field, calculated in the absence of phase twist. We saw earlier that this velocity field has two components, one longitudinal linked to the phase gradient $\theta(\boldsymbol{r})$ and phonons, the other transverse linked to vortices. The longitudinal component does not contribute to the above integral, since $\int \boldsymbol{v}^{\parallel}(\boldsymbol{r})\, {\rm d}^2r = 0$ if we impose periodic boundary conditions (without material flow) on the walls of the box. In this case, we can make the substitution

$$\langle v_{s,x}(\boldsymbol{r})\, v_{s,x}(\boldsymbol{r}')\rangle \longrightarrow \langle v_{s,x}^{\perp}(\boldsymbol{r})\, v_{s,x}^{\perp}(\boldsymbol{r}')\rangle. \quad \text{(IV.66)}$$

All that remains is to take the second derivative with respect to v_Θ to obtain the "renormalized" superfluid density ρ_s:

$$\rho_s = \rho_s^{(0)} - \frac{m(\rho_s^{(0)})^2}{k_{\rm B}T}\,\frac{1}{L^2}\iint \langle v_{s,x}^{\perp}(\boldsymbol{r})\, v_{s,x}^{\perp}(\boldsymbol{r}')\rangle\, {\rm d}^2r\, {\rm d}^2r'. \quad \text{(IV.67)}$$

This important result shows that the velocity field due to vortices is capable of reducing or even completely eliminating superfluid density. On the other hand, the presence of long-wavelength phonons, responsible for the field $\boldsymbol{v}^{\parallel}$, does not change the initial superfluid density; this is the result we stated in the previous chapter and which finds its justification here.

4-3 Superfluid density and vortex positions

To go one step further and set up the appropriate equations for the renormalization procedure, it is useful to express the superfluid density ρ_s in terms of the vortex positions rather than the velocity field they create. To do this, let us introduce a convergence factor $\mathrm{e}^{\mathrm{i}q_y(y'-y)}$ into the integral appearing in (IV.67), considering the limit $q_y \to 0$:

$$\iint \langle v_{s,x}^{\perp}(\boldsymbol{r})\, v_{s,x}^{\perp}(\boldsymbol{r}')\rangle {\rm d}^2r\, {\rm d}^2r' = \lim_{q_y\to 0}\iint \langle v_{s,x}^{\perp}(\boldsymbol{r})\, v_{s,x}^{\perp}(\boldsymbol{r}')\rangle\, \mathrm{e}^{\mathrm{i}q_y(y'-y)}{\rm d}^2r\, {\rm d}^2r'$$
$$= (2\pi)^2 \lim_{q_y\to 0}\langle \hat{v}_{s,x}^{\perp}(\boldsymbol{q})\, \hat{v}_{s,x}^{\perp}(-\boldsymbol{q})\rangle \quad \text{(IV.68)}$$

where we set $\boldsymbol{q} = (0, q_y)$ and introduce the Fourier transform of the transverse superfluid velocity field

$$\hat{\boldsymbol{v}}_s^{\perp}(\boldsymbol{q}) = \frac{1}{2\pi}\int \boldsymbol{v}_s^{\perp}(\boldsymbol{r})\, \mathrm{e}^{-\mathrm{i}\boldsymbol{q}\cdot\boldsymbol{r}}\, {\rm d}^2r. \quad \text{(IV.69)}$$

We gave in (IV.37) the Fourier transform $\hat{\boldsymbol{v}}_s^{\perp}(\boldsymbol{q})$ of the velocity field created by a vortex of charge $Q_j = 1$ localized at $\boldsymbol{r}_j = 0$. From this we deduce the velocity field created by the vortex assembly:

$$\hat{\boldsymbol{v}}_s^{\perp}(\boldsymbol{q}) = \mathrm{i}\,\frac{\hbar}{mq^2}\,\boldsymbol{q}\times\boldsymbol{u}_z\sum_j Q_j\,\mathrm{e}^{-\mathrm{i}\boldsymbol{q}\cdot\boldsymbol{r}_j}, \quad \text{(IV.70)}$$

or for the component $\hat{v}_{s,x}^{\perp}$ which is of interest for evaluating (IV.68) and the choice $\boldsymbol{q} = (0, q_y)$:

$$\hat{v}_{s,x}^{\perp}(\boldsymbol{q}) = \mathrm{i}\,\frac{\hbar}{mq_y}\,\sum_j Q_j \mathrm{e}^{-\mathrm{i}q_y\, y_j}. \quad \text{(IV.71)}$$

We therefore arrive at

$$\lim_{q_y\to 0}\langle \hat{v}_{s,x}^{\perp}(-\boldsymbol{q})\, \hat{v}_{s,x}^{\perp}(-\boldsymbol{q})\rangle = \frac{\hbar^2}{m^2}\lim_{q_y\to 0}\left[\frac{1}{q_y^2}\sum_{i,j}\boldsymbol{Q}_i\boldsymbol{Q}_j\mathrm{e}^{\mathrm{i}q_y\,(y_i-y_j)}\right]. \quad \text{(IV.72)}$$

To evaluate the limit $q_y \to 0$ of the bracketed expression, let us expand the exponential $\mathrm{e}^{\mathrm{i}q_y(y_i-y_j)}$ to order two in q_y:

$$\mathrm{e}^{\mathrm{i}q_y(y_i-y_j)} \approx 1 + \mathrm{i}q_y(y_i-y_j) - \frac{1}{2}q_y^2(y_i-y_j)^2 + \ldots \quad \text{(IV.73)}$$

The contribution of the first two terms is zero as we restrict ourselves to vortex assemblies of zero total topological charge, $\sum_i Q_i = 0$. The $q_y \to 0$ limit of the third term gives

$$\begin{aligned} \lim_{q_y\to 0} \langle \hat{v}^{\perp}_{s,x}(-\boldsymbol{q})\ \hat{v}^{\perp}_{s,x}(-\boldsymbol{q})\rangle &= -\frac{\hbar^2}{2m^2}\sum_{i,j} \boldsymbol{Q}_i\boldsymbol{Q}_j\ (y_i - y_j)^2 \\ &= -\frac{\hbar^2}{4m^2}\sum_{i,j} \boldsymbol{Q}_i\boldsymbol{Q}_j\ (\boldsymbol{r}_i - \boldsymbol{r}_j)^2. \quad \text{(IV.74)} \end{aligned}$$

This result can be expressed in terms of the vortex density $\rho_v(\boldsymbol{r}) = \sum_j Q_j\ \delta(\boldsymbol{r} - \boldsymbol{r}_j)$.

$$\begin{aligned} \sum_{i,j} \boldsymbol{Q}_i\boldsymbol{Q}_j\ (\boldsymbol{r}_i - \boldsymbol{r}_j)^2 &= \iint (\boldsymbol{r} - \boldsymbol{r}')^2\ \langle \rho_v(\boldsymbol{r})\,\rho_v(\boldsymbol{r}')\rangle\ \mathrm{d}^2r\ \mathrm{d}^2r' \\ &= L^2 \int r^2\ \langle \rho_v(\boldsymbol{r})\,\rho_v(0)\rangle\ \mathrm{d}^2r \quad \text{(IV.75)} \end{aligned}$$

so that from (IV.67)

$$\rho_s = \rho_s^{(0)} + \frac{\pi^2\hbar^2}{mk_{\mathrm{B}}T}\ (\rho_s^{(0)})^2 \int r^2\ \langle \rho_v(\boldsymbol{r})\ \rho_v(0)\rangle\ \mathrm{d}^2r. \quad \text{(IV.76)}$$

Finally, this expression can be written in a compact way using the phase-space density associated with the superfluid fraction $\mathcal{D}_s = \rho_s\lambda_T^2$:

$$\mathcal{D}_s = \mathcal{D}_s^{(0)} + \frac{\pi}{2}(\mathcal{D}_s^{(0)})^2 \int r^2\ \langle \rho_v(\boldsymbol{r})\,\rho_v(0)\rangle\ \mathrm{d}^2r. \quad \text{(IV.77)}$$

To evaluate the density-density correlation function for vortices, let us restrict ourselves to the first non-zero term, which corresponds to a vortex-antivortex pair, with either the $+$ vortex in 0 and the $-$ vortex in $\boldsymbol{r}$, or vice versa. This amounts to evaluating the first term in a expansion in powers of the vortex fugacity y_0. Using the Boltzmann weight found in (IV.25) for such a pair, and restricting ourselves to pairs with separation greater than a, we have

$$\int r^2\ \langle \rho_v(\boldsymbol{r})\ \rho_v(0)\rangle\ \mathrm{d}^2r \approx -\frac{2\,y_0^2}{a^4}\int_a^{+\infty} r^2\left(\frac{a}{r}\right)^{\mathcal{D}_s^{(0)}}\ 2\pi r\ \mathrm{d}r, \quad \text{(IV.78)}$$

which leads to, passing[2] of the function $\mathcal{D}_s$ to $1/\mathcal{D}_s$:

$$\frac{1}{\mathcal{D}_s} = \frac{1}{\mathcal{D}_s^{(0)}} + 2\pi^2 y_0^2 \int_a^{+\infty}\left(\frac{a}{r}\right)^{\mathcal{D}_s^{(0)}-3}\ \frac{\mathrm{d}r}{a}. \quad \text{(IV.81)}$$

Note that in this expression, the fugacity y_0 of a vortex is itself a function of the cutoff length a, since the vortex core energy contributing to y_0 depends on the boundary imposed on this core region.

4-4 The principle of renormalization

Renormalization for the BKT problem involves gradually increasing the distance scale a to absorb more and more aspects of short-distance physics, in particular bound vortex-antivortex pairs, into the superfluid density $\rho_s^{(0)}$. The question is whether, at the end of this process, $\rho_s^{(0)}$ will have converged to a zero or non-zero value. The action of the renormalization group can be seen as a succession of two steps [Kardar (2007), Chapters 4 and 8]:

- Starting from the coarse-grained average performed on the distance scale a, we slightly increase this scale $a \to \tilde{a} = a(1+\epsilon)$. The integral (IV.81) is rewritten:

$$\int_a^{+\infty} \ldots = \int_a^{a(1+\varepsilon)} \ldots + \int_{a(1+\varepsilon)}^{+\infty} \ldots \quad \text{(IV.82)}$$

  and the component between a and $a(1+\varepsilon)$ is incorporated into $1/\mathcal{D}_s^{(0)}$

[2] The relation $\mathcal{D}_s = \mathcal{D}_s^{(0)} + \alpha(\mathcal{D}_s^{(0)})^2$ with $\alpha\mathcal{D}_s^{(0)} \ll 1$ can indeed be written:

$$\frac{1}{\mathcal{D}_s} = \frac{1}{\mathcal{D}_s^{(0)} + \alpha(\mathcal{D}_s^{(0)})^2} = \frac{1}{\mathcal{D}_s^{(0)}}\,\frac{1}{1+\alpha\mathcal{D}_s^{(0)}} \approx \frac{1}{\mathcal{D}_s^{(0)}}\left(1 - \alpha\mathcal{D}_s^{(0)}\right) = \frac{1}{\mathcal{D}_s^{(0)}} - \alpha. \quad \text{(IV.79)}$$

Moreover, this relationship is written in several textbooks in terms of the quantity $K = \hbar^2\rho_s/mk_{\mathrm{B}}T = \mathcal{D}_s/2\pi$, which gives:

$$\frac{1}{K} = \frac{1}{K_0} + 4\pi^3 y_0^2 \int_a^{+\infty}\left(\frac{a}{r}\right)^{2\pi K_0 - 3}\ \frac{\mathrm{d}r}{a}. \quad \text{(IV.80)}$$

which becomes $1/\tilde{\mathcal{D}}_s^{(0)}$:

$$\frac{1}{\tilde{\mathcal{D}}_s^{(0)}} = \frac{1}{\mathcal{D}_s^{(0)}} + 2\pi^2 y_0^2 \int_a^{a(1+\varepsilon)} \left(\frac{a}{r}\right)^{\mathcal{D}_s^{(0)}-3} \frac{\mathrm{d}r}{a}. \tag{IV.83}$$

The equation (IV.81) is then written as

$$\frac{1}{\mathcal{D}_s} = \frac{1}{\tilde{\mathcal{D}}_s^{(0)}} + 2\pi^2 y_0^2 \int_{a(1+\varepsilon)}^{+\infty} \left(\frac{a}{r}\right)^{\mathcal{D}_s^{(0)}-3} \frac{\mathrm{d}r}{a}. \tag{IV.84}$$

- We then perform a scaling transformation on (IV.84) to bring $a(1+\varepsilon)$ back to a, which in particular modifies y_0: $y_0 \to \tilde{y}_0$:

$$\frac{1}{\mathcal{D}_s} = \frac{1}{\tilde{\mathcal{D}}_s^{(0)}} + 2\pi^2 \tilde{y}_0^2 \int_a^{+\infty} \left(\frac{a}{r}\right)^{\tilde{\mathcal{D}}_s^{(0)}-3} \frac{\mathrm{d}r}{a} \tag{IV.85}$$

with

$$\tilde{y}_0 = y_0 \, (1+\varepsilon)^{\left(4-\mathcal{D}_s^{(0)}\right)/2}. \tag{IV.86}$$

Note that we replaced $\mathcal{D}_s^{(0)}$ by $\tilde{\mathcal{D}}_s^{(0)}$ in the exponent of the integrand of (IV.85), thus ensuring the invariance of the equation after the action of the renormalization group. This point can be justified by looking at the next-order terms (order 4) in the power development of y_0 (Chaikin & Lubensky 2000).

The limit $\varepsilon \to 0$ in the two equations (IV.83) and (IV.86) then leads to the differential system for the pair of functions $\left[\mathcal{D}_s^{(0)}, y_0\right]$

$$\frac{\mathrm{d}[\mathcal{D}_s^{(0)}]^{-1}}{\mathrm{d}\varepsilon} = 2\pi^2 y_0^2 \tag{IV.87}$$

$$\frac{\mathrm{d}y_0}{\mathrm{d}\varepsilon} = \frac{1}{2}\left(4 - \mathcal{D}_s^{(0)}\right) y_0 \tag{IV.88}$$

We will not go into the details of how to solve this system which, since the initial articles by Kosterlitz (1974), Nelson (1977) and Jose (1977), has become a classic in the field of statistical field theory. Let us just mention here the main results, illustrated in figure IV.9:

- If we start with a superfluid density $\mathcal{D}_s^{(0)} < 4$, then we always end up with a zero superfluid density.

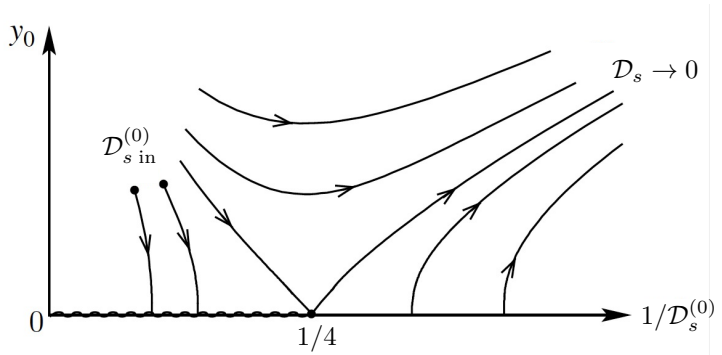

Figure IV.9. *Trajectories in the plane $\left[\mathcal{D}_s^{(0)}, y_0\right]$ obtained by the action of the renormalization procedure. Figure adapted from Kardar (2007).*

- If we start with a superfluid density $\mathcal{D}_s^{(0)} > 4$ and a fairly low fugacity y_0 (i.e., creating a vortex costs a significant energy), then we end the renormalization procedure still with $\mathcal{D}_s^{(0)} > 4$ and zero fugacity: the vortices have been erased and the gas is superfluid.

- If we start from a superfluid density $\mathcal{D}_s^{(0)} > 4$, but with a high fugacity for vortices (i.e., creating a vortex costs almost nothing in energy compared to $k_\mathrm{B}T$), we end up in a non-superfluid state. Note, however, that the conclusion for this situation can be invalidated for systems of finite size, as the limit of the renormalization procedure is not necessarily reached.

The BKT transition that occurs when $\mathcal{D}_s$ decreases to reach the critical value

$$\mathcal{D}_{s,\,\mathrm{crit.}} = 4 \tag{IV.89}$$

is very different from ordinary first- or second-order phase transitions:

- First of all, all thermodynamic functions are continuous and derivable at the transition point: we did not find the BKT transition by looking for singularities of the free energy and its derivatives with respect to the usual thermodynamic variables (chemical potential and temperature). There are therefore no critical exponents associated with the

transition. Superfluid density, on the other hand, is discontinuous, jumping from value 4 to value 0 at this point. This jump is often referred to as universal because its amplitude $\Delta\mathcal{D}_s = 4$ is independent of the strength $\tilde{g}$ of the interactions. We anticipated this result when we analyzed the probability of a free vortex appearing in the sample.

- This jump in superfluid density is accompanied by a change in the behavior of the one-body function $G_1(r)$. For $T < T_c$, in the superfluid zone, $G_1(r)$ decreases algebraically; this is the long-range quasi-order we studied in the previous chapter. For $T > T_c$, in the normal zone, G_1 decreases exponentially with distance. This is because isolated vortices proliferate in the gas, and there can be no significant phase coherence between two points if the probability of having a vortex between these two points is itself significant.

- We can show that this infinite-order transition is characterized by an extremely strong divergence of the correlation length as we approach the $T > T_c$ side. The function $G_1(r)$ decays exponentially in this non-superfluid zone, $G_1(r) \propto \mathrm{e}^{-r/\ell}$, but the decay length increases rapidly:

$$\ell \sim \lambda_T \exp\left(\frac{\sqrt{\zeta\, T_{\mathrm{BKT}}}}{\sqrt{T - T_{\mathrm{BKT}}}}\right) \qquad \text{(IV.90)}$$

where ζ is a constant. The size of the critical region is thus increased compared to a conventional transition, making finite-size effects play a more important role.

4-5 First experimental studies: helium films

Five years after BKT's theoretical papers, Bishop & Reppy (1978) provided excellent experimental confirmation of the existence of a superfluid transition in liquid helium films. These experiments, described in detail in Bishop, Krumhansl, et al. (1980), then Agnolet, McQueeney, et al. (1989), are carried out by depositing a very thin layer of helium atoms (between 1 and 10 atomic layers) on a sheet of Mylar. This foil, with a thickness of 6 μm, is rolled up on itself and has a total surface area of 0.4 m^2 in the 1978 experiments [2 m^2 for Agnolet, McQueeney, et al. (1989)].

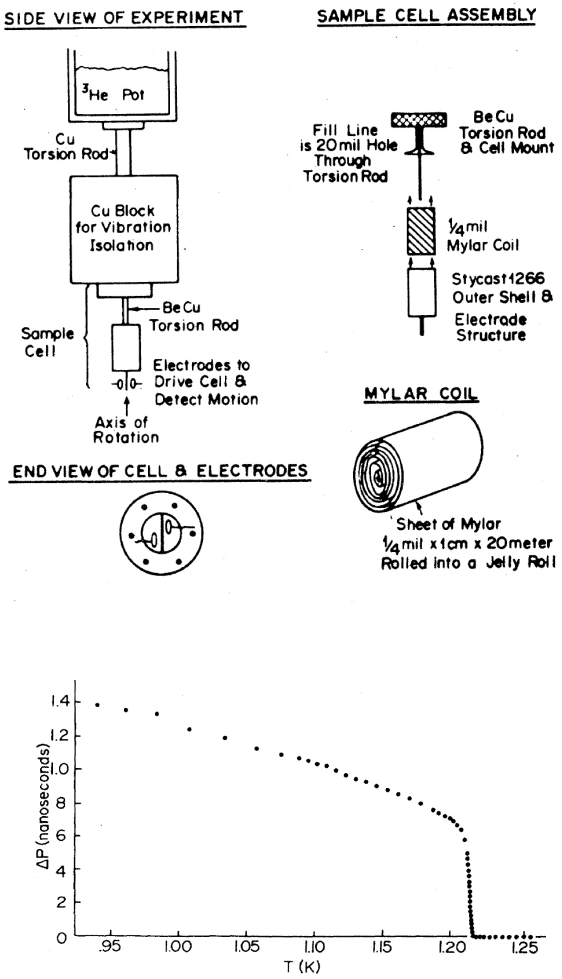

Figure IV.10. *Top: experimental diagram used by Bishop & Reppy (1978). A sheet of Mylar with surface area $\sim 0.4\,m^2$ is covered with a film of liquid helium. The film is only a few atomic layers thick. The Mylar sheet is mounted on a torsion pendulum to measure the moment of inertia of the Mylar+helium film assembly. Bottom: Example of results for the period of the torsion pendulum as a function of system temperature. The superfluid transition manifests itself as a sudden reduction in the moment of inertia. Figures taken from Bishop & Reppy (1978) and Bishop, Krumhansl, et al. (1980).*

The possible superfluidity of the helium film is tested by moving the Mylar sheet and measuring whether the helium film adsorbed on this surface also moves. If it does, the fluid is normal. If, on the other hand, a fraction of the fluid remains at rest, we are dealing with a superfluid. For precise measurement, the Mylar sheet is attached to a torsion pendulum with a high quality factor, $Q > 10^5$ (Andronikashvili experiment). The frequency of oscillation of the assembly is around 2.6 kHz and is measured with excellent relative accuracy, of the order of $5\ 10^{-9}$. The oscillation period, around 380 μs, is thus obtained with an accuracy of 2 picoseconds!

An example of how this period varies with temperature, for a film of given thickness, is shown in figure IV.10. It shows a constant period at "high" temperature, $T > 1.22$ K, and then a jump in this period of around 6 ns, corresponding to a reduction in the moment of inertia of the system. This can be interpreted as the fact that part of the helium film has become superfluid, and the corresponding mass is therefore not oscillating. As the film cools further, the reduction in period increases, indicating that a larger and larger fraction of the film becomes superfluid.

Since the superfluid fraction is measured around the frequency of 2.6 kHz and not at zero frequency, in order to give a quantitative account of this experiment it is necessary to extend the BKT theory to include the dynamical aspect of vortex motion. This extension was made by Ambegaokar, Halperin, et al. (1978) and the agreement with experimental measurements is excellent (figure IV.11). In particular, it explains why we do not observe in the strict sense a jump of the superfluid density corresponding to $\Delta\mathcal{D}_s = 4$, but rather a rapid variation over a range of the order of 5 mK. Repetition of these measurements for different quantities of helium deposited on the Mylar sheet is shown in figure IV.12. Each thickness corresponds to a couple "critical temperature – $\Delta\rho_s$ jump", and Bishop & Reppy (1978) were able to verify that the expected $\Delta\rho_s \propto T$ law was indeed satisfied.

Helium crystals and roughening transition. Another example of a BKT transition in cold helium is the roughening transition. This transition occurs at the interface between the ^{4}He superfluid and a helium crystal. Below the critical temperature, a flat facet develops in the direction of growth; above T_c, the surface is roughened. Experiments have confirmed many

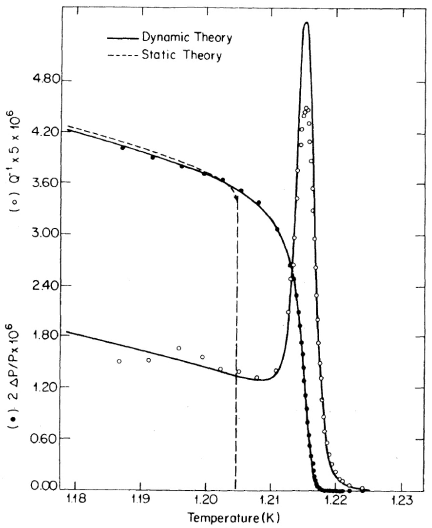

Figure IV.11. *Fitting experimental data with dynamical BKT theory by Ambegaokar, Halperin, et al. (1978). The dashed curve represents the static BKT theory studied in this chapter. The data in open symbols represents the excess dissipation Q^{-1} due to the superfluid (not discussed in this lecture). Figure taken from Bishop & Reppy (1978).*

of the characteristics of the BKT transition, for example by measuring the crystal growth rate as a function of temperature (Balibar & Castaing 1980; Wolf, Balibar, et al. 1983; Wolf, Gallet, et al. 1985; Gallet, Balibar, et al. 1987).

Hydrogen films. Finally, let us mention the study of a two-dimensional hydrogen gas adsorbed on the surface of a bath of liquid helium (Safonov, Vasilyev, et al. 1998). Hydrogen atoms float above the bath at a distance of around 8 micrometers. They do not form a stable gas: in a three-body collision, two atoms can recombine to form a H_2 molecule, with the third body carrying away the energy released. The rate of three-body processes varies as $\langle\rho^3\rangle$; in an ordinary gas, density fluctuations lead to $\langle\rho^3\rangle \approx 3!\,(\langle\rho\rangle)^3$. For a gas where density fluctuations are frozen (quasi-condensate), we expect $\langle\rho^3\rangle \approx (\langle\rho\rangle)^3$, a reduction of $3! = 6$. Safonov, Vasilyev, et al. (1998) actu-

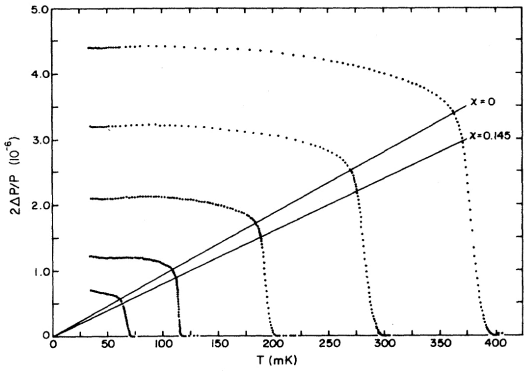

Figure IV.12. *Measurement of the BKT transition for different amounts of helium adsorbed on Mylar, showing the shift in transition temperature T_c and the jump in superfluid density ρ_s. The law $\Delta\rho_s \propto T$ predicted by BKT theory corresponds to the solid straight lines. The phenomenological parameter χ called* geometric hindrance *represents the fraction of superfluid that is not free to move relative to the Mylar due to imperfections in the foil winding; its experimental value, measured independently, is 0.145. Figure taken from Agnolet, McQueeney, et al. (1989).*

ally measured a reduction in the loss rate of about an order of magnitude by cooling the gas to a temperature comparable to that predicted by BKT theory.

Bibliography

Adhikari, Sadhan K. (1986), "Quantum scattering in two dimensions", in *American Journal of Physics* **54**, pp. 362–367.

Agnolet, Glenn, DF McQueeney & JD Reppy (1989), "Kosterlitz-Thouless transition in helium films", in *Physical Review B* **39**, p. 8934.

Ambegaokar, Vinay, B. I. Halperin, David R. Nelson & Eric D. Siggia (1978), "Dissipation in Two-Dimensional Superfluids", in *Phys. Rev. Lett.* **40** (12), pp. 783–786.

Ashcroft, N. W. & N. D. Mermin (1976), *Solid State Physics*, New York: Holt, Rinehardt and Winston.

Bagnato, V., D. E. Pritchard & D. Kleppner (1987), "Bose–Einstein condensation in an external potential", in *Phys. Rev. A* **35**, p. 4354.

Bagnato, V. S. & D. Kleppner (1991), "Bose–Einstein condensation in low-dimensional traps", in *Phys. Rev. A* **44**, pp. 7439–7441.

Balibar, S & B Castaing (1980), "Possible observation of the roughening transition in helium", in *Journal de Physique Lettres* **41**, pp. 329–332.

Berezinskii, V. L. (1971), "Destruction of long-range order in one-dimensional and two-dimensional system possessing a continous symmetry group - II. quantum systems", in *Soviet Physics JETP* **34**, p. 610.

Bishop, A.R., J.A. Krumhansl & S.E. Trullinger (1980), "Solitons in condensed matter: a paradigm", in *Physica D: Nonlinear Phenomena* **1**, pp. 1–44.

Bishop, D. J. & J. D. Reppy (1978), "Study of the Superfluid Transition in Two-Dimensional ^{4}He Films", in *Phys. Rev. Lett.* **40**, pp. 1727–1730.

Bloch, I., J. Dalibard & W. Zwerger (2008), "Many-body physics with ultracold gases", in *Rev. Mod. Phys* **80**, p. 885.

Bogoliubov, NN (1962), in *Physik. Abhandl. Sowjetunion* **6**, pp. 1–113–229.

Bramwell, S. T. & P. C. W. Holdsworth (1994), "Magnetization: A characteristic of the Kosterlitz–Thouless–Berezinskii transition", in *Phys. Rev. B* **49**, pp. 8811–8814.

Castin, Y (2001), "Bose-Einstein condensates in atomic gases: simple theoretical results", in *Coherent atomic matter waves (Les Houches Summer School 1999)*, ed. by Kaiser R., Westbrook C. & David F., EDP Sciences and Springer-Verlag.

Castin, Y. (2004), "Simple theoretical tools for low dimension Bose gases", in *Journal de Physique IV, France* **116**, p. 87.

Castro Neto, A. H., F. Guinea, N. M. R. Peres, K. S. Novoselov & A. K. Geim (2009), "The electronic properties of graphene", in *Rev. Mod. Phys.* **81** (1), pp. 109–162.

Chaikin, Paul M & Tom C Lubensky (2000), *Principles of condensed matter physics*, Cambridge university press.

Chiocchetta, Alessio, Andrea Gambassi & Iacopo Carusotto (2015), "Laser operation and Bose-Einstein condensation: analogies and differences", in *arXiv:1503.02816*.

Cohen-Tannoudji, Claude & Cécile Robilliard (2001), "Wave functions, relative phase and interference for atomic Bose–Einstein condensates", in *Comptes Rendus de l'Académie des Sciences-Series IV-Physics* **2**, pp. 445–477.

Connaughton, Colm, Christophe Josserand, Antonio Picozzi, Yves Pomeau & Sergio Rica (2005), "Condensation of Classical Nonlinear Waves", in *Phys. Rev. Lett.* **95** (26), p. 263901.

Damm, Tobias, Julian Schmitt, Qi Liang, David Dung, Frank Vewinger, Martin Weitz & Jan Klaers (2016), "Calorimetry of a Bose-Einstein-condensed photon gas", in *Nature communications* **7**.

De Groot, SR, GJ0039 Hooyman & CA Ten Seldam (1950), "On the Bose-Einstein condensation", in *Proceedings of the Royal Society of London. Series A. Mathematical and Physical Sciences* **203**, pp. 266–286.

Deutschländer, Sven, Patrick Dillmann, Georg Maret & Peter Keim (2015), "Kibble–Zurek mechanism in colloidal monolayers", in *Proceedings of the National Academy of Sciences* **112**, pp. 6925–6930.

Deutschländer, Sven, Antonio M Puertas, Georg Maret & Peter Keim (2014), "Specific heat in two-dimensional melting", in *Physical review letters* **113**, p. 127801.

Fasolino, Annalisa, JH Los & Mikhail I Katsnelson (2007), "Intrinsic ripples in graphene", in *Nature materials* **6**, pp. 858–861.

Gallet, F, S Balibar & E Rolley (1987), "The roughening transition of crystal surfaces. II. experiments on static and dynamic properties near the first roughening transition of hcp 4He", in *Journal de Physique* **48**, pp. 369–377.

Gardiner, Crispin & Peter Zoller (2004), *Quantum noise*, Springer Science & Business Media.

Giorgetti, L., I. Carusotto & Y. Castin (2007), "Semiclassical field method for the equilibrium Bose gas and application to thermal vortices in two dimensions", in *Phys. Rev. A* **76**, p. 013613.

Halperin, B. I. & David R. Nelson (1978a), "Theory of Two-Dimensional Melting", in *Phys. Rev. Lett.* **41**, pp. 121–124.

– (1978b), "Theory of Two-Dimensional Melting.", in *Phys. Rev. Lett.* **41** (7), pp. 519–519.

Herbut, Igor (2007), *A modern approach to critical phenomena*, Cambridge University Press.

Hohenberg, P. C. (1967), "Existence of Long-Range Order in One and Two Dimensions", in *Phys. Rev.* **158**, p. 383.

Illing, Bernd, Sebastian Fritschi, Herbert Kaiser, Christian L Klix, Georg Maret & Peter Keim (2017), "Mermin–Wagner fluctuations in 2D amorphous solids", in *Proceedings of the National Academy of Sciences* **114**, pp. 1856–1861.

José, Jorge V (2013), *40 years of Berezinskii-Kosterlitz-Thouless theory*, World Scientific.

Kagan, Y., B. V. Svistunov & G. V. Shlyapnikov (1987), "Influence on inelastic processes of the phase transition in a weakly collisional two-dimensional Bose gas", in *Sov. Phys. JETP* **66**, p. 314.

Kardar, Mehran (2007), *Statistical physics of fields*, Cambridge University Press.

Keim, Peter, Georg Maret & Hans-Hennig von Grünberg (2007), "Frank's constant in the hexatic phase", in *Physical Review E* **75**, p. 031402.

Ketterle, W. & N. J. vanDruten (1996), "Bose–Einstein condensation of a finite number of particles trapped in one or three dimensions", in *Phys. Rev. A* **54**, pp. 656–660.

Klaers, Jan, Julian Schmitt, T Damm, F Vewinger & M Weitz (2011), "Bose–Einstein condensation of paraxial light", in *Applied Physics B: Lasers and Optics* **105**, pp. 17–33.

Klaers, Jan, Julian Schmitt, Frank Vewinger & Martin Weitz (2010), "Bose-Einstein condensation of photons in an optical microcavity", in *Nature* **468**, pp. 545–548.

Kosterlitz, J. M. & D. J. Thouless (1973), "Ordering, metastability and phase transitions in two dimensional systems", in *J. Phys. C: Solid State Physics* **6**, p. 1181.

Leggett, A. J. (2006), *Quantum Liquids*, Oxford University Press.

Ma, Shang-Keng (1985), *Statistical Mechanics*, World Scientific.

Marelic, Jakov & RA Nyman (2015), "Experimental evidence for inhomogeneous pumping and energy-dependent effects in photon Bose-Einstein condensation", in *Physical Review A* **91**, p. 033813.

Marelic, Jakov, Lydia F Zajiczek, Henry J Hesten, Kon H Leung, Edward Y X Ong, Florian Mintert & Robert A Nyman (2016), "Spatiotemporal coherence of non-equilibrium multimode photon condensates", in *New Journal of Physics* **18**, p. 103012.

Mermin, N. D. (1968), "Crystalline Order in Two Dimensions", in *Phys. Rev.* **176** (1), pp. 250–254.

– (1979), "Erratum: Crystalline order in two dimensions", in *Phys. Rev. B* **20** (11), pp. 4762–4762.

– (2006), "Erratum: Erratum: Crystalline order in two dimensions [Phys. Rev. 176, 250 (1968)] [Phys. Rev. B 20, 4762 (1979)]", in *Phys. Rev. B* **74** (14), p. 149902.

Mermin, N. D. & H. Wagner (1966), "Absence of Ferromagnetism or Antiferromagnetism in One- or Two-Dimensional Isotropic Heisenberg Models", in *Phys. Rev. Lett.* **17**, p. 1133.

Minnhagen, Petter & G. G. Warren (1981), "Superfluid density of a two-dimensional fluid", in *Phys. Rev. B* **24**, pp. 2526–2532.

Mora, C. & Y. Castin (2003), "Extension of Bogoliubov theory to quasicondensates", in *Phys. Rev. A* **67**, p. 053615.

Mora, Christophe & Yvan Castin (2009), "Ground State Energy of the Two-Dimensional Weakly Interacting Bose Gas: First Correction Beyond Bogoliubov Theory", in *Phys. Rev. Lett.* **102**, p. 180404.

Mudry, Christopher (2014), *Lecture notes on field theory in condensed matter physics*, World Scientific Publishing Co Inc.

Nelson, David R (2002), *Defects and geometry in condensed matter physics*, Cambridge University Press.

Nelson, David R. & B. I. Halperin (1979), "Dislocation-mediated melting in two dimensions", in *Phys. Rev. B* **19**, pp. 2457–2484.

Nozières, P. & D. Pines (1990), *The Theory of Quantum Liquids, Superfluid Bose Liquids*, Addison-Wesley.

Onsager, Lars (1944), "Crystal statistics. I. A two-dimensional model with an order-disorder transition", in *Physical Review* **65**, p. 117.

Ozawa, Tomoki & Sandro Stringari (2014), "Discontinuities in the First and Second Sound Velocities at the Berezinskii-Kosterlitz-Thouless Transition", in *Phys. Rev. Lett.* **112** (2), p. 025302.

Peierls, R. E. (1934), in *Helv. Phys. Acta* **7**, p. 81.

Peierls, R. E. (1935), "Quelques propriétés typiques des corps solides", in *Ann. Inst. Henri Poincaré* **5**, p. 177.

Petrov, D. S., D. M. Gangardt & G. V. Shlyapnikov (2004), "Low-dimensional trapped gases", in *J. Phys. IV* **116**, pp. 5–44.

Petrov, D. S. & G. V. Shlyapnikov (2001), "Interatomic collisions in a tightly confined Bose gas", in *Phys. Rev. A* **64**, p. 012706.

Picozzi, Antonio, Josselin Garnier, Tobias Hansson, Pierre Suret, Stephane Randoux, Guy Millot & Demetrios N Christodoulides (2014), "Optical wave turbulence: Towards a unified nonequilibrium thermodynamic formulation of statistical nonlinear optics", in *Physics Reports* **542**, pp. 1–132.

Pilati, S., J. Boronat, J. Casuelleras & S. Giorgini (2005), "Quantum Monte Carlo simulation of a two-dimensional Bose gas", in *Phys. Rev. A* **71**, p. 023605.

Pitaevskii, L. & S. Stringari (2016), *Bose–Einstein Condensation and Superfluidity*, 2nd edition, Oxford: Oxford University Press.

Popov, V. N. (1972), "On the theory of the superfluidity of two- and one-dimensional bose systems", in *Theoretical and Mathematical Physics* **11**, pp. 565–573.

– (1987), *Functional Integrals and Collective Modes*, Cambridge: Cambridge University Press.

Pricoupenko, Ludovic & Maxim Olshanii (2007), "Stability of two-dimensional Bose gases in the resonant regime", in *Journal of Physics B: Atomic, Molecular and Optical Physics* **40**, p. 2065.

Prokof'ev, N. V. & B. V. Svistunov (2002), "Two-dimensional weakly interacting Bose gas in the fluctuation region", in *Phys. Rev. A* **66**, p. 043608.

Safonov, A. I., S. A. Vasilyev, I. S. Yasnikov, I. I. Lukashevich & S. Jaakkola (1998), "Observation of Quasicondensate in Two-Dimensional Atomic Hydrogen", in *Phys. Rev. Lett.* **81**, p. 4545.

Schick, M. (1971), "Two-Dimensional System of Hard-Core Bosons", in *Phys. Rev. A* **3**, p. 1067.

Schmitt, Julian, Tobias Damm, David Dung, Frank Vewinger, Jan Klaers & Martin Weitz (2014), "Observation of grand-canonical number statistics in a photon Bose-Einstein condensate", in *Physical review letters* **112**, p. 030401.

Schmitt, Julian, Tobias Damm, David Dung, Christian Wahl, Frank Vewinger, Jan Klaers & Martin Weitz (2016), "Spontaneous symmetry breaking and phase coherence of a photon Bose-Einstein condensate coupled to a reservoir", in *Physical review letters* **116**, p. 033604.

Schoelz, JK, P Xu, V Meunier, P Kumar, M Neek-Amal, PM Thibado & FM Peeters (2015), "Graphene ripples as a realization of a two-dimensional Ising model: A scanning tunneling microscope study", in *Physical Review B* **91**, p. 045413.

Schweikhard, V., S. Tung & E. A. Cornell (2007), "Vortex Proliferation in the Berezinskii–Kosterlitz–Thouless Regime on a Two-Dimensional Lattice of Bose–Einstein Condensates", in *Phys. Rev. Lett.* **99**, p. 030401.

Sondhi, S. L., S. M. Girvin, J. P. Carini & D. Shahar (1997), "Continuous quantum phase transitions", in *Rev. Mod. Phys.* **69** (1), pp. 315–333.

Strandburg, Katherine J. (1988), "Two-dimensional melting", in *Rev. Mod. Phys.* **60**, pp. 161–207.

Strandburg, Katherine J, ed. (1992), *Bond-orientational order in condensed matter systems*, Springer Science & Business Media.

Sun, Can, Shu Jia, Christopher Barsi, Sergio Rica, Antonio Picozzi & Jason W Fleischer (2012), "Observation of the kinetic condensation of classical waves", in *Nature Physics* **8**, pp. 470–474.

Svistunov, Boris V, Egor S Babaev & Nikolay V Prokof'ev (2015), *Superfluid states of matter*, Crc Press.

Thompson-Flagg, Rebecca C, Maria JB Moura & M Marder (2009), "Rippling of graphene", in *EPL (Europhysics Letters)* **85**, p. 46002.

Thouless, D. J., M. Kohmoto, M. P. Nightingale & M. den Nijs (1982), "Quantized Hall Conductance in a Two-Dimensional Periodic Potential", in *Phys. Rev. Lett.* **49**, pp. 405–408.

Wierschem, Keola & Efstratios Manousakis (2011), "Simulation of melting of two-dimensional Lennard-Jones solids", in *Phys. Rev. B* **83** (21), p. 214108.

Wigner, E. (1932), "On the Quantum Correction For Thermodynamic Equilibrium", in *Phys. Rev.* **40** (5), pp. 749–759.

Wolf, PE, S Balibar & F Gallet (1983), "Experimental Observation of a Third Roughening Transition on hcp He 4 Crystals", in *Physical review letters* **51**, p. 1366.

Wolf, PE, F Gallet, S Balibar, E Rolley & Ph Nozieres (1985), "Crystal growth and crystal curvature near roughening transitions in hcp 4He", in *Journal de Physique* **46**, pp. 1987–2007.

Young, A. P. (1979), "Melting and the vector Coulomb gas in two dimensions", in *Phys. Rev. B* **19** (4), pp. 1855–1866.

Ziman, John M (1960), *Electrons and phonons: the theory of transport phenomena in solids*, Oxford university press.